



TAMPEREEN TEKNILLINEN YLIOPISTO
TAMPERE UNIVERSITY OF TECHNOLOGY

DIEGO ALONSO
NARROWBAND INTERFERENCE REJECTION STUDIES FOR
GALILEO SIGNALS VIA SIMULINK

Master of Science

Examiner: Assoc. Prof. Elena-Simona Lohan
Examiner: Prof. Jari Nurmi
Examiner and topic approved by the
Faculty Council of the Faculty of
Electronics and Communications Engineering
on 20th April 2015

ABSTRACT

DIEGO ALONSO: Narrowband interference rejection studies for Galileo signals via Simulink

Tampere University of Technology

Master of Science, 67 pages

July 20, 2015

Master's Degree Program in Satellite Technology

Major: Wireless Communication and Navigation

Examiner: Assoc. Prof. Elena-Simona Lohan

Examiner: Prof. Jari Nurmi

Keywords: *GNSS, Galileo E5/E5a, Interferences, Mitigation Techniques, Acquisition*

Four Global Navigation Satellite System (GNSS) are scheduled to be fully operational orbiting the Earth in the coming years. A considerably high number of signals, coming from each of the satellites that will constitute those constellations, will share the radio electric spectrum. Aeronautical Radio Navigation Systems (ARNS) share the E5 Galileo band. Examples of ARNS are Distance Measuring Equipment (DME) and Tactical Air Navigation system (TACAN). It should also be mentioned that electronic attacks (jamming or spoofing) have always been a latent threat for satellite services. All of this are important interference sources which can partially or completely disable a GNSS system. These interferences must be, and are currently being studied together with interference mitigation methods.

The aim of the work presented in this thesis is to study the narrowband interference effects in Galileo E5 band and to assess three mitigation techniques against two types of narrowband interferences, Continuous Wave Interference (CWI) and DME signals. Cancellation techniques can be classified into two major groups: time-domain approaches and frequency-domain approaches. Methods that combine time and frequency together are also given in the literature (e.g. cyclostationarity-based methods) but their implementations are very costly with high sampling rates as those used for example in Galileo E5 signals.

The mitigation techniques that are addressed in this thesis are zeroing, dynamic notch filtering and blanking pulse methods. All of them can be understood as filtering techniques that remove any signal above a certain threshold. This thesis shows that zeroing is more suitable for CWI and blanking is better against DME signals. These techniques have been developed within a Matlab-Simulink based simulator initiated in 2007 at Tampere University of Technology. The implemented simulator could be a great help tool for future research and development projects.

PREFACE

This Master of Science Thesis has been written at the Department of electrical Engineering at the Tampere University of Technology (TUT), Tampere, Finland. This thesis work has been carried out in the signal processing for wireless positioning group at the Department of Electronics and Communications Engineering during the years 2014-2015.

This thesis has been possible thanks to the help of several people. First of all, I would like to express my heartfelt thanks to my supervisor, Dr. Elena-Simona Lohan and Prof. Jari Nurmi. They gave me the opportunity to work with them and learn a lot. I must particularly thank my parents, for giving me the necessary means to be what I am today and helping me when I needed it. Last but not least, I would like to thank Patricia Herrera for her unconditional support, help, patience and love.

Tampere, July 20, 2015

Diego Alonso

TABLE OF CONTENTS

1. Introduction, state-of-the-art and motivation	1
1.1 The use of satellite positioning	1
1.2 GNSS landscape	2
1.2.1 Global Positioning System (GPS)	3
1.2.2 GLObal NAVigation Satellite System (GLONASS)	4
1.2.3 BeiDou Navigation Satellite System (BDS)	5
1.2.4 Galileo	6
1.3 Interferences study motivation	7
1.4 Author's contribution	8
2. Galileo Signals	10
2.1 Frequency bands and services	10
2.2 General signal structure	13
2.3 GNSS modulations	14
2.3.1 Binary Phase Shift Keying (BPSK) modulation	14
2.3.2 Binary Offset Carrier (BOC) modulation	15
2.3.3 Alternative Binary Offset Carrier (AltBOC) modulation	16
2.4 E5 signals	18
2.4.1 E5 transmitted signal	19
2.4.2 E5 Power Spectral Density (PSD)	20
2.4.3 E5 Cross-Correlation Function (CCF)	22
2.4.4 E5 received signal and operating principles	22
3. Error sources in Galileo	24
3.1 Overview	24
3.2 Narrowband interferences models: CWI and DME/TACAN signals	27
3.2.1 CWI signals	27
3.2.2 DME signals	28

4. Narrowband interference mitigation techniques	30
4.1 Time domain and frequency domain approaches	30
4.1.1 Pulse blanking method	31
4.1.2 Zeroing method	33
4.1.3 Dynamic notch filtering method	35
4.2 Comparative notes	39
5. Simulink-based algorithmic implementation	40
5.1 Transmitter	41
5.2 Channel & interferences	44
5.3 Receiver	48
5.3.1 Mitigation techniques block	48
5.3.2 Acquisition unit	49
5.3.3 Tracking unit	53
5.4 Main variables and defined-user parameters	57
6. Simulation results	59
6.1 Performance criteria	59
6.2 Simulation results	62
7. Conclusions and open directions	66
Bibliography	68

LIST OF FIGURES

1.1	Example of a GNSS system architecture.	2
1.2	Galileo ground segment locations	7
2.1	Current Frequency Bands for GNSS.	10
2.2	Galileo tiered code structure	14
2.3	PSD of SinBOC(10,5) and CosBOC(10,5)	16
2.4	E5 modulation [52]	19
2.5	Constellation diagram of $s_{e5}(t)$	20
2.6	E5 Power Spectral Density	21
2.7	Auto-Correlation Function (upper plot) and cross-correlation function (lower plot)	22
2.8	Code delay computation[35].	23
3.1	Wideband vs Narrowband spectra	26
3.2	Continuous Wave Interference representation in frequency domain (upper plot) and time domain (lower plot).	28
3.3	DME Interference representation. RF signal in time domain (Upper plot) and pulses envelope (lower plot).	29
3.4	DME Interference representation in frequency domain.	29
4.1	System model used.	31
4.2	Pulse blanking performance in time domain.	32
4.3	Pulse blanking performance in frequency domain. A DME interference is harming the GNSS signal in the upper plot and its blanking is showed in the lower plot.	32

4.4	Zeroing performance in frequency domain. A CWI interference is harming the GNSS signal in the upper plot and its zeroing samples are showed in the lower plot.	34
4.5	Zeroing performance in time domain against one CWI. The contaminated GNSS signal in the upper plot and the cleaned GNSS signal in the lower plot.	34
4.6	Zeroing performance in frequency domain against DME pulses. The contaminated GNSS signal in the upper plot and the cleaned GNSS signal in the lower plot.	35
4.7	Zeroing performance in time domain against DME pulses. The contaminated GNSS signal in the upper plot and the cleaned GNSS signal in the lower plot.	35
4.8	Second order IIR notch filter transfer function.	36
4.9	Block diagram of the dynamic notch filtering method.	37
4.10	$s_{rx}(t)$ mean power in the presence of three CWIs.	37
4.11	Notch performance in frequency domain against three CWIs. The contaminated GNSS signal in the upper plot and the cleaned GNSS signal in the lower plot.	38
4.12	Notch performance in frequency domain against DME pulses. The contaminated GNSS signal in the upper plot and the cleaned GNSS signal in the lower plot.	39
5.1	End-to-end Galileo E5 signal simulator block diagram.	41
5.2	Transmitter block diagram.	42
5.3	Above, the PSD before down-sample. Below, the PSD after down-sample. The x axis bounds are between $-f_{sample}/2$ and $f_{sample}/2$ due to the Matlab FFT representation. In the upper plot $f_{sample} = 126MHz$ and in the lower plot $f_{sample} = 31.5MHz$	43
5.4	Comparison between the real part of the E5 and E5a normalized ACF.	44
5.5	Comparison between the absolute value of the E5 and E5a normalized ACF.	44

5.6	Channel and interferences block diagram.	45
5.7	E5a ACF before and after the multipath block. Array for multipath delay = [2 25 85] chip, Array for multipath gain = [0 -3 -6] dB. . . .	46
5.8	Galileo E5 signal PSD before (upper plot) vs after (lower plot) the noise addition block. No multipath effect is considered.	47
5.9	Interferences block diagram.	47
5.10	Mitigation techniques block diagram.	48
5.11	ACF to assess the zeroing method against two CWIs.	49
5.12	Block diagram of the acquisition process carried out in GE5-TUT simulator.	50
5.13	Acquisition time-frequency grid. $C/N_0 = 60$ dB/Hz, $N_C = 1$, $N_{NC} = 1$. No multipath effects nor interference signal are present.	50
5.14	One CWI. No-mitigation technique is used.	51
5.15	Zeroing method against one CWI.	51
5.16	Notch-Filtering method against one CWI.	52
5.17	DME interference with 3000 pps density. No-mitigation technique is used.	52
5.18	Notch-Filtering method against DME interference with 3000 pps density.	53
5.19	Blanking method against DME interference with 3000 pps density.	53
5.20	Tracking subsystem block diagram.	54
5.21	Carrier-wipe-off block diagram.	55
5.22	channel correlation and discriminator block diagram.	56
5.23	Tracking error along 0.5 second of simulation, 1 ms of non-coherent integration and $C/N_0 = 60$ dB/Hz.	56
5.24	Initial pop-up menu.	57

6.1	Statistical scenario.	60
6.2	Statistical scenario for $SIR = -30$ dB and $C/N_0 = 50$ dB. Above no mitigation technique is applied while picture below shows the zeroing behavior.	61
6.3	Statistical scenario for $SIR = -50$ dB and $C/N_0 = 50$ dB. Above no mitigation technique is applied while picture below shows the zeroing behavior.	61
6.4	P_d performance without any mitigation technique and different values of interference power. CWI and DME signal are considered.	62
6.5	CWI rejection performance at interference powers between 0 and 45 dB.	63
6.6	DME interference rejection performance at interference powers between 0 and 60 dB. Pulse density of 500 pps.	63
6.7	DME interference rejection performance at interference powers between 0 and 60 dB. Pulse density of 3000 pps.	64
6.8	Mitigation techniques efficiency. C/N_0 was fixed to 42 dB/Hz.	65

LIST OF TABLES

2.1 Galileo carriers and bandwidths. Galileo OS SIS ICD Issue 1 Revision 1 September 2010 [13].	11
2.2 GPS and Galileo signals features	13
4.1 Comparative table between the method described along the chapter. .	39
5.1 GE5-TUT main parameters.	58

LIST OF ABBREVIATIONS AND SYMBOLS

Abbreviations

ACF	Auto-Correlation Function
AltBOC	Alternative Binary Offset Carrier
ARNS	Aeronautical Radio Navigation Services
AWGN	Additive white Gaussian noise
BDS	BeiDou Navigation Satellite System
BOC	Binary Offset Carrier
CCF	Cross Correlation Function
CDMA	Code Division Multiplex Access
CFAR	Constant False Alarm Rate algorithm
CS	Commercial Service
CWI	Continuous Wave Interference
DFT	Discrete Fourier Transform
DLL	Delay Locked Loop
DME	Distant Measuring Equipment
EML	Early Minus Late discriminator
ESA	European Space Agency
EU	European Union
FDMA	Frequency Division Multiplex Access
FFT	Fast Fourier Transform
FLL	Frequency Locked Loop
FOC	Full Operational Capability
GCC	Ground Control Centers
GEO	Geostationary Earth Orbit
GE5-TUT	Galileo E5 TUT simulator
GLONASS	GLOBAL NAVIGATION Satellite System
GNSS	Global Navigation Satellite System
GPS	Global Positioning System
GSS	Galileo Sensor Stations
GUI	Graphical User Interface
IF	Intermediate Frequency
IGSO	Inclined Geosynchronous Orbit satellite
IIR	Infinite Impulse Response
IOV	In-Orbit-Validation
LEO	Low Earth Orbit

LFSR	Linear Feedback Shift Registers (LFSR)
MEO	Medium Earth Orbit
MCS	Master Control Station
MS	Monitoring Station
MUX	Multiplexor
NCO	Numerically controlled Oscillator
OS	Open Service
PLL	Phase Locked Loop
pps	Pair of pulses per second
PRS	Public Regulated Service
PSD	Power Spectral Density
PRN	Pseudo-Random Noise
PVT	Position Velocity Time Radio-Frequency
QPSK	Quadrature phase-shift keying
RF	Radio-Frequency
RMS	Root Mean Square
RNSS	Radio Navigation Satellite Service
SAR	Search and Rescue Service
SCC	System Control Center
SIS	Signals In Space
SIR	Signal-to-Interference Ratio
SLR	Laser Ranging Station
SoL	Safety-of-Life
SNR	Signal-to-Noise Ratio
SV	Space Vehicle
TACAN	TACTical Air Navigation system
TOA	Time Of Arrival
TOF	Time Of Flight
TOT	Time Of Transmission
TT&C	Telemetry, Tracking and Command
TUT	Tampere University of Technology
SINR	Signal to Interference and Noise Ratio
UHF	Ultra High Frequency
ULS	Up-link Local Station
UWB	Ultra-Wideband
VHF	Very High Frequency

Symbols

BW_{E5}	Galileo E5 Bandwidth
BW_{E5a}	Galileo E5a Bandwidth
$C(t)$	Spreading code
$C_{E5a-I}(t)$	Unencrypted ranging code
$C_{E5a-Q}(t)$	Unencrypted ranging code
$C_{E5b-I}(t)$	Unencrypted ranging code
$C_{E5b-Q}(t)$	Unencrypted ranging code
C/N_0	Carrier-to-Noise-density Ratio
c	Light speed
$D(t)$	Navigation message
d	Distance between GNSS receiver and one satellite
$e_{5a-I}(t)$	E5a sequence of navigation data modulated with $C_{E5a-I}(t)$ (data channel)
$e_{5a-Q}(t)$	E5a sequence of $C_{E5a-Q}(t)$ (pilot channel)
$e_{5b-I}(t)$	E5b sequence of navigation data modulated with $C_{E5b-I}(t)$ (data channel)
$e_{5b-Q}(t)$	E5b sequence of $C_{E5b-Q}(t)$ (pilot channel)
f_c	Chip frequency
$f_{Doppler}$	Doppler frequency
f_{E5}	E5 Carrier frequency
f_{IF}	Intermediate frequency
f_{sample}	Sample frequency
$f_{subcarr}$	Galileo E5 sub-carrier frequency
$j(t)$	Interference signal
$j_{cwi}(t)$	CWI signal
$j_{dme}(t)$	Interference signal from DME system
N_0	Noise power spectral density
N_C	Number of coherent integrations
N_{NC}	Number of non-coherent integrations
n	GLONASS frequency channel
$s_{E5}(t)$	Galileo E5 transmitted signal
$s_{e5}(t)$	Galileo E5 complex envelope
$s_{rx}(t)$	Received input signal
$s_{out}(t)$	Galileo E5 signal after the multipath block
$sc_s(t)$	Complex squared wave sub-carrier for the single signals
$sc_p(t)$	Complex squared wave sub-carrier for the product signals
T_c	Chip period
$T_{sc,E5}$	Galileo E5 sub-carrier period

T_{sym}	Symbol period
x_i	i th satellite latitude
x_u	User's latitude
y_i	i th satellite longitude
y_u	User's longitude
z_i	i th satellite altitude
z_u	User's altitude
α_i	Complex gain for the i -th path
β	Notch filter parameter to control the central frequency
$\delta(t)$	Dirac pulse
Δf_{interf}	Frequency shift (in MHz) with respect to the Galileo E5a sub-carrier
ρ	Pseudorange between satellite and receiver
τ	Clocks bias
τ_i	Delay time for the i -th path
ϕ_0	Galileo E5 phase at $t = 0$
ω_N	Notch angular frequency

1. INTRODUCTION, STATE-OF-THE-ART AND MOTIVATION

1.1 The use of satellite positioning

As time goes by, radio-navigation are becoming more and more useful for a hundred of situations and a large list of applications in our daily life. One technological field in which radio-communications are experiencing an extraordinary progress is satellite navigation. Some words such as evolution, innovation or development are continuously present at the environment of any Global Navigation Satellite System (GNSS).

A GNSS system is formed by a constellation of satellites orbiting at an altitude of more than nineteen thousand kilometers and transmitting constantly Radio-Frequency (RF) signals that allow users to obtain the position (i.e. latitude, longitude and height) and velocity of one receiver in real-time at any part of the Earth surface. Therefore, in order to provide a good geopositioning service, global coverage must be assured with enough satellites distributed in several orbits with an appropriated inclination.

Although the initial developments of the satellite navigation technology were meant for military applications to raise the accuracy of weapons (Transit System, 1960), technological progress and inexpensive receivers have helped that civil applications are growing by leaps and bounds [6]. Some of them are considered indispensable for many years such as road navigation (almost everybody has had, or knows someone who has had, an in-car navigation device) or maritime navigation. Also air navigation is benefiting more and more from the satellite navigation systems. In the future, GNSS systems are expected to assist pilots in all flight phases. Personal applications (e.g. pedestrian or outdoor navigation, indoor navigation assistance, social networking and location based services), road applications (e.g. tolling, traffic management, fleet management and tracking services) or industry applications (e.g. agriculture accuracy, package and container tracking or surveillance services) are some examples that satellite navigation is offering. There are also futuristic environments

such as autonomous driving/flying where GNSS systems are the key system for the recent developments on this area [39].

1.2 GNSS landscape

The purpose of this section is to give a general idea about the development stage of each GNSS system. It also describes briefly the basic operational principle of a GNSS. This section starts with describing GNSS systems in general, and it ends up with a description of Galileo, because Galileo is the system used in this thesis.

Currently, there are four GNSS systems at different development stage, NAVSTAR Global Positioning System (GPS) from United States, GLObal Navigation Satellite System (GLONASS) from Russia, Compass/BeiDou-2 System (BDS) from China and Galileo from Europe. Despite their differences between these systems, all of them share the same general architecture. This aspect is illustrated in Figure 1.1.

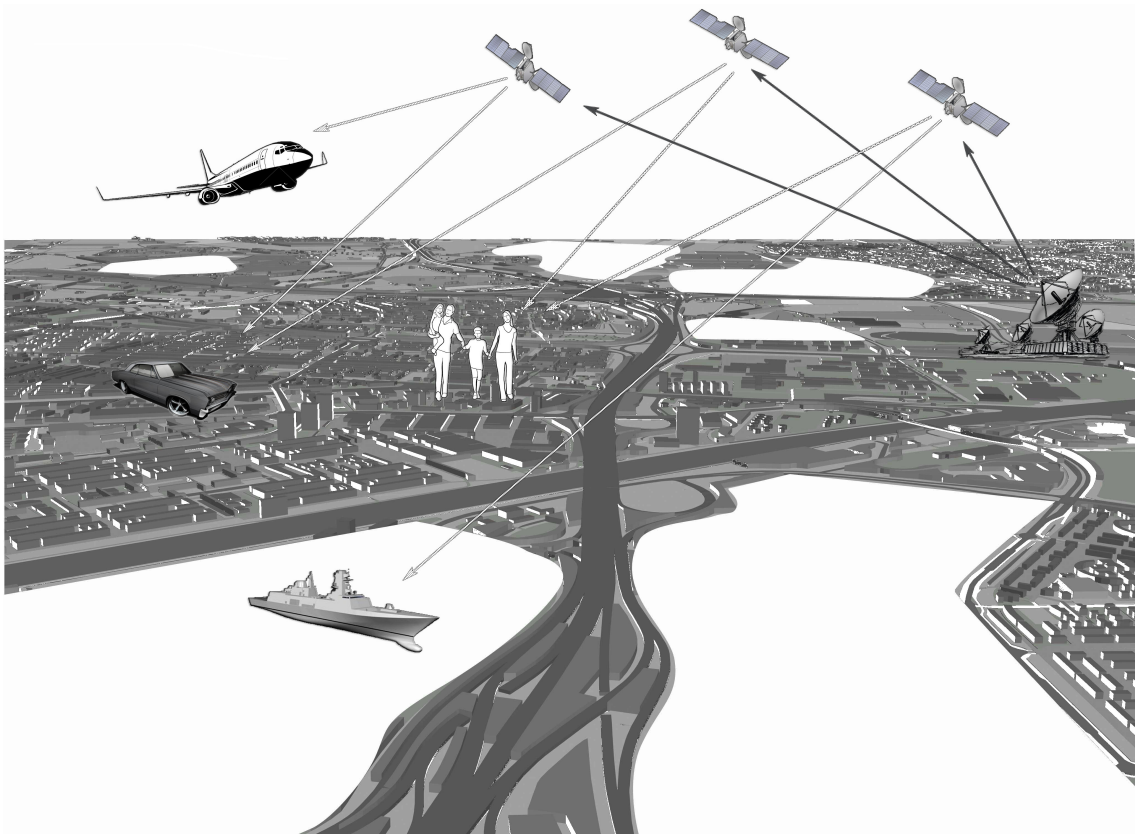


Figure 1.1 Example of a GNSS system architecture.

Each GNSS has the following three architectural segments:

- Space Segment, formed by all the spacecrafts or Space Vehicles (SV) and RF signals.
- Ground Segment, formed by control centers and a global network of transmitting and receiving stations to control or maintain the constellation and the health of every SV sending orbital or clock corrections.
- User segment, wherein are included users equipment that are able to receive each satellite signal and compute the user position, velocity and time (PVT).

In general, each satellite broadcasts simultaneously, in several frequency-bands, radio signals, called Signals In Space (SIS), carrying with them information about satellite orbital characteristics (almanac and ephemeris). With the data, user receiver is able to obtain the time of transmission (TOT), the time of arrival (TOA) and then get the time of flight (TOF) value to calculate its distance (d) to each satellite multiplying this among by the light speed ($c = 299,792,458m/s$).

$$TOF = TOA - TOT, \quad (1.1)$$

$$d = TOF \times c, \quad (1.2)$$

In this context, it can be said that just three satellites are enough by the user receiver to acquire its position at any time thanks to a multilateration technique, but to do this, there should be a perfect synchronization between both the satellite clock and the user receiver clock. At the moment, this is impossible due to the imperfect clock stability at the receiver side. This limitation means that another satellite is needed to calculate both the receiver position and the temporary deviation. For more information see [39],[7], [49].

The main differences between each GNSS system lie in the number of satellites, number or type of orbits, inclination of each orbit with respect to the equatorial plane, radio interface parameters and number of control centers and global network elements. In the next sections this points are discussed.

1.2.1 Global Positioning System (GPS)

The first GNSS system was the NAVSTAR, commonly called GPS. It was developed by the United States Department of Defense (DoD) in 1973 (military control). The first launch was in 1978 and it was not until April of 1995 that GPS was declared

as a system with Full Operational Capability (FOC). The GPS is growing and the last launch was the 25th of March 2015. [58].

At least 24 SV are needed to provide global service 95% of the time. The United States Air Force is responsible of this system and to ensure all the requirements several improvements have been carried out as well as a greater number of SV, more signal and more frequency bands.

- ***Current space segment:*** There are 31 operative satellites and 1 spare at an altitude of 20,200 km. The constellation is structured in 6 orbits with an inclination of approximately 55° grades with respect to the equatorial plane. Regarding to the SIS transmitted using the Code Division Multiplex Access (CDMA), the GPS started using the L1 band (centered at 1575.42 MHz) and the L2 (1227.60 MHz) but later, the L5 (1176.45 MHz) band and other improvements (additional RF signals like L1C and L2C) began to be incorporated into the GPS modernization program, which is ongoing. Civil, military and Safety-of-Life (SoL) services are provided through this band.
- ***Current ground segment:*** One Master Control Station (MCS), as the core of this network located in Colorado Springs, an alternate master control station, 16 Monitoring Stations (MS) to collect the GPS data and 12 ground antennas to send information to each satellite spread around all the world.

For more information about GPS see [29], [41] and [56].

1.2.2 GLObal NAVigation Satellite System (GLONASS)

The second GNSS system was the Russian system. Initiated in 1982 by the Soviet Union armed forces, GLONASS was originally developed for military purposes. It was declared fully operational with 24 SV in 1995, but due to the economic crisis which lasted until 1999, GLONASS was almost abandoned leaving the constellation with only 6 operational SV. To avoid the dependence of Russia on the American GPS, the program was restarted in 2001 and the constellation was completed with 24 operational satellites in April, 2013. In the same way as GPS, GLONASS is increasing and the last launch was in November, 2014 [58].

- ***Current space segment:*** There are 24 operative SV, 1 spare, 1 under check and 2 in “flight test phase” at an altitude of 19,100 km. All of these SV are

distributed along 3 orbital planes with an inclination of approximately 64.8° . Unlike GPS, this system makes use of the Frequency Division Multiplex Access (FDMA) technique in order to separate the satellites. Hence each satellite has its own carrier frequency in the L1 band ($1602 \text{ MHz} + n \times 0.5625 \text{ MHz}$, $n \in [-7,6]$), and L2 band ($1246 \text{ MHz} + n \times 0.44375 \text{ MHz}$, $n \in [-7,6]$) where n is the frequency channel for civil and military services. In fact, CDMA is still used to spread the navigation data even in FDMA case, but same pseudorandom code (see section 2.4.4 for better understanding of this codes) is employed for all satellites. Soon, GLONASS will start using the CDMA technique through the L3 band (1207.14 MHz) especially suitable for SoL services. Also CDMA-based signals will be broadcast in L1, L2 and L5 band in the next years. Important modifications to the future GLONASS are also being studied, such as moving from 3 to 6 orbits, rise the number of SV to 30 and remove gradually the FDMA signal [39], [21]. These can overcome the problem that GLONASS bands are not perfectly overlapping with GPS bands and thus, the complexity of the interoperability would reduce significantly.

- **Current ground segment:** Providing the same capabilities as the GPS ground segment, GLONASS is formed by one System Control Center (SCC) in Moscow region, 5 Telemetry, Tracking and Command centers (TT&C), one central clock, 2 Laser Ranging Stations (SLR), 3 Upload Stations (UL) and an increasing network of surveillance stations deployed mainly in Russian territory, as well as in neighboring countries, Antarctica and Brazil.

1.2.3 BeiDou Navigation Satellite System (BDS)

The first phase of the Chinese satellite navigation system was Beidou-1. It was an experimental regional navigation system formed by 4 Geostationary Earth Orbit (GEO) satellites (3 operative satellites and one backup satellite). BeiDou-1 was fully operational since 2003 until 2012 when the second phase, called BeiDou-2, started offering **regional** services in Asia-Pacific region with FOC. BeiDou-2 consists of 14 satellites, 5 GEO, 5 Inclined Geosynchronous Orbit satellites (IGSO) (about 55°) and 4 Medium Earth Orbit (MEO) satellites [31]. The first BeiDou-2 launch was in 2007 and the last, until the date of this thesis, was on the 30th of April 2015 [58]. The ultimate objective planned by 2020 is a **global** system (BDS) of 35 SV, of which 5 are GEO, 27 are MEO and 3 are IGSO (third phase) [39].

- **Current space Segment:** At the present time, COMPASS is supplying service for the whole Asia-Pacific region through 16 SV, 5 Medium Earth

Orbit (MEO) satellites (one is partially operable), 5 GEO satellites and 6 IGSO (one is in commissioning). B1 (1561.098 MHz), B2 (1258.520 MHz) and B3 (1207.140 MHz) are the spectrum zones where each SV transmits its signals using quadrature phase-shift keying (QPSK) modulation [37].

- ***Current ground Segment:*** The functionality of this subsystem is the same as mentioned for the above systems. One MCS, two update stations and several MS still being deployed are the main structures.

1.2.4 Galileo

The last of the 4 GNSS systems which are fully operative or still being developed, is the Galileo system, named in honor of the famous scientist Galileo Galilei. This system was created with the aim of being the first GNSS intended exclusively for civil purposes and thus to untie the Europe dependence on other systems under military control such as those mentioned previously. The initiative of Galileo emerged thanks to the European Union (EU) and the European Space Agency (ESA). The first phase of Galileo, called In-Orbit-Validation (IOV), was completed in 2014 when 4 satellites were launched (the first two in 2011 and the next two in 2012) and their validation tests were successfully assessed. These 4 IOV satellites will constitute the core of the Galileo constellation. Initial Operational Capability (IOC) is the second phase and is planned to be ended around 2016. By then, 18 SV will be in orbit and primary services will be working for the users. The last phase, Full Operational Capability (FOC), will mean the complete deployment of the full system planned by 2020 [39]. An updated launch schedule can be found in [58] and [53]

- ***Current space Segment:*** Right now, the constellation is formed by 8 satellites (3 operative, one temporally unavailable and 4 in commissioning) [12]. Galileo will be a 30 MEO satellites system (27 operational and 3 spare) at an altitude of 23,222 km with an inclination of approximately 56° . As Galileo is the system around which this thesis is involved, its frequency bands as well as its offered services and the transmitted signals are discussed in chapter 2.
- ***Current ground Segment:*** Two Ground Control Centers (GCC) are the core infrastructure in charge of monitoring the constellation and managing the navigation system control. One is located in the Fucino Control Center (Italy) and the other is situated in Oberpfaffenhofen (Germany). Their tasks are accomplished thanks to a worldwide network of 5 Telemetry, Tracking and Command (TTC) and a global network of 15 Galileo Sensor Stations (GSS)

and 5 Up-link Local Station (ULS) [16] and [40]. Figure 1.2 shows the world locations of each element.

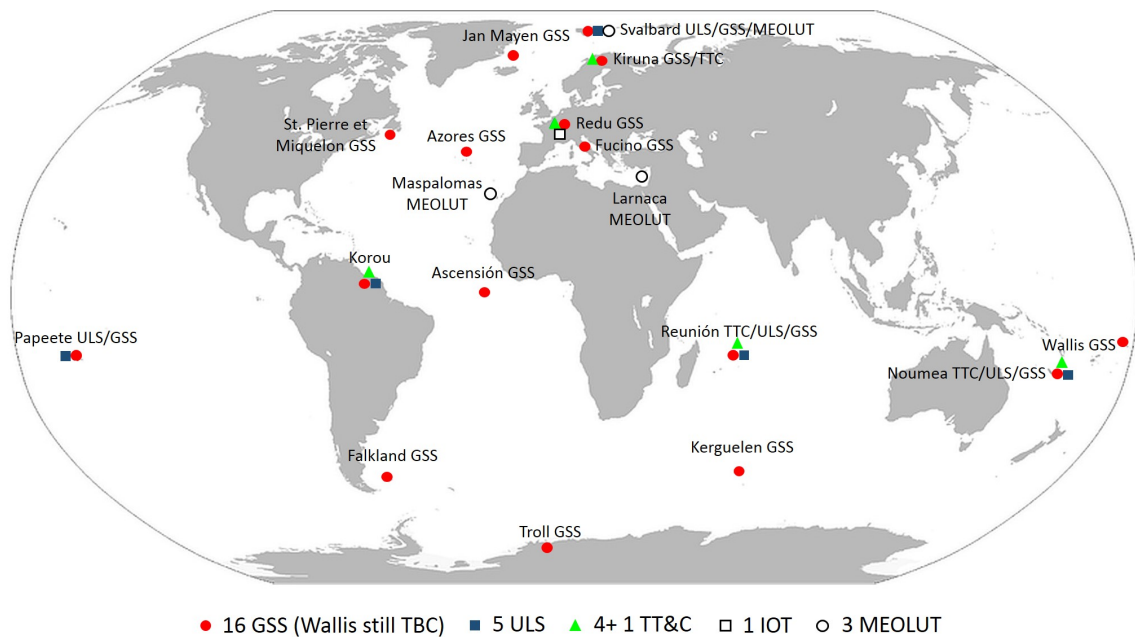


Figure 1.2 Galileo ground segment locations

1.3 Interferences study motivation

Interference signals can be classified as narrowband or wideband, depending on their relative bandwidth to GNSS signal. Unintentional or intentional interference classes can be another classification. Over the years, GNSS receivers have been in situations in which SIS was impossible to acquire momentarily or permanently because of interferences signals. Some of these situations are mentioned below:

- At Stanford University in 1999, a camera with a digital images transmitter incorporated was installed to monitoring a construction inside the campus. The secondary frequency of this transmitter was quite close to the GPS L1 band and caused the GPS signal loss within a 1 km radius (narrowband and unintentional).
- At Moss Landing Harbor, California in 2001, more than one commercial VHF/UHF television antenna disabled the GPS L1 signal tracking due to its built-in preamplifier within a 3 km radius (narrowband and unintentional).

- Inside an hangar, in a German airport, a GNSS repeater was installed to provide coverage to indoor devices. This repeater had a power leak outside its placement and was causing loss of signal or giving wrong measurements to pilots (narrowband and unintentional).
- An engineering firm worker in New Jersey purchased a GPS jammer device to avoid his boss could know his position at any time while he is driving the company truck. When the offender drove near Newark airport in New Jersey, the jammer blocked the GPS signal reception (narrowband and intentional).

Because of unintentional reasons, some RF devices failures, as well as deliberate attacks or camouflage countermeasures, the GNSS signal could be seriously jammed or violated. Therefore, the need to investigate how all of these issues can be approached is critically important to make any GNSS system robust. Consequently, it is very important to make research projects about interference signals to which Galileo (or other GNSS systems) might be exposed. Further in the chapter 3 different kinds of interference signals are addressed in detail (e.g jamming, meaconing and spoofing as the three main types of interference encountered in GNSS) as well as its effects and some techniques to deal with them. This thesis focuses on narrowband interference both intentional and unintentional.

The reader can find more information regathering the incidents commented above in [9], [44], [43]and [36].

1.4 Author's contribution

The thesis focuses on the TUT Galileo E5 Matlab-Simulink simulator intended to be a useful student tool for interferences and mitigation techniques studies. The main contributions are:

- Previous TUT model adaptation from Matlab-Simulink 2007a - 32 bits to Matlab-Simulink 2014a - 64 bits and updating the outdated blocks.
- Studies and implementation of narrowband interference signals.
- Studies and implementation of three interferences rejection techniques: pulsed blanking, dynamic notch filtering and zeroing method.
- Creation of a basic Graphical User Interface (GUI) to allow the user to modify several parameters easily and launch each simulation faster.

- Validation tests and illustrations in alternative scenarios.

This thesis is structured as follows. Chapter 2 discusses briefly the Galileo E5 signals as well as its main properties. Chapters 3 and 4 summarize the existing interference signals and some mitigation techniques. After that, the Galileo E5 TUT simulator is explained in a detailed manner with some graphic examples at various stages in chapter 5. Simulation results are addressed in chapter 6 and finally, the thesis concludes with chapter 7 in which conclusions and open directions are given.

2. GALILEO SIGNALS

This chapter deals generally with the most significant aspects of Galileo SIS. First of all, an overview is given for the different Galileo frequency bands as well for the services available when the system is fully operational. This is followed by a brief SIS structure explanation and after that the chapter focuses on Galileo E5 signals. Also, the operating principles of satellite receivers will be explained further on.

2.1 Frequency bands and services

Every GNSS system, as mentioned in the first chapter, usually works in several frequency bands at the same time to offer different services. Figure 2.1 shows which are the zones of the spectrum where each system works.

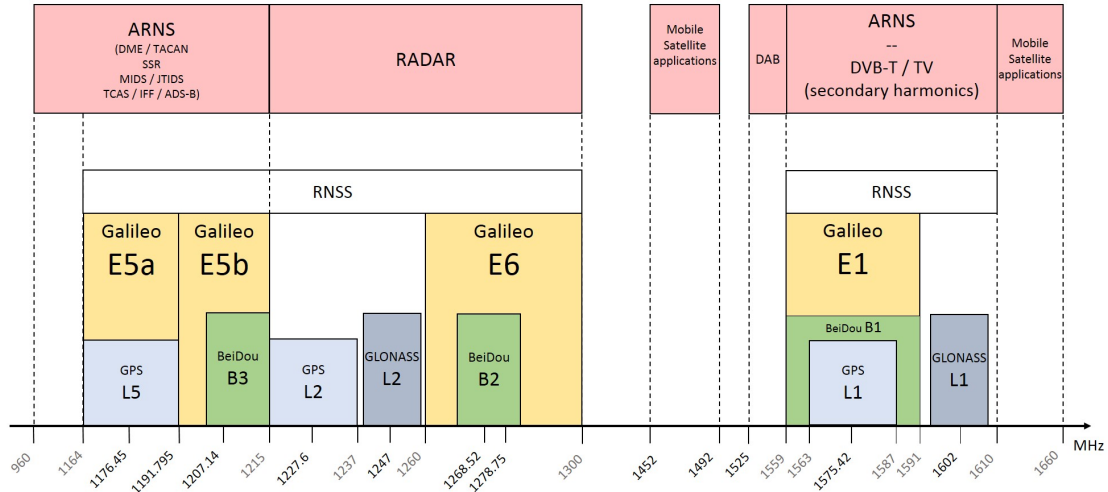


Figure 2.1 Current Frequency Bands for GNSS.

As seen in figure 2.1, Galileo satellites transmit permanently its CDMA signals throughout three frequency bands namely E5 (which in turn is separated in two bands, E5a and E5b), E6 and E1. These are placed in the allocated spectrum for Radio Navigation Satellite Service (RNSS) and, at the same time, E5 and E1

bands are included in the allocated spectrum for Aeronautical Radio Navigation Services (ARNS) which is intended for Civil-Aviation users, and allowing dedicated safety-critical applications. The overlap between frequency bands observed in figure 2.1 enable interoperability among different GNSS systems.

Table 2.1 shows the carrier frequencies of each Galileo frequency bands and its bandwidth. carriers and bandwidth

Table 2.1 Galileo carriers and bandwidths. Galileo OS SIS ICD Issue 1 Revision 1 September 2010 [13].

Signal	Carrier Frequency (MHz)	Receiver Reference Bandwidth (MHz)
E1	1575.420	24.552
E6	1278.750	40.920
E5	1191.795	51.150
E5a	1176.450	20.460
E5b	1207.140	20.460

At the moment, Galileo is notably interoperable with GPS. By 2025, GLONASS will employ CDMA method instead of FDMA in order to transmit interoperable signals with GPS and Galileo at L1/E1 and L5/E5 bands. In addition, BeiDou has also initiated plans to migrate its B1 and B2 bands toward L1/E1 band and L5/E5 respectively. Researches are currently under way to achieve interoperability between the four GNSS systems at signal and system level. For more information about interoperability see [39], [18] and [54].

It is expected that Galileo will be able to offer some satellite-only services with global or European coverage and full independence from other systems making use of one or a combination of more than one SIS [39]:

- **Galileo Open Service (OS)** is the basic service that Galileo will offer globally. It targets the mass-market applications. This service focuses on satellite radio-navigation and location-based mobile devices services without any cost to the user. The OS will be a combination of GPS and Galileo signals, E1/L1 and E5 signals. Various combinations are also possible according to the number of frequency bands a user receiver is able to manage. There are dual frequency services using L1/E1 and E5a (for best channel error cancellation) or single frequency services (at L1/E1, E5a, E5b or E5a and E5b together) in which case some atmosphere errors are suppressed using a mathematical model

(section 3.1, Ionospheric and tropospheric delays), and even triple frequency services making use of all the signals at the same time (L1, E5a and E5b), which can be utilized for very accurate applications.

- ***Galileo Safety of Life (SoL)*** is being re-profiled. It has been a major factor in defining the Galileo ground infrastructure and signal structure. Its original mission was to offer a global integrity service, satisfying the stringent requirements of aviation communities, among others.

For various reasons, the competent authorities decided to re-profile the SoL into a lighter service, which will provide integrity in likely cooperation with other regions.

- ***Galileo Public Regulated Service (PRS)*** is an encoded and uninterrupted navigation service developed to be more robust against jamming, spoofing and unintentional interference. It combines the robust benefits of a military GNSS signal with the enormous potential of a civilian-controlled system. The PRS will use a dual band signal (through both E1-A and E6-A signals) that makes it much more resistant to interference. This service is intended for government-authorized bodies such as police or coast-guards and Member States will maintain control of its distribution.
- ***Galileo Search and Rescue Service (SAR)*** is the contribution of Europe to the international COSPAS-SARSAT system, which is aimed at humanitarian search and rescue situations.

The SAR service will improve notably the current system, adding:

- Near real-time reception of SOS messages transmitted from any part of the world (now the elapsed time is around one hour).
- A position accuracy of few meters (if COSPAS-SARSAT receivers are equipped with Galileo receivers) while the current specification for location accuracy is 5 km.
- Several SV detection in case of one fail for any reason.
- Higher availability of the space segment, since there will be 27 MEO satellites and only four Low Earth Orbit (LEO) satellites and three GEO satellites in the current system.

Each SV receives the distress alert from any COSPAS-SARSAT beacon emitting an alert in the 406 - 406.1 MHz band, and broadcasts this alert to dedicated ground stations throughout the E1-B component. The SAR service is expected to be operative in 2016 [22].

- **Galileo Commercial Service (CS)** was one of the key elements intended to allow private partners to recover their investment. However, it was not possible to obtain such investment for the development of the Galileo project and therefore it was a program fully EU-funded. Under these premises the other services were prioritized and it is now when CS is steaming ahead.

The CS with early service expected to start in 2016, would offer a range of added-value features, including positioning accurate to decimeter-level and an authentication element, which could support professional or commercial applications. The CS will provide access adding two encrypted signals to the OS signal on the E6 band (E6-B and E6-C), delivering a higher data throughput rate and higher accuracy than offered by the OS [15].

The table 2.2 presents the main characteristics of both GPS and Galileo satellite signals to compare them [32]:

Table 2.2 GPS and Galileo signals features

System	Carrier (MHz)	Signal	Type	Modulation	Chipping rate (Mcps)	Code Length	Full length (ms)
GPS	L1 1575,420	C\A	Data	BPSK	1.023	1023	1
		P(Y)	Military	BPSK	10.23	for 7 days	7 days
		M	Military	BOCs(10,5)	5.115	-	-
	L2 1227,60	L2 CM	Data	TM and BPSK	0.5115	10230	20
		L2 CL	Pilot		0.5115	767250	1500
		P(Y)	Military	BPSK	10.23	for 7 days	7 days
		M	Military	BOCs(10,5)	5.115	-	-
	L5 1176,450	I	Data	QPSK	10.23	10230	1
		Q	Pilot		10.23	10230	1
	Galileo	E1 1575,42	A	PRS	BOCc(15,2,5)	10.23	25575 * 1
B			Data	BOCs(1,1)	1.023	4092 * 1	4
C			Data		1.023	4092 * 25	100
E6 1278,720		A	PRS	BOCc(10,5)	5.115	51150 * 1	10
		B	Data	BPSK(5)	5.115	5115 * 1	1
		C	Pilot		5.115	10230 * 50	100
E5 1191,795 a:1176,450 b:1207,140		a-I	Data	AltBOC (15,10)	10.23	10230 * 20	20
		a-Q	Pilot		10.23	10230 * 100	100
		b-I	Data		10.23	10230 * 4	4
		b-Q	Pilot		10.23	10230 * 100	100

2.2 General signal structure

All the necessary information to allow user receivers get its PVT is contained in a navigation message (NAV DATA, $D(t)$). This message is modulated a bit sequence

known as the Pseudo-Random Noise (PRN) code, also known as ranging code, ($C(t)$) which has a bit rate (chip rate) much higher to spread the spectrum of the transmitted signal. The resulting signal is the spread data ($s_{spread_data}(t) = D(t) \times C(t)$). This is a spread spectrum modulation technique, called direct-sequence spread spectrum (DSSS) that is used in the CDMA access method. A modulated PRN code provides the ability to recover ranging information due to its properties of time correlation commented in section 2.4.3.

Each GNSS system uses different types PRN codes. For example, GPS uses Gold codes [57] whereas Galileo uses tiered codes which are a combination of medium length primary codes with a smaller length secondary codes. Some secondary code are stored in memory instead of generated by a linear feedback shift registers (LFSR), thus they are harder to decipher [39] (figure 2.2). Every signal has its own PRN code (primary and secondary) with different length and chip rate as the table 2.2 indicates (see also the Galileo SIS Interface Control Document [13]).

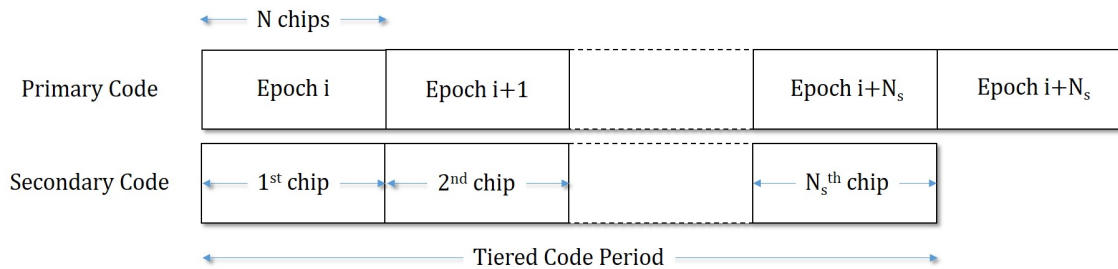


Figure 2.2 Galileo tiered code structure

2.3 GNSS modulations

As seen in table 2.2, several modulations are used by Galileo signals. Due to this thesis focuses on Galileo signals and especially in Galileo E5a signal, the modulation used in these bands are briefly presented in this section.

2.3.1 Binary Phase Shift Keying (BPSK) modulation

BPSK modulation is very important and useful in satellite navigation which was in fact the first one to be used for Satellite Navigation. A BPSK-modulated signal can be expressed as the convolution between a code part (including navigation data $D(t)$) and a modulation pulse ($p_{Tc}(t)$) as [60]:

$$s(t) = p_{T_c}(t) * \sum_{n=-\infty}^{+\infty} D_n \sum_{k=1}^{SF} c_{k,n} \delta(t - nT_{sym} - kT_c) \quad (2.1)$$

$$= s_{BPSK}(t) * s_{spread_data}(t) \quad (2.2)$$

$$D_n \in \{-1, +1\} \quad , \quad p_{T_c} = \begin{cases} 1 & \text{if } 0 < t < T_c \\ 0 & \text{otherwise} \end{cases} \quad (2.3)$$

where $*$ is the convolution operator, T_{sym} is the code symbol period, $c_{k,n}$ is the k -th chip corresponding to the n -th symbol, D_n is the n -th data symbol, $\delta(t)$ is the Dirac Pulse and T_c is the chip period that together with T_{sym} define SF which is the spread factor ($SF = T_{sym}/T_c$).

It is quite common in the literature to see BPSK(n). That means the code symbol rate ($1/T_{sym}$) is $n \times 1.023$ MHz. Galileo E6 CS will use a BPSK(5) modulation and also some receiver devices will operate with a BPSK(10) signal to acquire the Galileo E5 signal [4].

2.3.2 Binary Offset Carrier (BOC) modulation

This modulation is less known than the previous one. It was introduced by J.W. Betz for the GPS modernization program. BOC modulation is a square sub-carrier modulation, where the signal $s_{spread_data}(t)$ is multiplied by a rectangular waveform sub-carrier. This sub-carrier waveform is equal to the sign of a sine or a cosine waveform.

Whether a sine or a cosine form is used, a sine-phased BOC (SinBOC) or cosine-phased BOC (CosBOC) is generated respectively. A common way to refer to a BOC signal is BOC(m,n) where $m = f_{subcarr}/1.023$ and $n = f_c/1.023$ ($f_{subcarr}$ and f_c in MHz). As with the BPSK signal, Sin/CosBOC signal can be seen as the convolution between sub-carrier and a modulating waveform as follows:

$$s(t) = s_{Csin/cosBOC}(t) * \sum_{n=-\infty}^{+\infty} D_n \sum_{k=1}^{SF} c_{k,n} \delta(t - nT_{sym} - kT_c) \quad (2.4)$$

$$= s_{Csin/cosBOC}(t) * s_{spread_data}(t) \quad (2.5)$$

Where the rectangular waveform sub-carriers are:

$$\begin{cases} s_{C_{sinBOC}}(t) = \text{sign} \left[\sin \left(\frac{\Phi_{boc}\pi t}{T_c} \right) \right], 0 < t < T_c \\ s_{C_{cosBOC}}(t) = \text{sign} \left[\cos \left(\frac{\Phi_{boc}\pi t}{T_c} \right) \right], 0 < t < T_c \end{cases} \quad (2.6)$$

where $\text{sign}(\cdot)$ is the sign function and $\Phi_{boc} = 2f_{subcarr}/f_c = 2m/n$ must be an integer. The spectrum is divided into two parts due to the sub-carrier (figure 2.3). The mathematical expressions for Sin/CosBOC Power Spectral Density (PSD) can be found in [4].

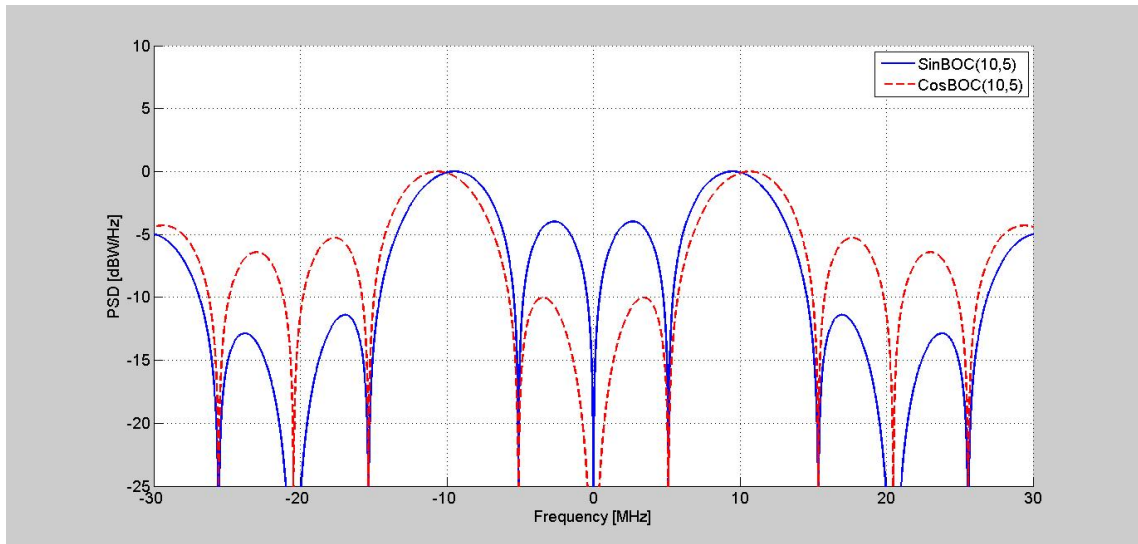


Figure 2.3 PSD of $\text{SinBOC}(10,5)$ and $\text{CosBOC}(10,5)$

2.3.3 Alternative Binary Offset Carrier (AltBOC) modulation

AltBOC modulation is quite similar to the BOC modulation. The main difference is that AltBOC has a high spectral isolation between the two upper main lobes and the two lower main lobes (if I and Q channels are considered independents). This is achieved by employing a different PRN code for each main lobe. Hence, it is possible to receive each lobe separately [4].

A complex sub-carrier was initially used to shift and not split up (as in BOC case) the spectrum to higher or lower frequencies. AltBOC signal can be seen as the multiplication of PRN codes and a complex sub-carrier:

$$s_{AltBOC}(t) = (s_{spread_data_L}^I + js_{spread_data_L}^Q)sc(t) + \quad (2.7)$$

$$(s_{spread_data_U}^I + js_{spread_data_U}^Q)sc^*(t) \quad (2.8)$$

Where $*$ is the conjugation operator, the subscripts L/U denote the low/up lobe and the superscripts I/Q denote the I/Q channel. $sc(t)$ is the complex sub-carrier that is as follow:

$$sc(t) = sign[\cos(2\pi f_{subcarr}t)] + jsign[\sin(2\pi f_{subcarr}t)] \quad (2.9)$$

However, the AltBOC signal defined above (which is the general case of the AltBOC modulation) lacks a constant envelope that the original BOC modulation possessed. Constant envelope is essential to avoid distortion problems in the satellite. The solution was to modify the signal as indicated in equation 2.10:

$$\begin{aligned} s_{AltBOC}(t) = & (s_{spread_dataL}^I + js_{spread_dataL}^Q) [sc_s(t) - js_c_s(t - \frac{T_s}{4})] \\ & + (s_{spread_dataU}^I + js_{spread_dataU}^Q) [sc_s(t) - js_c_s(t - \frac{T_s}{4})] \\ & + (\bar{s}_{spread_dataL}^I + j\bar{s}_{spread_dataL}^Q) [sc_p(t) - js_c_p(t - \frac{T_s}{4})] \\ & + (\bar{s}_{spread_dataU}^I + j\bar{s}_{spread_dataU}^Q) [sc_p(t) - js_c_p(t - \frac{T_s}{4})] \end{aligned} \quad (2.10)$$

Where the dashed signals are:

$$\bar{s}_{spread_dataL}^I = s_{spread_dataU}^I s_{spread_dataU}^Q s_{spread_dataL}^Q \quad (2.11)$$

$$\bar{s}_{spread_dataL}^Q = s_{spread_dataU}^I s_{spread_dataU}^I s_{spread_dataL}^I \quad (2.12)$$

$$\bar{s}_{spread_dataU}^I = s_{spread_dataL}^I s_{spread_dataL}^Q s_{spread_dataU}^Q \quad (2.13)$$

$$\bar{s}_{spread_dataU}^Q = s_{spread_dataL}^I s_{spread_dataL}^I s_{spread_dataU}^I \quad (2.14)$$

and the four-valued sub-carrier functions for the single signals and the product

signals respectively are:

$$\begin{aligned} s_{c_s}(t) = & \frac{1}{2}(\text{sign}[\cos(2\pi f_{\text{subcarr}}t)]) + \frac{\sqrt{2}}{4}(\text{sign}[\cos(2\pi f_{\text{subcarr}}t - \frac{\pi}{4})]) \\ & + \frac{\sqrt{2}}{4}(\text{sign}[\cos(2\pi f_{\text{subcarr}}t + \frac{\pi}{4})]) \end{aligned} \quad (2.15a)$$

$$\begin{aligned} s_{c_p}(t) = & \frac{1}{2}(\text{sign}[\cos(2\pi f_{\text{subcarr}}t)]) - \frac{\sqrt{2}}{4}(\text{sign}[\cos(2\pi f_{\text{subcarr}}t - \frac{\pi}{4})]) \\ & - \frac{\sqrt{2}}{4}(\text{sign}[\cos(2\pi f_{\text{subcarr}}t + \frac{\pi}{4})]) \end{aligned} \quad (2.15b)$$

Similarly, as in BPSK and BOC subsections, a common way to refer to an AltBOC signal is AltBOC(m,n). Figure 2.6 shows the AltBOC PSD. The following section focuses on Galileo E5 and the properties exhibited by this type of modulation.

2.4 E5 signals

The E5 Galileo band must be highlighted because its design and properties. It supplies a broadband signal with a nominal bandwidth around 90 MHz centered at 1191.795 MHz. (However, the authorized bandwidth is 51.15 MHz according to the Galileo SIS Interface Control Document [13]). The E5 signal makes use of a constant envelope AltBOC(15,10) modulation, in order to bring along four different spread signals ($e_{5a-I}(t)$, $e_{5a-Q}(t)$, $e_{5b-I}(t)$ and $e_{5b-Q}(t)$). The main advantage of this signal is providing a code-range noise incredibly low in comparison with the rest of the signals. Thanks to this particular modulation, a code-range measurements at the centimeter level and better mitigation of multipath effects can be carried out.

One of the features of E5 band is that the signal can be acquired in two ways: taking only one of side bands E5a or E5b, or processing the overall E5 signal. However, the major challenge is the receiver implementation, due to large E5 bandwidth and its complex demodulating scheme [23], [11].

Given all the aforementioned reasons, this thesis focuses on the E5 signal and also on some techniques to make it more robust. The most noteworthy characteristics are briefly described below.

2.4.1 E5 transmitted signal

Through AltBOC modulation mentioned above, a carrier signal is modulated by two navigation messages ($D_{E5a-I}(t)$, $D_{E5b-I}(t)$), four PRN codes ($C_{E5a-I}(t)$, $C_{E5a-Q}(t)$, $C_{E5b-I}(t)$, and $C_{E5b-Q}(t)$) and two complex square wave sub-carriers ($sc_s(t)$, $sc_p(t)$) through an AltBOC multiplexor (MUX). Figure 2.4 shows the block diagram of this modulation.

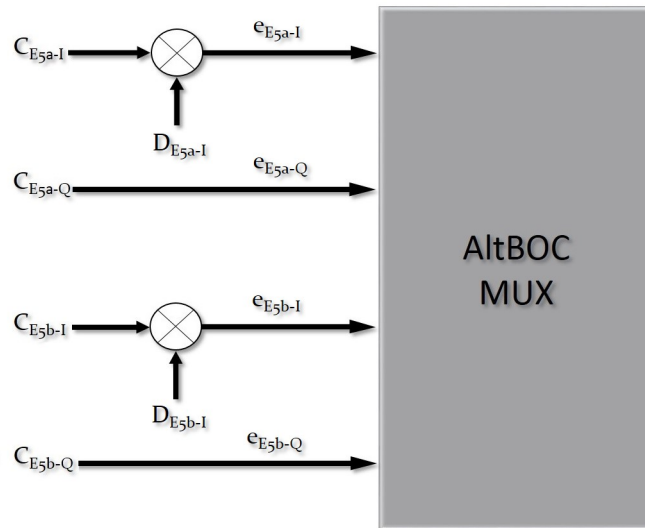


Figure 2.4 E5 modulation [52]

The expression of the band pass Galileo E5 transmitted signal can be depicted as:

$$S_{E5}(t) = \Re[s_{e5}(t) e^{j(2\pi f_{E5}t + \phi_0)}] \quad (2.16)$$

$$= \Re[s_{e5}(t)] \cos(2\pi f_{E5}t + \phi_0) - \Im[s_{e5}(t)] \sin(2\pi f_{E5}t + \phi_0) \quad (2.17)$$

where \Re is the real part operator, f_{E5} is the carrier frequency equal to 1191.795 MHz, ϕ_0 is the initial phase and $s_{E5}(t)$ is the complex envelope or baseband E5 signal that can be written as:

$$\begin{aligned}
s_{e5}(t) &= s_{e5-I}(t) + s_{e5-Q}(t) \\
&= (e_{5a-I}(t) + je_{5a-Q}(t)) [sc_s(t) - jsc_s(t - \frac{T_s}{4})] \\
&\quad + (e_{5b-I}(t) + je_{5b-Q}(t)) [sc_s(t) - jsc_s(t - \frac{T_s}{4})] \\
&\quad + (\bar{e}_{5a-I}(t) + j\bar{e}_{5a-Q}(t)) [sc_p(t) - jsc_p(t - \frac{T_s}{4})] \\
&\quad + (\bar{e}_{5b-I}(t) + j\bar{e}_{5b-Q}(t)) [sc_p(t) - jsc_p(t - \frac{T_s}{4})] \tag{2.18}
\end{aligned}$$

This expression comes from equation 2.10. For more information see Galileo SIS ICD and [52]. The complex square wave sub-carriers signal are responsible the constellation diagram of the E5 AltBOC complex envelope signal is like a 8-PSK (Phase-Shift Keying) modulation which is illustrated in figure 2.5.

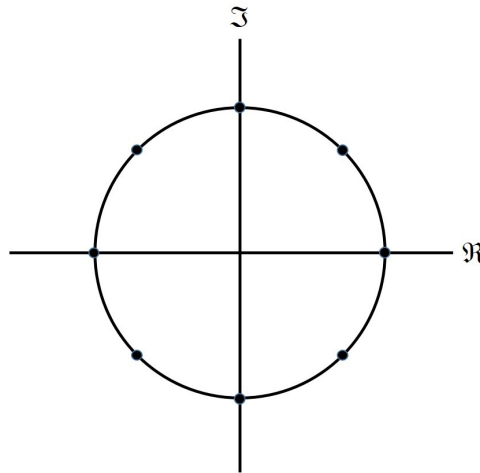


Figure 2.5 Constellation diagram of $s_{e5}(t)$

2.4.2 E5 Power Spectral Density (PSD)

As it was mentioned, the E5 signal is a constant envelope modulation. Its PSD is not a direct calculation, therefore if a detailed development is desired, see Rebeyrol and Macabiau (2005). The final mathematical expression for both constant (C) and non-constant (NC) envelope can be written as:

$$G_{AltBOC(m,n)}^C(f) = \frac{4f_c}{\pi^2 f^2} \frac{\cos^2\left(\frac{\pi f}{f_c}\right)}{\cos^2\left(\frac{\pi f}{2f_{subcarr}}\right)} + \left[\cos^2\left(\frac{\pi f}{2f_{subcarr}}\right) - \cos\left(\frac{\pi f}{2f_{subcarr}}\right) - 2 \cos\left(\frac{\pi f}{2f_{subcarr}}\right) \cos\left(\frac{\pi f}{4f_{subcarr}}\right) + 2 \right] \quad (2.19)$$

$$G_{AltBOC(m,n)}^{NC}(f) = 8f_c \left[\frac{\cos\left(\frac{\pi f}{f_c}\right)}{\pi f \cos\left(\frac{\pi f}{2f_{subcarr}}\right)} \right]^2 \left(1 - \cos\left(\frac{\pi f}{2f_{subcarr}}\right) \right) \quad (2.20)$$

where $f_{subcarr} = m \times 1.023 MHz$ is the sub-carrier frequency and $f_c = n \times 1.023 MHz$ is the chip frequency. Constant envelope AltBOC(15,10) is the modulation used by the E5 signal. Figure 2.6 shows the differences between the constant and non-constant envelope modulation AltBOC(15,10). The blue graph is the PDS of the E5 signal generated by the Simulink E5-Galileo simulator which is addressed in chapter 5. As it can be noted, the theoretical line and the simulated line are very similar.

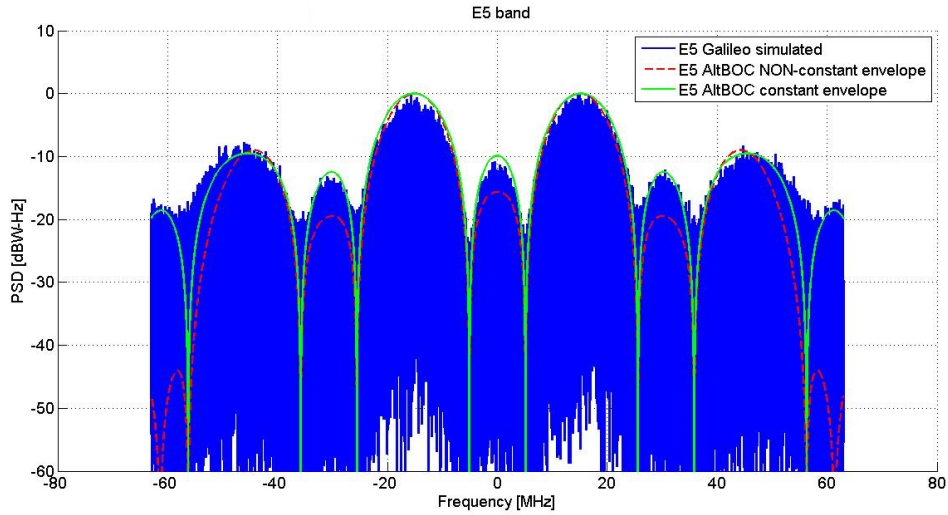


Figure 2.6 E5 Power Spectral Density

2.4.3 E5 Cross-Correlation Function (CCF)

The correlation function is the main key which makes possible to acquire and track every SIS from each SV. Before obtaining the PVT value, the receiver must know which signal belongs to each satellite, and to do this, the receiver uses the cross correlation function (CCF) value between incoming GNSS signal and a local replica (this process is explained in next section). PRN codes are not only different signal by signal, but also satellite by satellite. The property illustrated in picture 2.7 says: “The cross correlation function is very high if both range codes are equal, and very low if not” [39].

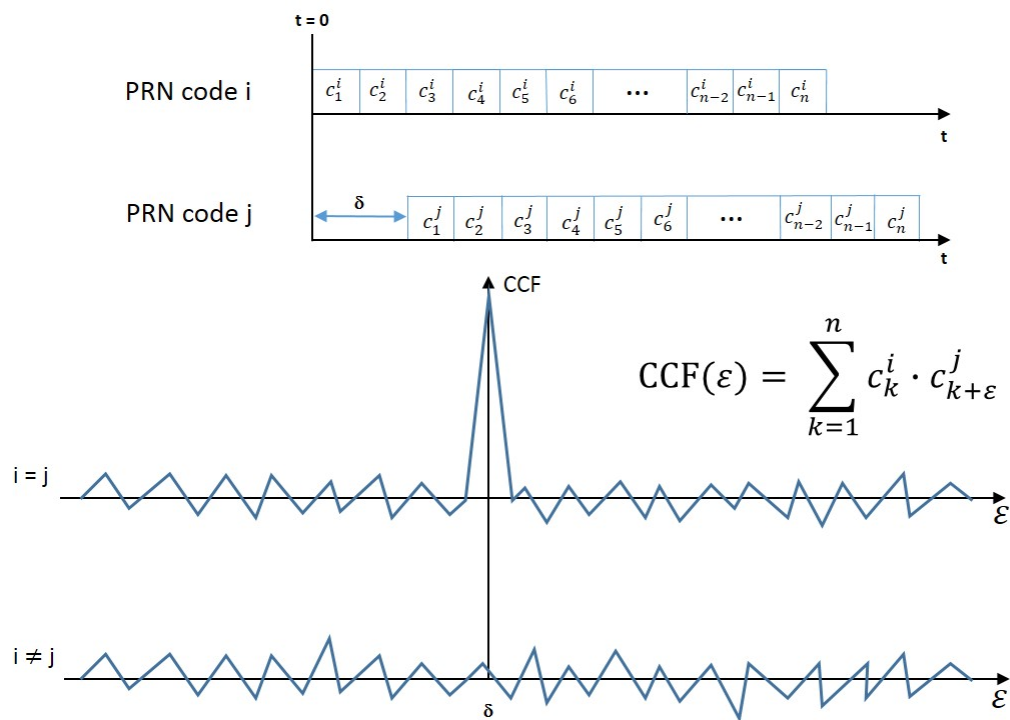


Figure 2.7 Auto-Correlation Function (upper plot) and cross-correlation function (lower plot)

2.4.4 E5 received signal and operating principles

The receiver correlates the incoming signal with one internal replica of each PRN code ($C(t)$), and thus, it obtains the **code delay**. The distances between every SV and receiver (called **pseudoranges**) are obtained by multiplying the code delay by the speed of light, as shown in figure 2.8. Also a frequency span is done to obtain the Doppler frequency due to the satellite and the receiver movement (**carrier phase**). To compute the receiver PVT by triangulation principles at least four pseudoranges

are need due to the clocks of satellites and receiver are not perfectly synchronized. Latitude, longitude, altitude and the clocks offset τ are the unknown parameters.

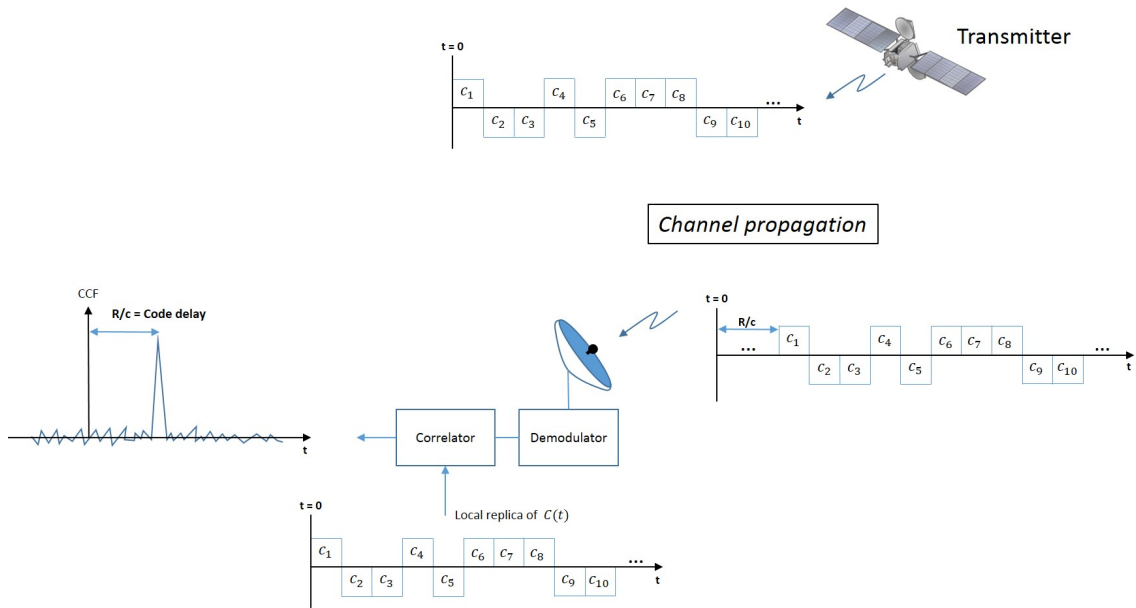


Figure 2.8 Code delay computation[35].

When the receiver knows the rough value of code delay and carrier phase (**acquisition process**), a **tracking process** is initiated to track one specific satellite and therefore demodulate the navigation data. With this navigation data the receiver is able to get its position (x_u, y_u, z_u) thank to these equations:

$$\left. \begin{aligned} \rho_1 &= \sqrt{(x_1 - x_u)^2 + (y_1 - y_u)^2 + (z_1 - z_u)^2} + \tau \cdot c \\ \rho_2 &= \sqrt{(x_2 - x_u)^2 + (y_2 - y_u)^2 + (z_2 - z_u)^2} + \tau \cdot c \\ \rho_3 &= \sqrt{(x_3 - x_u)^2 + (y_3 - y_u)^2 + (z_3 - z_u)^2} + \tau \cdot c \\ \rho_4 &= \sqrt{(x_4 - x_u)^2 + (y_4 - y_u)^2 + (z_4 - z_u)^2} + \tau \cdot c \end{aligned} \right\} \quad (2.21)$$

where ρ_i are the pseudoranges mentioned above, (x_i, y_i, z_i) are the coordinates of the i^{th} satellite and [39] [55].

3. ERROR SOURCES IN GALILEO

3.1 Overview

Now is the moment to talk about diverse error sources within a GNSS environment. The errors can be of two types, internal sources or external sources to the GNSS system.

Internal sources might include clock synchronism errors, internal noise of electronic equipment, instrumental delays or the Antenna Phase Center (APC) effect [24]. This errors are minimized in the design phase but not completely eliminated. By means of correction factors or additional calculations, these issues can be utterly suppressed.

External error are given by causes related to the signals propagating. The principal effects are caused by the atmosphere status and the characteristics of the local environment of the receiver. The most remarkable are the ionospheric and tropospheric delays, multipath errors and finally the interference signals.

- ***Ionospheric and tropospheric delays:*** The atmosphere of the Earth can be mainly divided in two parts:
 - Troposphere (between the surface and 40 km of altitude), whose main effect is a group delay on transmitted signal due to water vapor and the dry gases. This delay is not dependent on the frequency (dispersive media up to 15GHz) therefore, the only way to mitigate tropospheric delay is to use models and/or to estimate it from observational data [34].
 - Ionosphere layer (between 70 km and 900 km of altitude), which is the ionized part of the atmosphere due to the ultra rays from the sun. It induces a dispersive group delay that is several orders of magnitude larger than the troposphere delay. As this effect is inversely proportional to the square of frequency (dispersive media), dual-frequency receivers can eliminate it by a linear combination of code or carrier phase measurements

at different frequency values named *ionosphere-free* [25]. For single frequency receivers, mathematical models are available such as Klobuchar Ionospheric Model for GPS and NeQuick Ionospheric Model for Galileo. The GPS/Galileo satellites broadcast the parameters needed to run these ionospheric models [26].

- **Multipath error:** This is one of the most harmful error sources. Multipath occurs when the received signal arrives through several paths at the antenna because of the scattering, reflection or refraction of the signals against obstacles (e.g. buildings or trees). The propagation channel is a time and frequency selective channel and it may affect the phase and the code measurements. The receivers get several delayed replicas of the desired signal that can distort the CCF at the acquisition block and hence, an error is computed in the pseudorange measurement. Improving the antenna quality, making use of dual-frequency receivers or incorporate new correlation techniques like “narrow correlator spacing” are some solutions to reduce this problem [27].

- **Interference signals:** Another error source that can severely degrade or even completely block the system performance are the interference RF signals. On a simple way, interference can be defined as “*whatever signal, from whatever service, working in the same frequency as the satellite receiver and could annoy it*”. Undesired transmitted signals (with the same carrier frequency than the GNSS signals) are not only threatening, but also high level spurious or small leakages inside the GNSS bands. In the picture 2.1, is depicted to what extent different services from ARNS share the spectrum with the GPS/Galileo bands.

In radio-navigation satellite systems, the SV signals are received at the Earth with very little power (minimum power around -157 dBW for the E1 OS signals [13]) and thus a deep analysis about undesired signals and its effects has become more necessary. Although CDMA technique has a good process gain, alternative methods are required for medium and high interference level. Some of these methods are described in chapter 4.

There are various ways of classifying interferences. Taking account their spectral characteristics, e.g. the ratio between the bandwidth of the interference BW_{int} and the GNSS signal BW_{gnss} (Figure 3.1):

- *Wideband interferences*, when $BW_{int} \gg BW_{gnss}$, e.g. Ultra-Wideband (UWB) technology which transmits a huge amount of information with a very low power using a large bandwidth. Communications and sensors (e.g. wireless connection of computer peripherals, smart healthcare systems, high internet access and multimedia applications) and radars and imaging

systems (e.g. techniques that allow high penetration in a wide range of surfaces or high resolution and detectability) are some applications [45] [46]. Inter-system interferences between satellites from different GNSSs; or intra-system interferences between satellites from the same GNSS are other potential interference sources. The spectrum is becoming overwhelmed due to all satellite systems deployed.

- *Narrowband interferences*, when $BW_{int} \ll BW_{gnss}$, e.g. TV harmonics (real case can be found in [5]), inter-modulation products or signal from Very High Frequency (VHF) and Ultra High Frequency (UHF) stations. The narrowest interference is a simple tone also called Continuous Wave Interference (CWI) and it can have a severe impact on the acquisition and tracking process decreasing the received Signal to Interference and Noise Ratio (SINR).

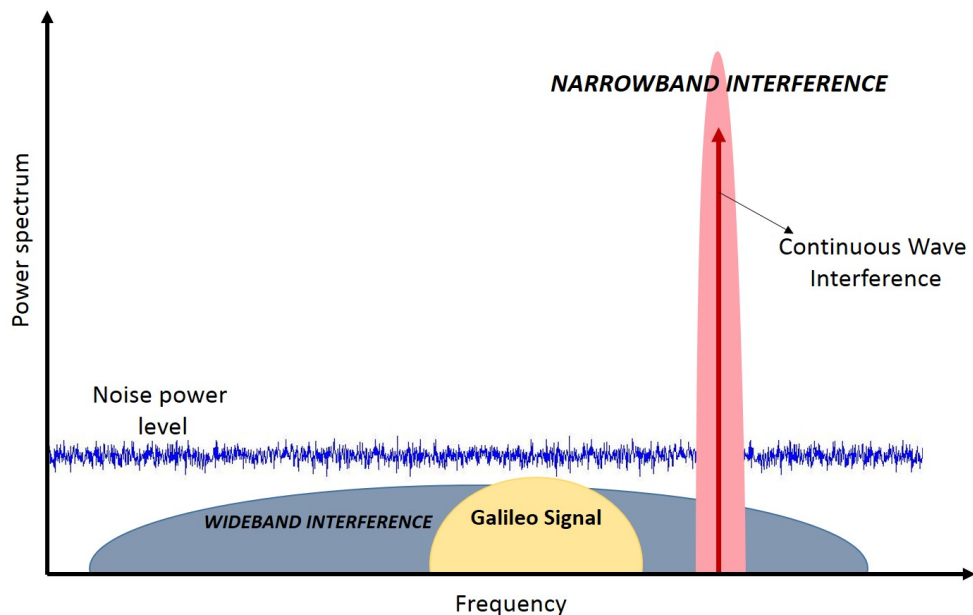


Figure 3.1 Wideband vs Narrowband spectra

Another classification criterion could be the purpose for which the interference source has been created:

- *Unintentional interferences*, There are many signals generated by systems such as Distance Measuring Equipment (DME) or tactical air navigation system (TACAN) which measures distance to a ground or ship-borne station by the

TOA of VHF or UHF radio signals. Also amateur radio, surveillance radars or wind profiler radars transmit in the same bands [50].

- *Intentional interferences* which in turn can be separated as [2]:
 - *Jamming signals* that deliberately block or interfere with authorized wireless communications through illegal devices decreasing the SINR. These illegal devices are quite cheap and their operating range is around 10 km. The user is aware that is unable to compute the PVT values.
 - *Spoofing signals*, which fake the SIS and may hack a hostile vehicle GNSS receiver. The purpose of spoofing is to catch on the tracking loop of the receiver deceived with an spoofing signal. Once this is accomplished, the PVT can be manipulated. The user is not aware that is being deceived.
 - *Meaconing signals*, which are the interception and rebroadcast of navigation signals. The deceived device takes the true GNSS signal and a delayed version of this. The strongest component is the acquired one. Also, the user is not conscious that is being duped.

3.2 Narrowband interferences models: CWI and DME/TACAN signals

As the thesis title indicates, special attention has been paid to narrowband interference rejection for Galileo. To do this, two interference signals have been simulated and studied. These are CWI and pulsed signals such as those generated by the DME or TACAN systems (from now on DME signals).

3.2.1 CWI signals

These signals can be just a pure tone (Figure 3.2) or a combination of pure tones given by the expressions:

$$j_{cwi}(t) = A \sin 2\pi \Delta f_{cwi} t + \phi_0 \quad (3.1)$$

where A is the amplitude, Δf_{cwi} is the frequency offset with respect to the GNSS frequency and ϕ_0 is the initial phase; and

$$j_{\Sigma cwi}(t) = \sum_{i=1}^N A_i \sin 2\pi \Delta f_{cwi,i} t + \phi_{0,i} \quad (3.2)$$

where N is the number of interference waves. Figure 3.2 shows the case $N = 1$.

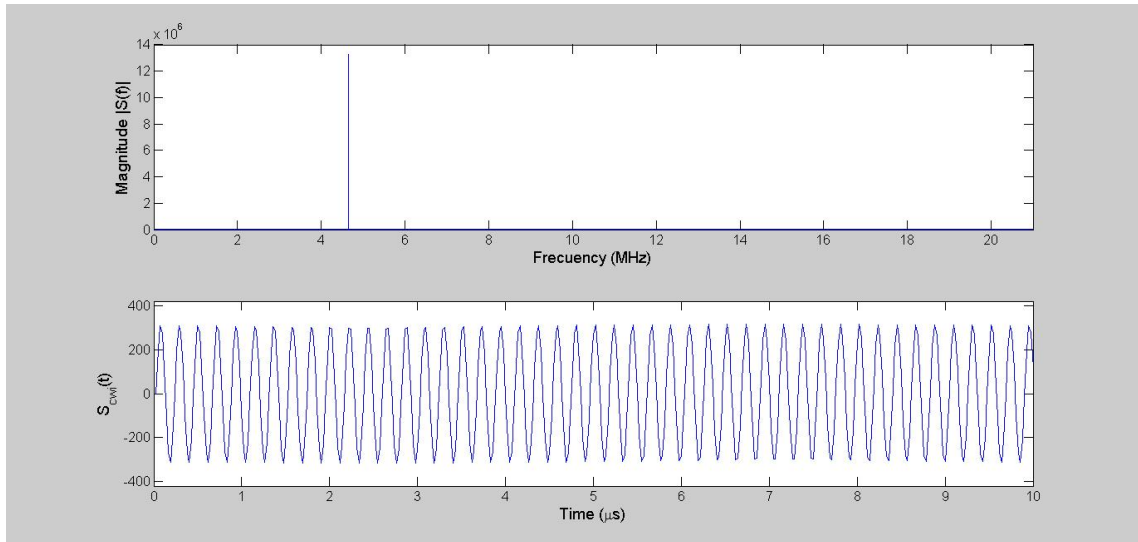


Figure 3.2 Continuous Wave Interference representation in frequency domain (upper plot) and time domain (lower plot).

Regarding to the possible damage caused by the CWI, the Low Noise Amplifier (LNA) or the Automatic Control Gain (ACG) can be saturated. Also the CCF may have associated positioning errors.

3.2.2 DME signals

Signals from air radio-navigation systems such as DME or TACAN, consist of Gaussian RF pulses paired $12 \mu s$ separated and each pulse lasts $3.5 \mu s$. Figures 3.3 and 3.4 show the time and frequency behavior at intermediate frequency ($f_{IF} = 12$ MHz). The maximum repetition rate is about 3000 pair of pulses per second (pps). DME systems are designed to provide service for 100 planes simultaneously. The power transmitted may vary from 50 W to 2kW. Finally, the Gaussian envelope is given by the next expression:

$$j_{dme-pair}(t) = A \left[e^{-\frac{\alpha}{2}(t-\frac{\Delta t}{2})^2} + e^{-\frac{\alpha}{2}(t+\frac{\Delta t}{2})^2} \right] \quad (3.3)$$

where $\alpha = 4.5 \times 10^{11} s^2$ controls the width of each pulse and $\Delta t = 12 \times 10^{-6}$ controls the time gap. The DME system frequency goes from 960 MHz to 1215 MHz, hence it is overlapped with the Galileo E5 band.

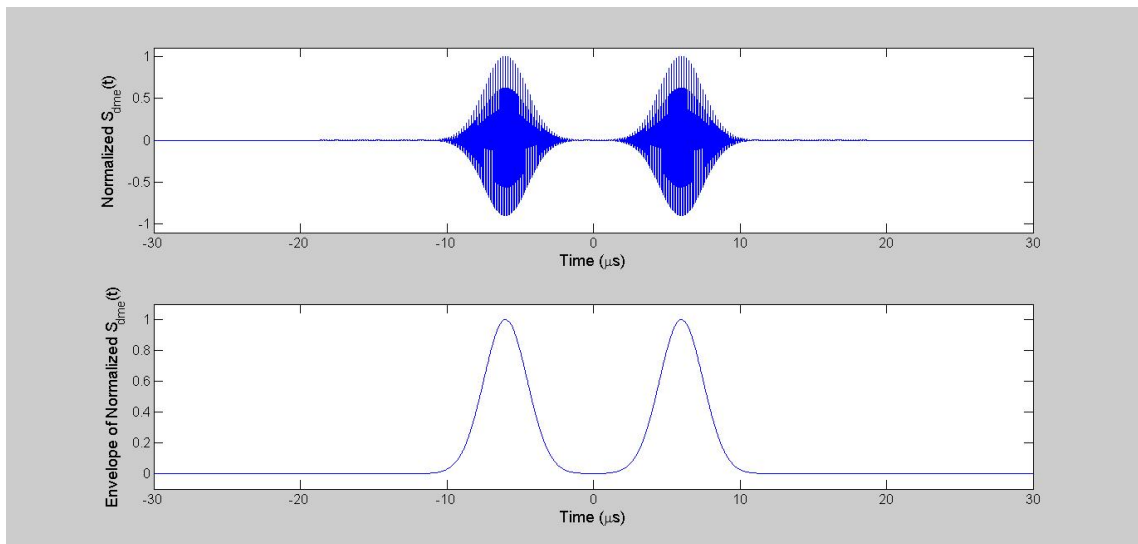


Figure 3.3 DME Interference representation. RF signal in time domain (Upper plot) and pulses envelope (lower plot).

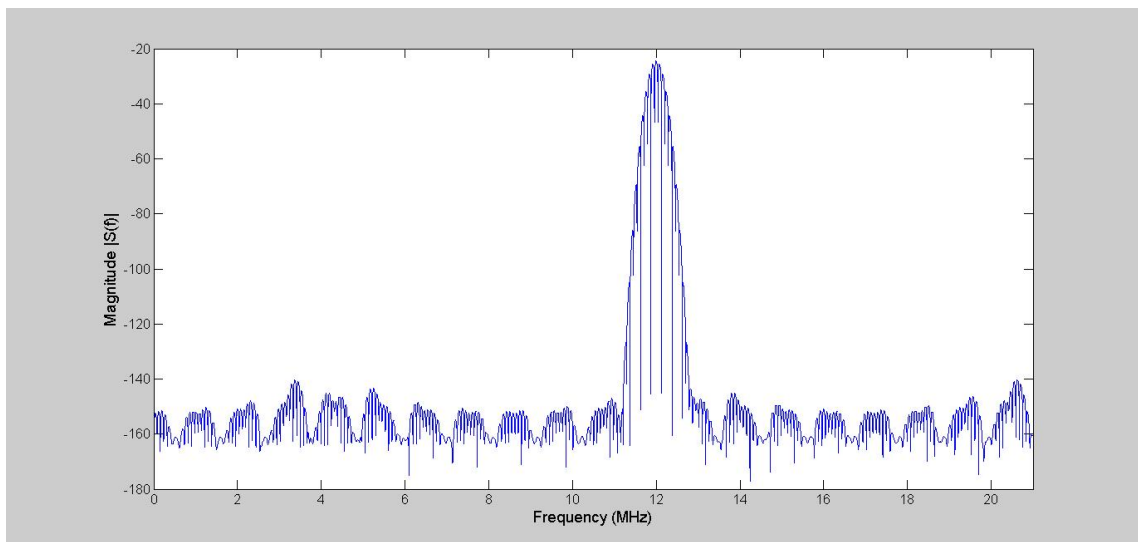


Figure 3.4 DME Interference representation in frequency domain.

4. NARROWBAND INTERFERENCE MITIGATION TECHNIQUES

All the approaches explained in this chapter are associated with both CWI and DME interferences signals mentioned in chapter 3. This approaches can be categorized in two groups: time-domain and frequency-domain techniques.

4.1 Time domain and frequency domain approaches

Time-domain mitigation techniques are those which make only use of mathematical calculation without any operation in frequency domain. Heavy computational loads area avoided and complexity is lower. Non-linear methods [47], filtering methods based on convolution operations [59] or blanking methods [17] are some of proposed approaches.

On the other hand, frequency-domain mitigation techniques are also widely presented in the literature. The zeroing technique [61] and a cyclostationary approach [48] can be found inside this group. Alternative methods based on wavelet transform have also been proposed [1], but their trade-off between complexity and performance is not as good as expected.

For the purpose of this study three mitigation techniques have been elected, zeroing method, adaptive notch filter method and pulse blanking method, to face up the interferences simulated. For the sake of clarification, figure 4.1 shows the system model used along the research and development process

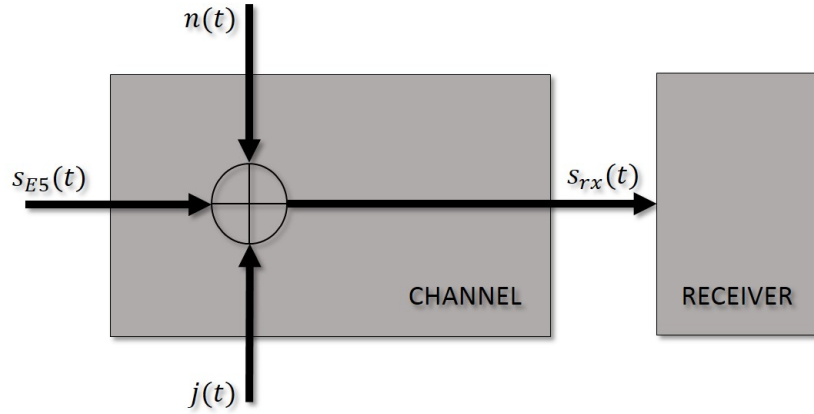


Figure 4.1 System model used.

where $n(t)$ is an additive Gaussian white noise with zero mean and two side PSD $N_0/2$ and $j(t)$ is the damaging signal.

4.1.1 Pulse blanking method

As a time-domain approach, the pulse blanking method does not need any computationally heavy operation. This is a simple method to implement which blanks the incoming signal that exceeds a certain threshold (figure 4.2). The threshold is chosen according to the mean value of the mean of the absolute value of the received signal ($s_{rx}(t)$).

$$Th_{blanking} = kE(|s_{rx}(t)|) \quad (4.1)$$

where $E(.)$ is the average operation and k is fixed at 3,5 for a good trade-off between removing as much DME pulses as possible and attenuate as little as possible the useful navigation signal.

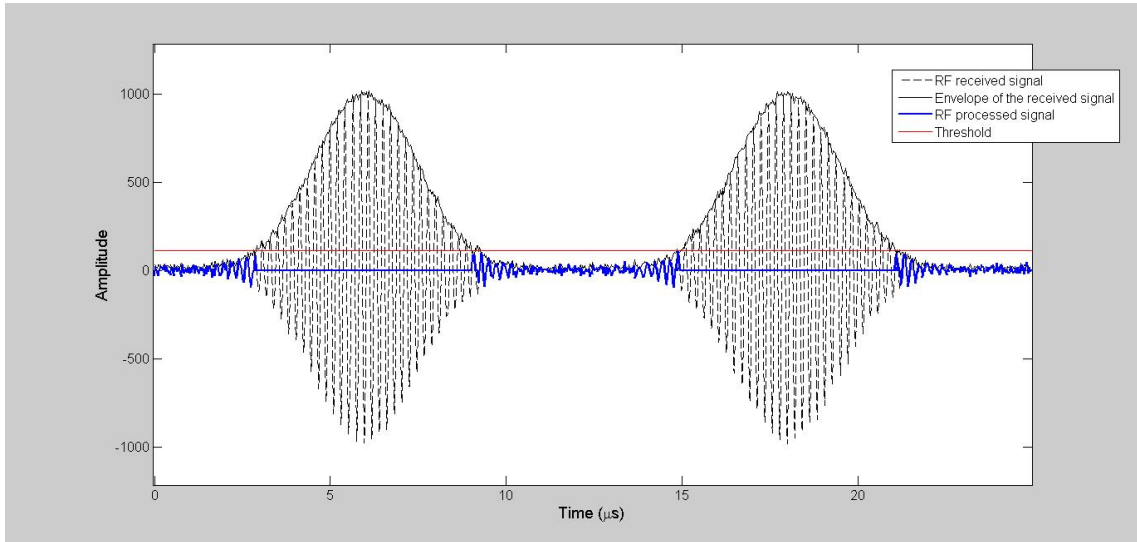


Figure 4.2 Pulse blanking performance in time domain.

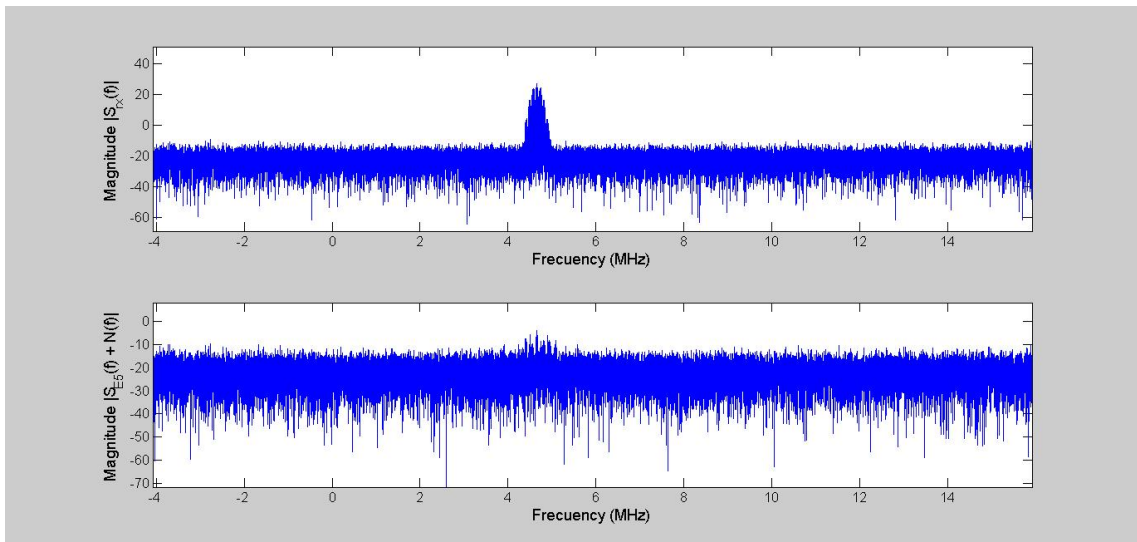


Figure 4.3 Pulse blanking performance in frequency domain. A DME interference is harming the GNSS signal in the upper plot and its blanking is showed in the lower plot.

As shown in figure 4.3 the pulse blanking can introduce a considerable improvement of around 20 dB of SINR gain. This method is quite effective but it does not eliminate the interference completely. Indeed, the remains of the Gaussian tails can be detected which persist even after processing. It is not effective against weak pulses due to the threshold can not be exceeded and the interference energy may sneak into the receiver decreasing the SINR value. Another remarkable drawback is that while the pulses are blanked, the GNSS signal is also removed. Therefore,

for a given environment with high pulse density, the performance decreases as the outcomes of chapter 6 show.

4.1.2 Zeroing method

A Fast Fourier Transform (FFT) based method is also assessed. As the simulator presented in chapter 5 process the signal in time blocks this method can be an adequate technique. The number of samples per block is $N = f_{sample} \times 1ms$. The Discrete Fourier Transform (DFT) of each block can be presented by:

$$S_{rx}[k] = \sum_{n=0}^{N-1} s_{rx}[n] e^{-j \frac{2\pi}{N} kn}; \quad k = 0, \dots, N - 1 \quad (4.2)$$

where $s_{rx}[n]$ is the GNSS sampled signal and N is the number of points the DFT has.

This is a more complex approach because of the FFT algorithm operations but also more effective than the previous one in terms of energy leaked. Narrowband interferences can be rejected just zeroing the spectral samples above certain threshold. This time, the threshold is obtained according to the mean and the variance of the absolute value of $S_{rx}[k]$ as shown in equation 4.3.

$$Th_{zeroing} = E(|S_{rx}[k]|) + \alpha Var(|S_{rx}[k]|) \quad (4.3)$$

where $Var(.)$ is the variance operator and α is the factor to adjust the threshold over the noise. In this thesis $\alpha = 0.5$. There is an alternative of this method in which instead of zeroing, the samples (also in frequency domain) are given a predefined value to avoid fast amplitude transitions in the spectrum [48].

Figure 4.4 shows an important enhancement in frequency domain before and after using the zeroing method. It removes completely the CWI. Also the time domain is presented in figure 4.5 but the upgrade is less obvious. It works also when several CWI are present.

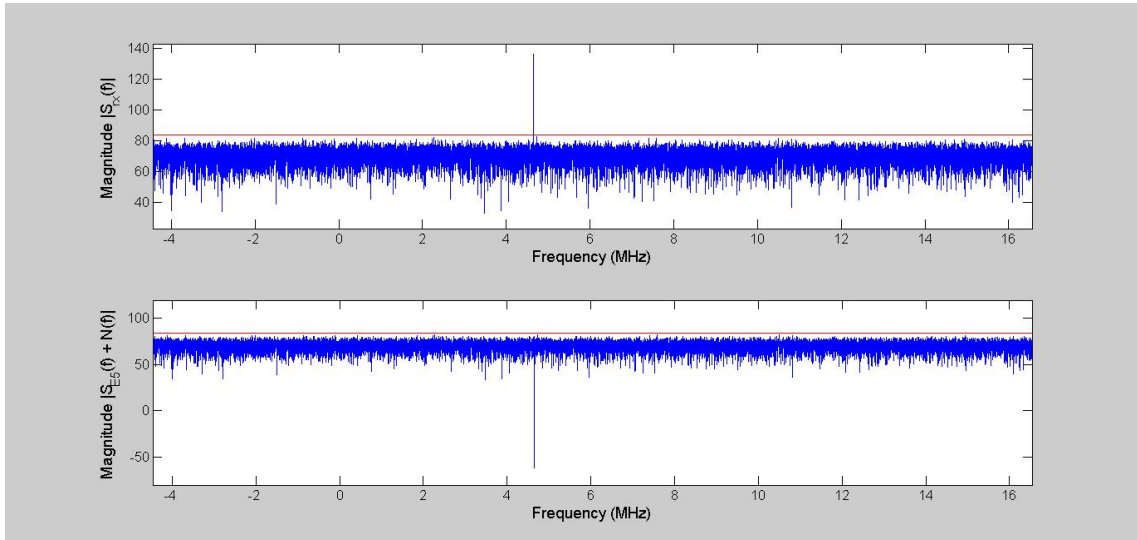


Figure 4.4 Zeroing performance in frequency domain. A CWI interference is harming the GNSS signal in the upper plot and its zeroing samples are showed in the lower plot.

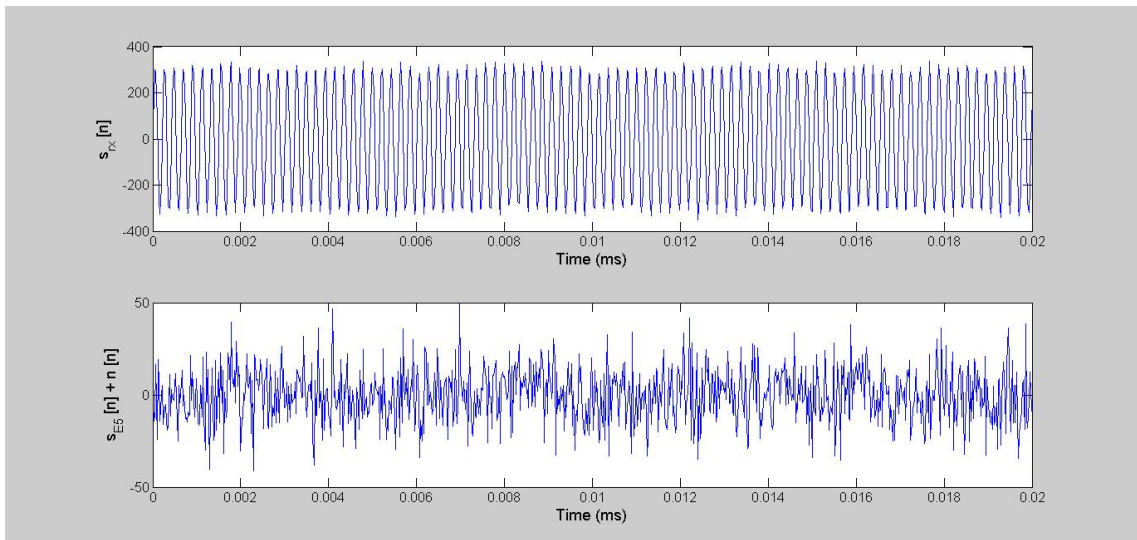


Figure 4.5 Zeroing performance in time domain against one CWI. The contaminated GNSS signal in the upper plot and the cleaned GNSS signal in the lower plot.

Unlike blanking approach, this method can be used for both CWI and DME interferences. However, it is less effective than blanking method against DME interference. The spread of the spectrum due to the steep variation in time domain makes more difficult to separate the useful signal from DME signal. Some energy from DME pulses remains after the zeroing method as shown in figures 4.6 and 4.7.

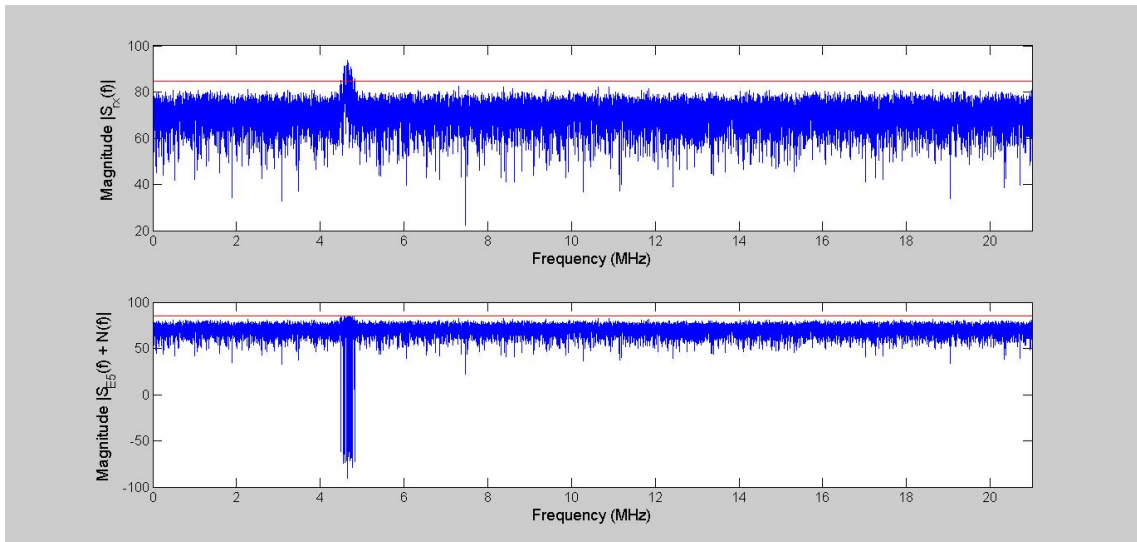


Figure 4.6 Zeroing performance in frequency domain against DME pulses. The contaminated GNSS signal in the upper plot and the cleaned GNSS signal in the lower plot.

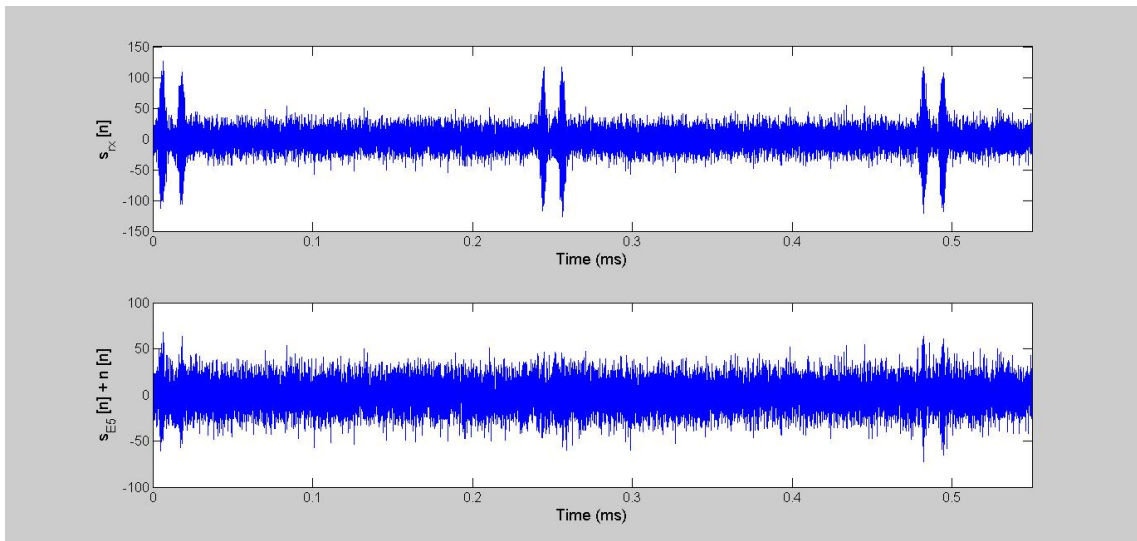


Figure 4.7 Zeroing performance in time domain against DME pulses. The contaminated GNSS signal in the upper plot and the cleaned GNSS signal in the lower plot.

4.1.3 Dynamic notch filtering method

The last studied method was implemented with a second order infinite impulse response (IIR) notch filter, which is a band-stop filter with a narrow stop band [59]. Its transfer function in Z-domain is shown at figure 4.8 and it is given by:

$$H_{Notch}(z) = \frac{1 + \alpha}{2} \frac{1 - 2\beta z^{-1} + z^{-2}}{1 - \beta(1 + \alpha)z^{-1} + \alpha z^{-2}} \quad (4.4)$$

where α and β can be expressed as:

$$\alpha = \frac{1 - \tan(BW_{-3dB}/2)}{1 + \tan(BW_{-3dB}/2)} \quad \beta = \cos(\omega_N); \quad \omega \in [0\pi] \quad (4.5)$$

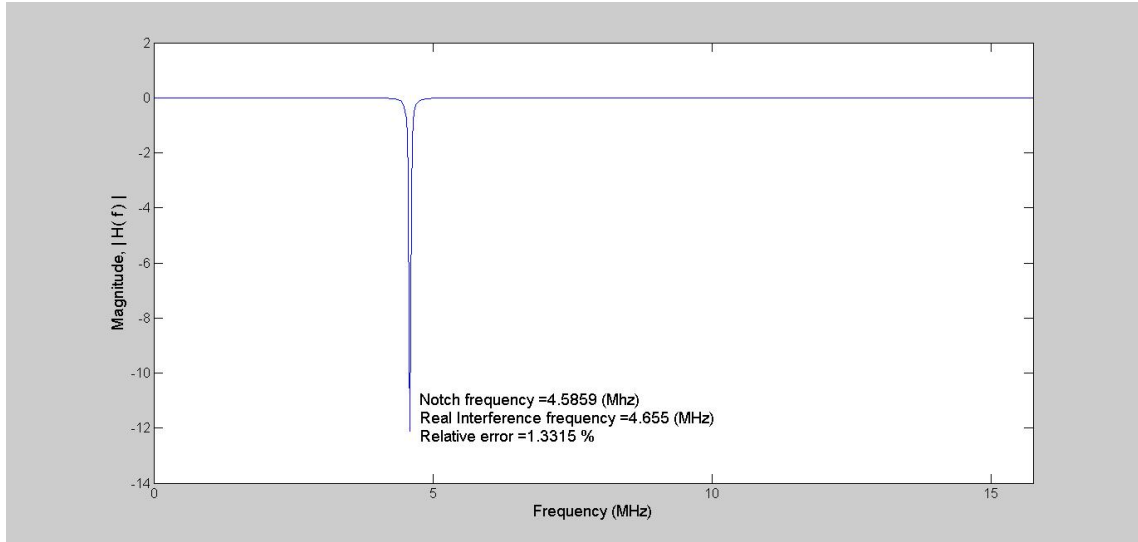


Figure 4.8 Second order IIR notch filter transfer function.

We note that the filter -3 dB bandwidth (BW_{-3dB}) is controlled by α and the central frequency by β . These parameters are independent of each other. As it can be seen in [48], $\alpha = 0.989$ to minimize the attenuation of the GNSS signal. A block diagram is depicted in figure 4.9 to better understand this recursive model called *the minimum power method* [48].

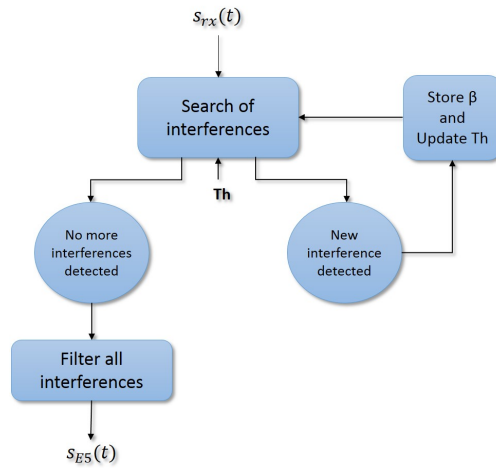


Figure 4.9 Block diagram of the dynamic notch filtering method.

First, the incoming signal is filtered overall the spectrum by giving to β successive values between $[-1, 1]$. For each output its mean power are stored. When all mean power values are calculated, the method is able to depict a picture as figure 4.10. This image shows the mean power for every frequency and each peak represents the frequency of one interference. When the central frequency of the filter matches with the frequency of one interference the mean power of the output signal decrease considerably. If one of these peaks are lower than a certain threshold according to the mean power, hence an interference is declared and its β value is stored. Finally, when no more interferences are detected, the notch filter uses the storage and removes all the harming signals.

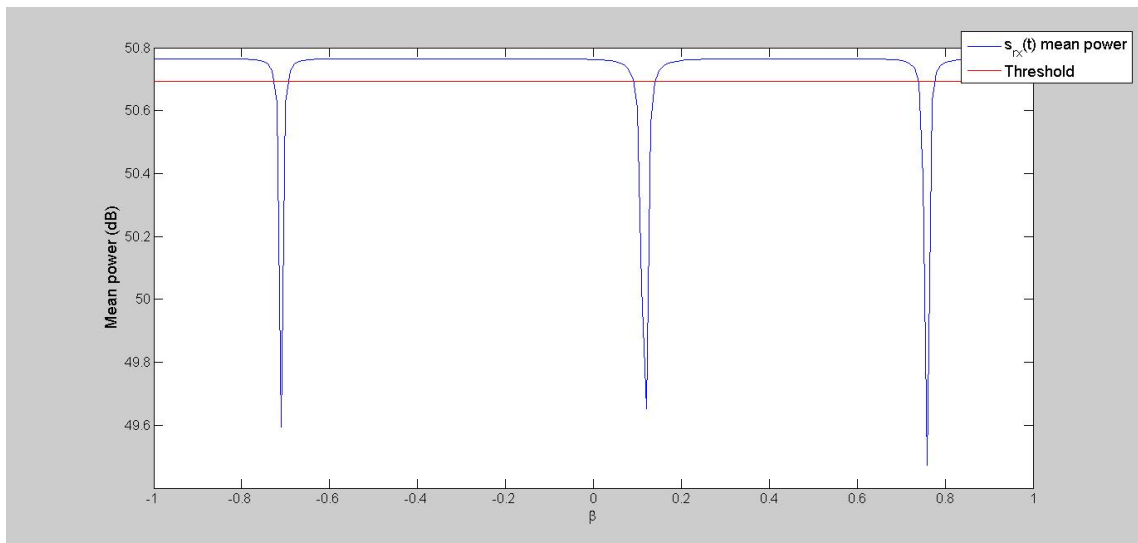


Figure 4.10 $s_{rx}(t)$ mean power in the presence of three CWIs.

This is considered a time approach because it does not require FFT block. The computational load would be very low if the filter had a fixed central frequency but, due to the search over the frequency range, the time increases considerably. From another point of view this drawback can be seen as an advantage since the filter only works when a CWI is declared and hence, the GNSS signal is not always suppressed. This method is suitable for both CWI and DME interference and it is able to deal with more than one interference at the same time but, again the time is an obstacle, even more for DME pulses. In the following figures an improvement between 30 and 40 dB is illustrated against both interferences.

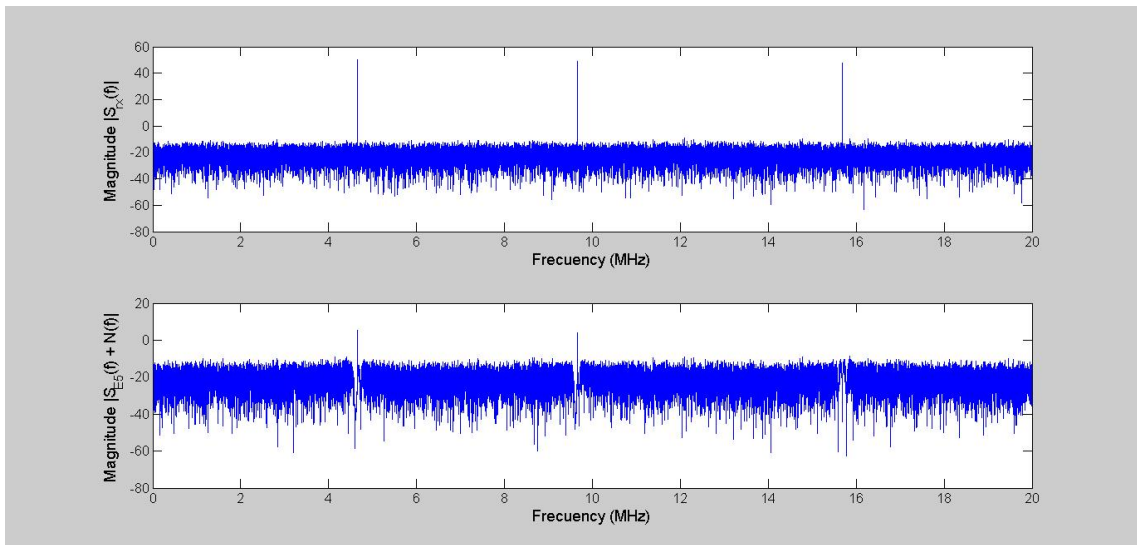


Figure 4.11 Notch performance in frequency domain against three CWIs. The contaminated GNSS signal in the upper plot and the cleaned GNSS signal in the lower plot.

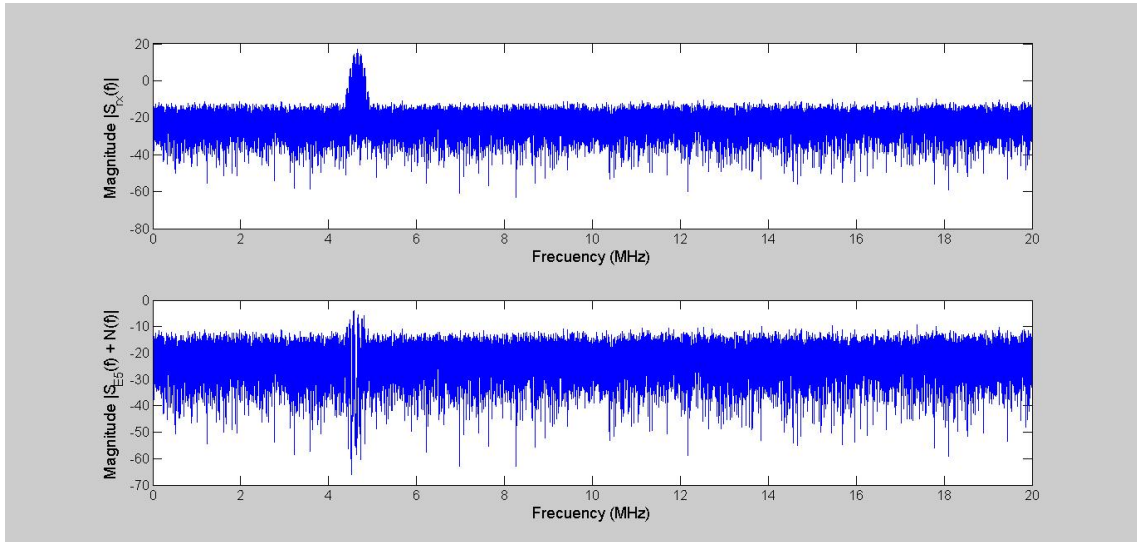


Figure 4.12 Notch performance in frequency domain against DME pulses. The contaminated GNSS signal in the upper plot and the cleaned GNSS signal in the lower plot.

4.2 Comparative notes

The table 4.1 shows the strengths and weaknesses of each solution.

Table 4.1 Comparative table between the method described along the chapter.

Method	Suitable for CWI	Suitable for DME	Computational load	Time required	Power cancellation (dB) ***
Blanking	✗	✓	low	low	≈25
Zeroing	✓	✗	moderate	moderate	Inversely proportional to the SINR value.
Dynamic Notch Filtering	✓	✓	high *	high **	25 - 40

* The operations are in themselves very fast.

** High run time due to the frequency sweep.

*** The difference between the spectral maximum of the contaminated signal (dB) and the spectral maximum of the cleaned signal (dB).

5. SIMULINK-BASED ALGORITHMIC IMPLEMENTATION

Simulation process helps to represent, research and assess future production models prior to implementing them. In the cases of GNSS systems, simulators are an essential part because unexpected situations hardly can be corrected if they have not been taken into account. Low deployment costs, flexibility and big ability to control many scenarios and process a huge amount of data make simulators an indispensable tool.

There are some developed GNSS simulators such as GNSS-Lab Tool (gLAB)[51], SX3 multi-GNSS software receiver[20] or GRANADA (Galileo Receiver ANALysis and Design Application) Bit-True Software Receiver simulator[28]. The model which is thoroughly described in this thesis is the E5 Galileo simulator (hereinafter called ***GE5-TUT***) which is a Simulink-based model from Technical University of Tampere (TUT), Finland.

The GE5-TUT model was initiated in 2009 within the Galileo Ready Advanced Mass Market Receiver (GRAMMAR) project[10]. It has since evolved with the incorporation of new blocks and features. This thesis represents the continuation of GE5-TUT which consisted of three blocks: transmitter, propagation channel and receiver block. Currently, two more blocks have been added, namely the interference generator and mitigation techniques block to assess the impact of multipath and interference situations. The end-to-end block diagram of GE5-TUT is depicted in figure 5.1 and its main blocks are described deeply in the next sections.

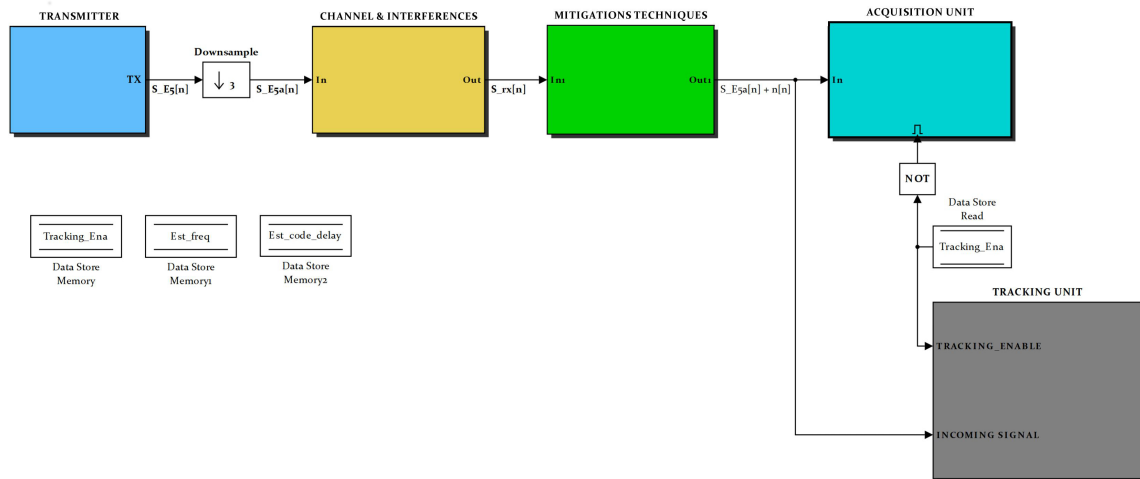


Figure 5.1 End-to-end Galileo E5 signal simulator block diagram.

5.1 Transmitter

Figure 5.2 shows how the transmitter is implemented. As discussed in chapter 2, the transmitted signal is implemented based on AltBOC(15,10) modulation following the scheme depicted in figure 2.4. It was said that E5 signal can be described as an 8-PSK. The idea is to allocate any of the 4 codes ($e_{5a-I}(t)$, $e_{5a-Q}(t)$, $e_{5b-I}(t)$ and $e_{5b-Q}(t)$) and 8 sub-carrier phases combinations to a phase state in the constellation, using a look-up table. These 4 codes (+1 or -1) lead to $2^4 = 16$ code combinations and the two complex square wave sub-carriers have 8 values per period. As the 8-PSK depends also on time, the time is partitioned first in sub-carrier intervals $T_{sc,E5}$ and further sub-divided in 8 equal sub-periods. That is why the look-up table dimensions are 16×8 . For more information one could read the Galileo SIS ICD [13]. The look-up table enables the generation of the I and Q signals before the digital-to-analog conversion.

The frequency of these sub-carriers is $f_{subcarr} = 15 \times 1.023 \text{ MHz} = 15.345 \text{ MHz}$. Thus, E5a signal is allocated at $f_{E5} - f_{subcarr} = 1176.45 \text{ MHz}$ and E5b signal is allocated at $f_{E5} + f_{subcarr} = 1207.14 \text{ MHz}$. The chip rate is $f_c = 10.23 \text{ MHz}$ and the PRN codes are stored in memory (See table 2.2). The navigation data is a random sequence of $-1sand + 1s$. Finally, the signal is moved to intermediate frequency (IF) f_{IF} to be transmitted. Currently, f_{IF} is set to 20 MHz.

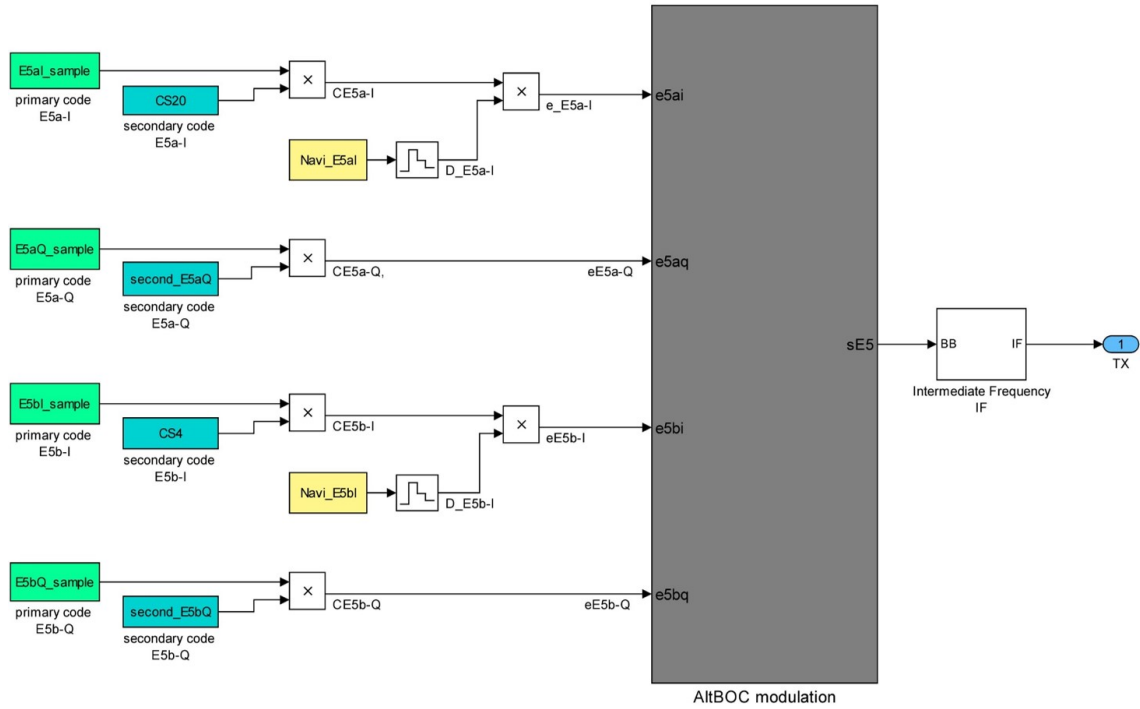


Figure 5.2 Transmitter block diagram.

Downsampling from Galileo E5 to Galileo E5a

Regarding to the main characteristics of the AltBOC modulation commented in section 2.4, the E5 signal can be considered as two QPSK signals because each side band can be acquired independently (*single side-band acquisition*). Hence a down-sample process by a factor of K is suitable to save computational burden due to the useful information is only in one side-band (the E5a signal in this case). Its bandwidth is much narrower ($BW_{E5a} = 20.46$ MHz) than the full E5 signal ($BW_{E5} > 50$ MHz).

If the full Galileo E5 signal is intended to be acquired, the sample rate (f_{sample}) may be at least 100 MHz to satisfy the Nyquist-Shannon sampling theorem (right now, the whole E5 signal is sampled with $f_{sample} = 126$ MHz). Therefore, to acquire just the E5a band (single side-band acquisition), with $K = 4$ the E5a sample rate would be equal to $126/4 = 31.5$ MHz without losing useful information. Figure 5.3 shows the power spectral density addressed in section 2.4.2 whether a down-sample is done or not.

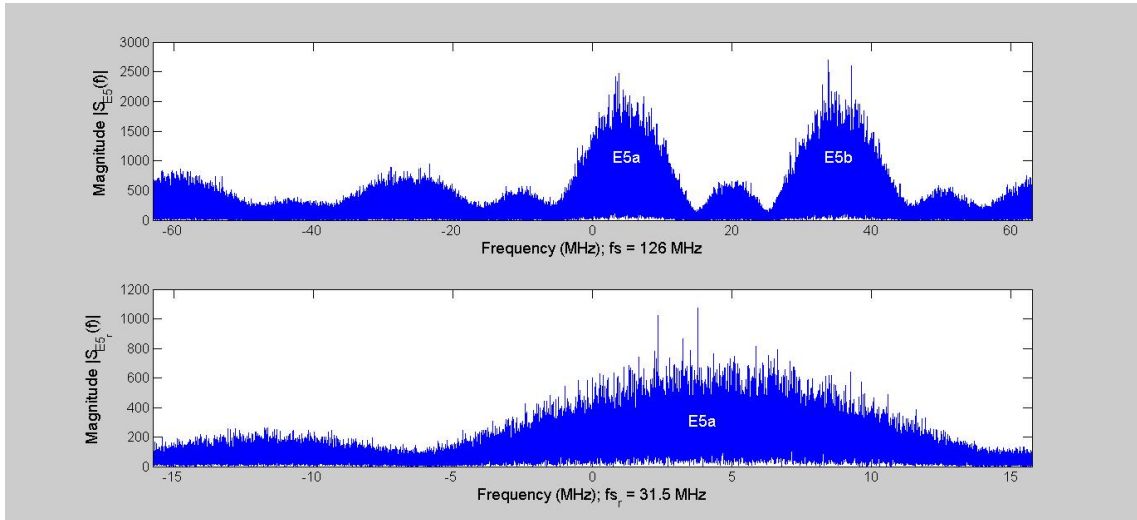


Figure 5.3 Above, the PSD before down-sample. Below, the PSD after down-sample. The x axis bounds are between $-f_{sample}/2$ and $f_{sample}/2$ due to the Matlab FFT representation. In the upper plot $f_{sample} = 126MHz$ and in the lower plot $f_{sample} = 31.5MHz$

As the PSD function is the Fourier transform of the Auto-Correlation Function (ACF), the shape of this function is also different whether the whole E5 signal is acquired or other components of the E5 signal such as the E5 pilot, the E5 data signals or one of the separated bands (E5a or E5b) [52]. In this thesis, the signal is acquired only through the E5a signal in a BPSK-like manner, similarly to a current GPS receiver. The real part and the absolute value of the ACF of both E5 and E5a signal are depicted in figure 5.4 and figure 5.5 respectively. As it can be appreciated, the E5a signal is free from the sub-carriers influence given rise to a triangular shape (as if it was a BPSK signal ACF).

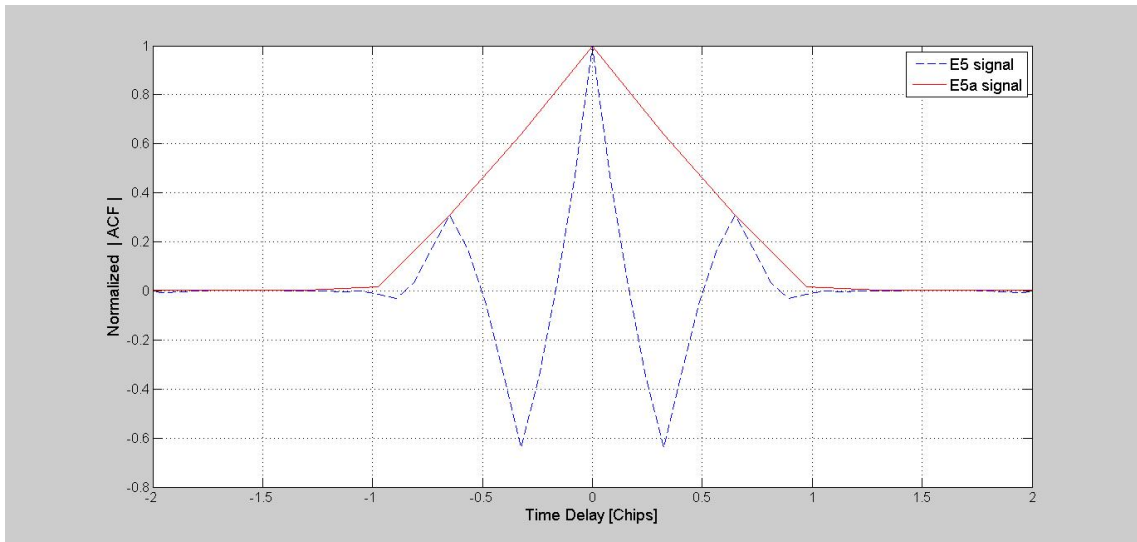


Figure 5.4 Comparison between the real part of the E5 and E5a normalized ACF.

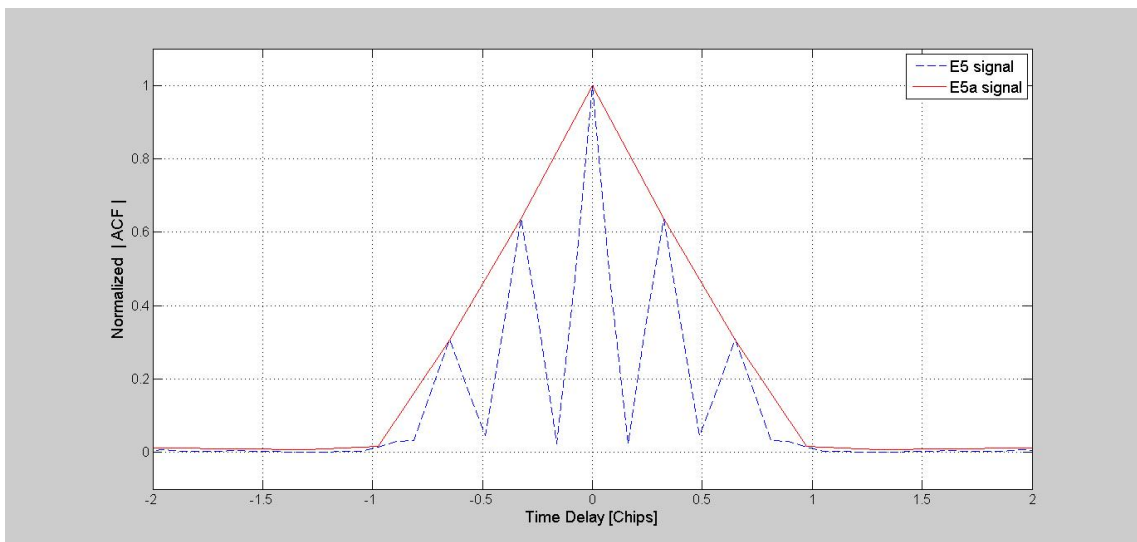


Figure 5.5 Comparison between the absolute value of the E5 and E5a normalized ACF.

5.2 Channel & interferences

The channel and interferences block are responsible for generating the multipath error, noise and interference signals. Figure 5.6 is a snapshot of this block. This subsystem depends on several parameters entered manually by the user at the beginning of the simulation (pop-up menu). The initial menu and its parameters are explained at the end of this chapter.

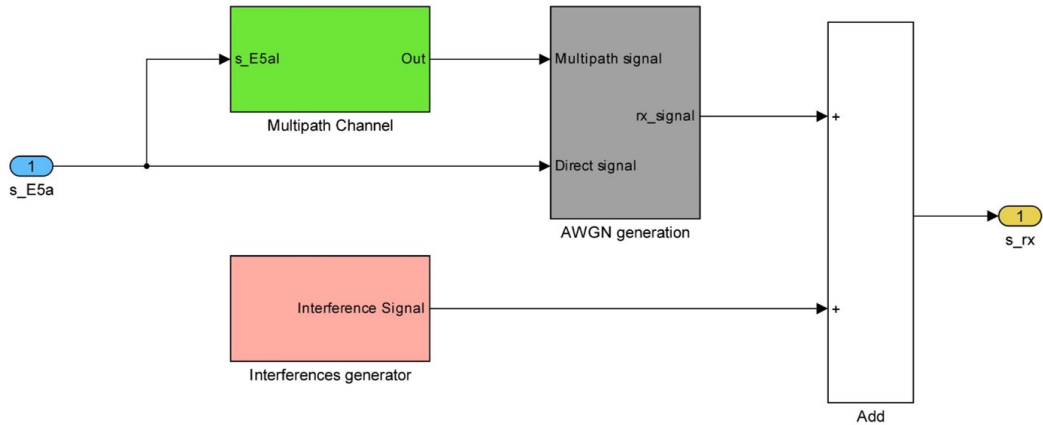


Figure 5.6 Channel and interferences block diagram.

- **Multipath delay:** the user is able to set two types of multipath models, *static* or *time variant* model. The *static channel* is modeled by the expression:

$$s_{out}(t) = \sum_{i=1}^N \alpha_i s_{E5}(t - \tau_i) \quad (5.1)$$

where N is the number of electromagnetic paths (currently $N = 5$ and $i = 1$ represents the line-of-sight propagation) and α_i and τ_i are the path complex gain (real in this case) and path delay for the i -th path.

On the other hand, *time variant channel* include the *multipath induced fading* effect which is the attenuation affecting a signal over the channel that may vary depending on time, position or frequency [8]. The fading effect is often modeled as a random process. The process used by GE5-TUT is the *Rayleigh fading* based on a Land and Mobile Multipath Channel Model from DLR [33].

For the sake of simplicity, this thesis has been written using only the multipath static model. The ACF provides the necessary information to know the delay experienced by the GNSS signal in each path. Figure 5.7 represents the E5a signal along three different paths. The most direct path has 2 chips of delay whilst the other two have 25 and 85 chips. The gain of each path is also modified with 0 dB, -3 dB and -6 respectively.

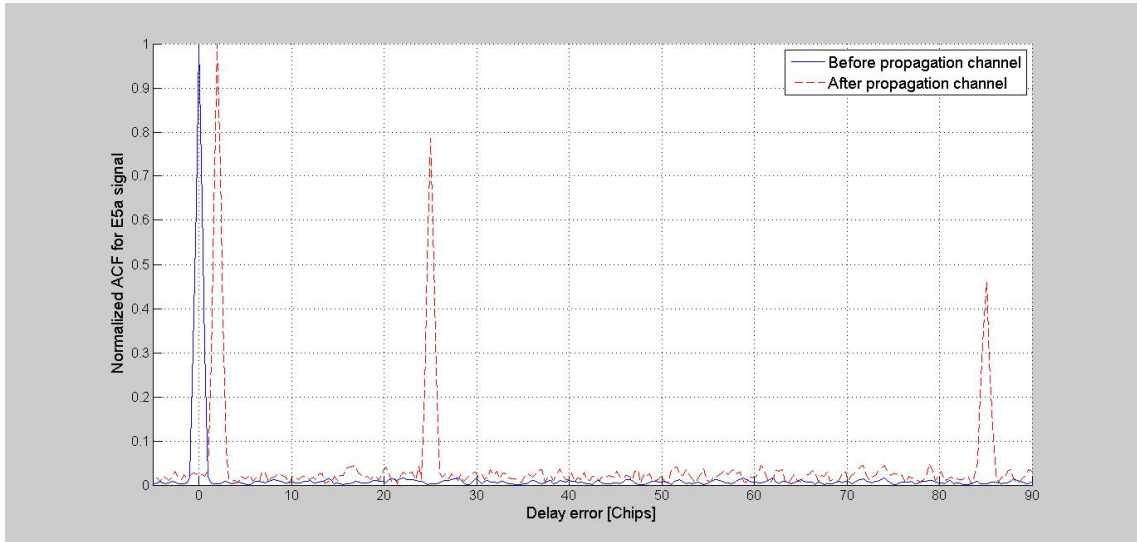


Figure 5.7 E5a ACF before and after the multipath block. Array for multipath delay = [2 25 85] chip, Array for multipath gain = [0 -3 -6] dB.

- **Gaussian noise:** It is modeled as an Additive white Gaussian noise (AWGN). This is a random processes that has a uniform power spectral density N_0 (expressed as watts per hertz). It also has a zero mean normal distribution and a variance depending on the user-defined Carrier-to-Noise-density Ratio (C/N_0) in dB/Hz, given by the expression [38] [30] [19]:

$$\sigma_{noise} = 10^{-SNR/20} \quad (5.2)$$

where,

$$SNR = C/N_0 - 10\log_{10}(BW) - 10\log_{10}(10230 * f_{sample}/f_{chip}) \quad (5.3)$$

- SNR (signal-to-noise ratio) is the RMS (root mean square) signal level divided by the RMS noise level expressed in dB.
- BW is the noise equivalent bandwidth of the last filter stage in the RF front-end of the receiver in Hz. 30KHz is the value assumed.
- The factor $10230 * f_{sample}/f_{chip}$ is included to add the noise at sample level after the correlator in the acquisition process, which works millisecond by millisecond. In one millisecond there are 10230 chips and the simulator computes f_{sample}/f_{chip} samples per chip. In order to a better appreciation figure 5.8 shows the whole Galileo E5 PSD before and after the noise addition.

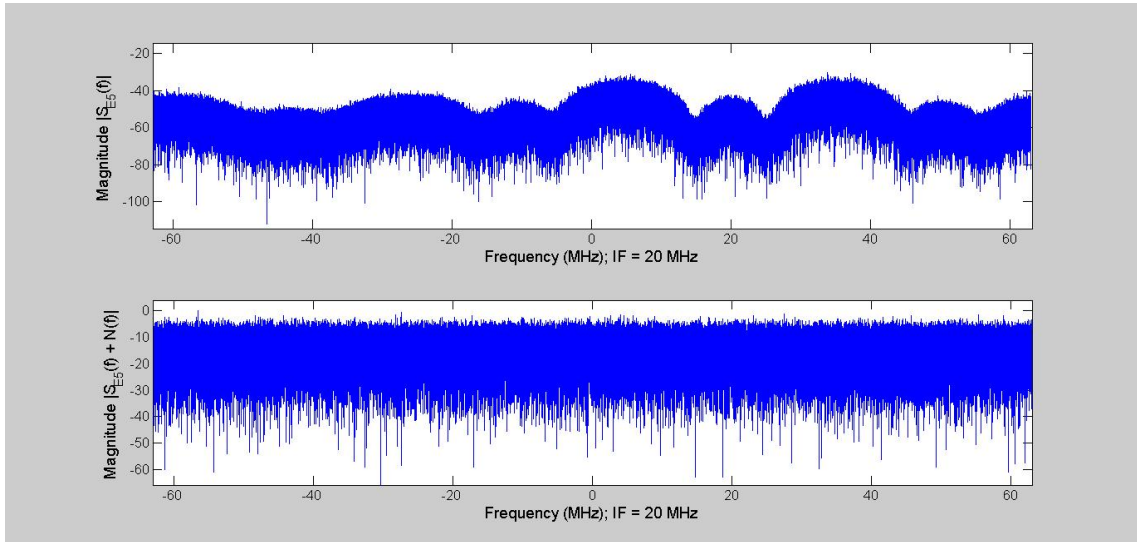


Figure 5.8 Galileo E5 signal PSD before (upper plot) vs after (lower plot) the noise addition block. No multipath effect is considered.

- **Interference signals:**

The interference generator block is one of the major contributions of this thesis to the GE5-TUT. In figure 5.9 one can appreciate that through the control flag called *ID_Type_Interference* the user is able to select the desired harming signals described in section 3.2.

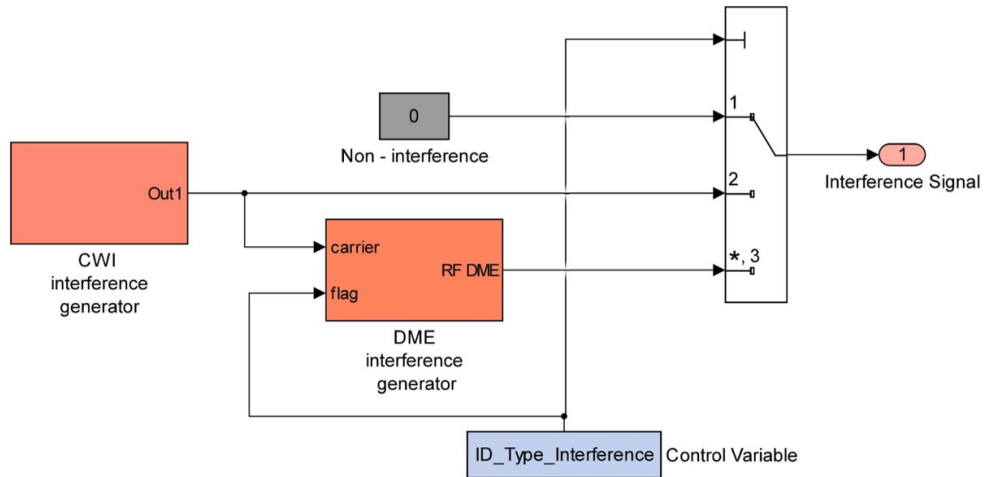


Figure 5.9 Interferences block diagram.

The signal used to generate CWIs is the same which is used as a carrier signal to generate the pulsed RF DME signal. There are two parameters that user

can modify freely. One is the *Signal-to-Interference Ratio (SIR)* that is the quotient between the RMS (root mean square) E5 signal level and the RMS interference level expressed in dB. The second one is the *interference carrier frequency (Δf_{interf})* which is defined as the frequency shift (in MHz) with respect to the Galileo E5a sub-carrier.

As many interference signal as user wants can be generated at the same time. CWIs with different amplitudes/frequency or a high/low density of RF DME pulses during the simulation can be added. It has been assumed that, for the sake of clarity, interference signals are not affected by multipath propagation. However, if desired, add this effect to the simulator may be easily implemented.

5.3 Receiver

Once the signal is transmitted and passed through the channel propagation, the receiver starts working. This section address the main activities undertaken within the receiver block. Currently, as mentioned in the preceding chapters, the GE5-TUT receiver only operates in the E5a band (single band receiver).

5.3.1 Mitigation techniques block

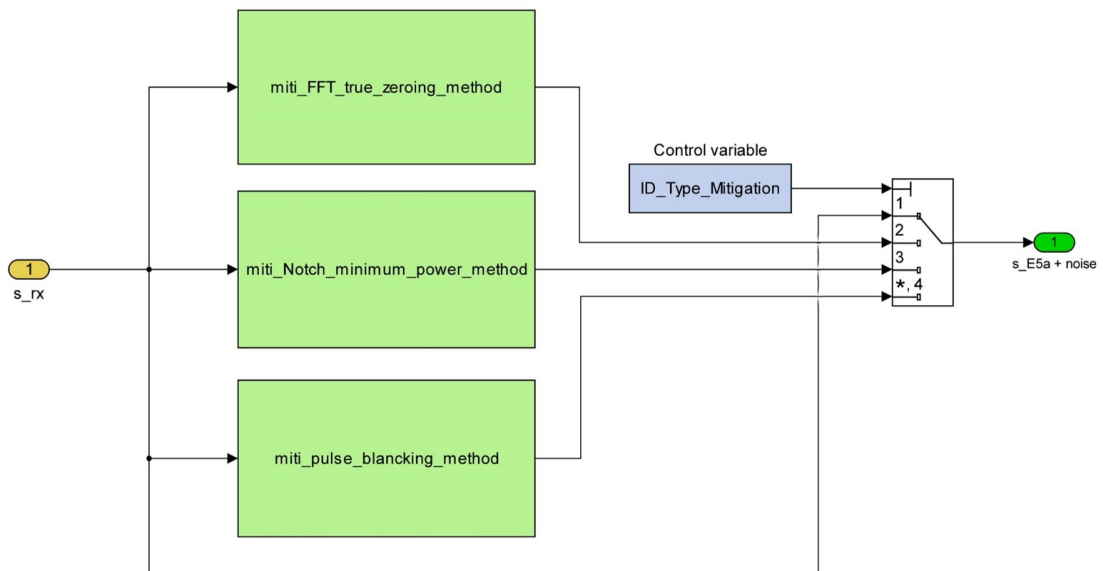


Figure 5.10 Mitigation techniques block diagram.

Figure 5.10 depicts the second main contribution of this thesis to the GE5-TUT simulator. The main aim of this block is to cancel as much as possible the interference

signals present in the channel. The methods used herein and their performances were explained in chapter 4. Not only the spectrum/time representations give useful information about the performance mitigation techniques but also the ACF. Making use of the ACF, it is possible to observe the improvement carried out in interference cancellation. For example, figure 5.11 depicts the zeroing performance against two CWI. $C/N_0 = 50$ dB/Hz, no multipath effects, $SIR_{cwi1} = -40$ dB, $SIR_{cwi2} = -38$ dB, $\Delta f_{interf1} = 0$ MHz and $\Delta f_{interf2} = 0.5$ MHz.

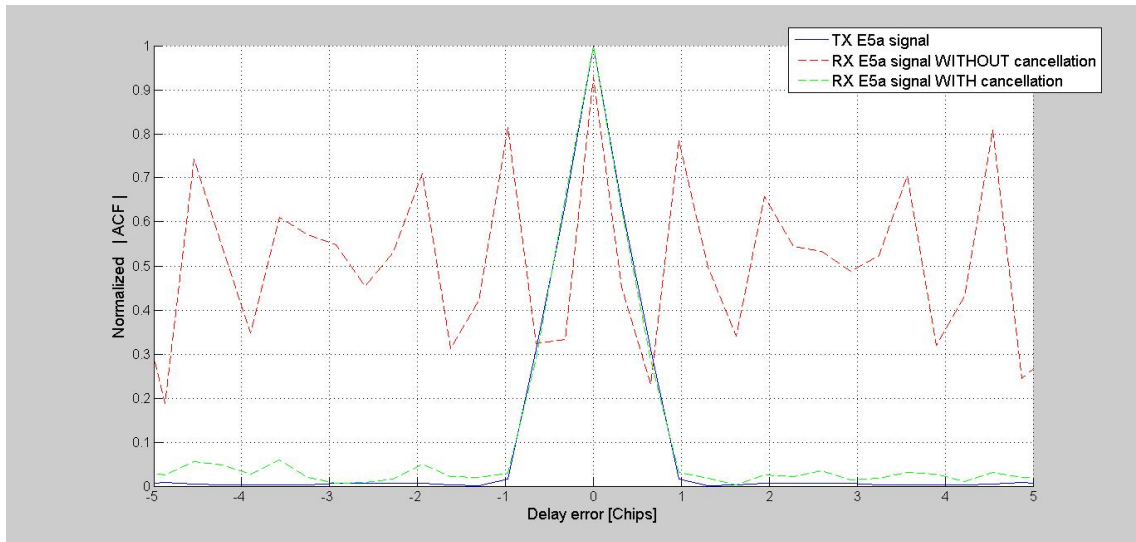


Figure 5.11 ACF to assess the zeroing method against two CWIs.

5.3.2 Acquisition unit

In section 2.4.4 the receiver fundamentals of operation were briefly explained. Before obtaining the pseudorange measures, the receiver must acquire the E5a signal. The aim of the acquisition process is to estimate roughly the *code delay* (θ) and the *Doppler frequency shift* ($f_{Doppler}$) of the incoming signal from each satellite in view. To do that, a bi-dimensional search is carried out throughout all possible code phases and Doppler shifts. The receiver correlates blocks of samples (1 ms of duration means $f_{sample}/0.001$ samples) with a local replica of the desired satellite signal. The local code position is swept over an uncertainty time slot (one epoch of the primary code, 10230 chips) and also the local frequency is varied inside the Doppler uncertainty domain. When a correlation peak is found at the output of the correlator and this peak is higher than a certain detection threshold (Th), the tracking process starts working. This search strategy could be seen as a window of time-frequency bins (code-Doppler shift). Figures 5.12 and 5.13 shows the acquisition diagram and an example of this time-frequency grid.

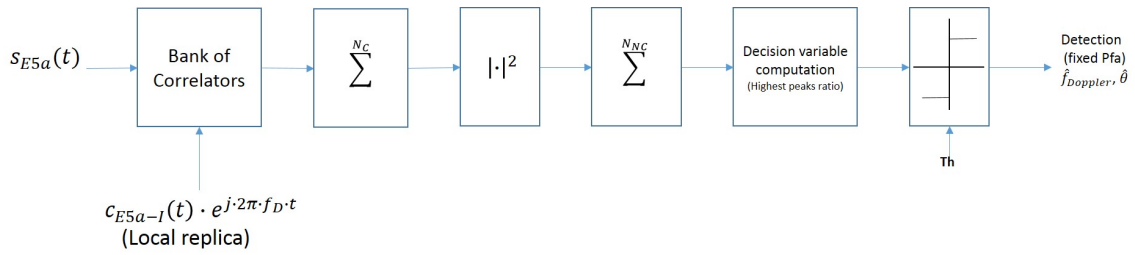


Figure 5.12 Block diagram of the acquisition process carried out in GE5-TUT simulator.

Where $c_{E5a-I}(t)$ is the local primary code replica, N_C is the number of coherent integrations and N_{NC} is the number of non-coherent integrations. The acquisition block uses FFT-based correlations and it is implemented according to the Constant False Alarm Rate (CFAR) algorithm of Pajala et al. [42] based on the ratio $highest_correlation_peak / second_correlation_highest_peak$ of the grid.

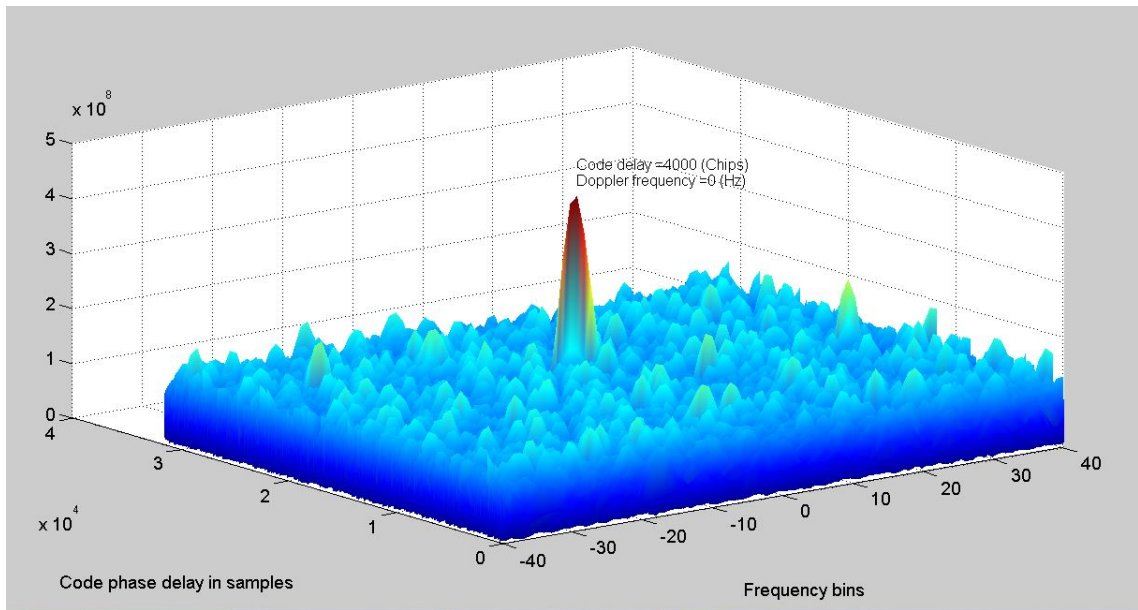


Figure 5.13 Acquisition time-frequency grid. $C/N_0 = 60$ dB/Hz, $N_C = 1$, $N_{NC} = 1$. No multipath effects nor interference signal are present.

Interference signal may prevent the correlator from acquiring the ratio of the peak. Thanks to the proposed techniques, this issue can be solved satisfactorily. The following illustrations show how the performance is improved using different approaches throughout the time-frequency grid explained above. Noise and multipath effect are not contemplated. Simulation was carried out with $C/N_0 = 55$ dB/Hz, $SIR = -50$ dB, $N_C = 1$, $N_{NC} = 4$.

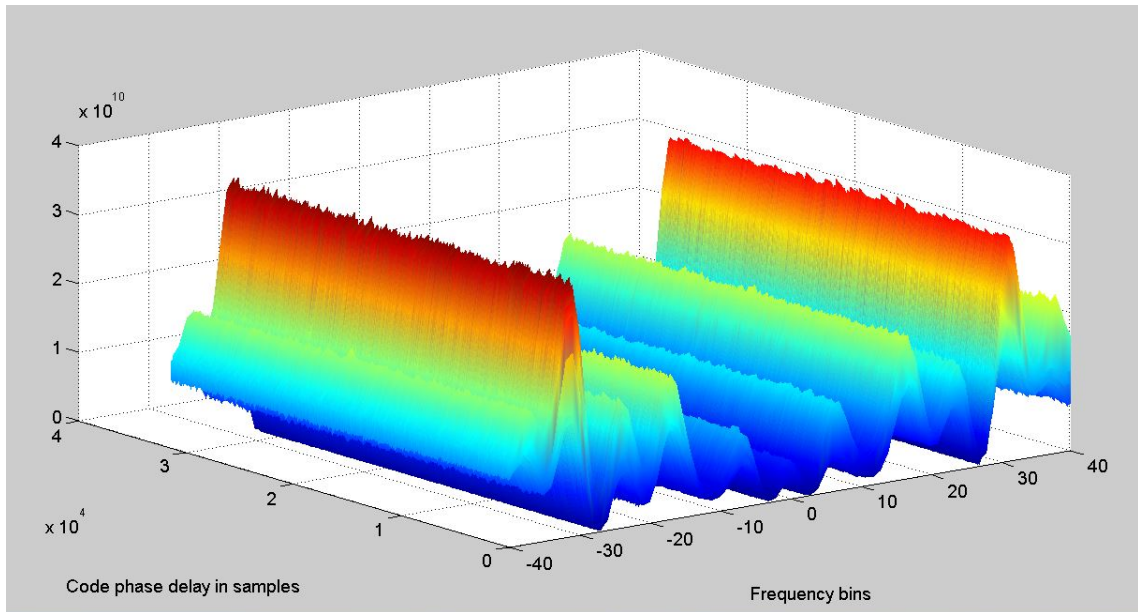


Figure 5.14 One CWI. No-mitigation technique is used.

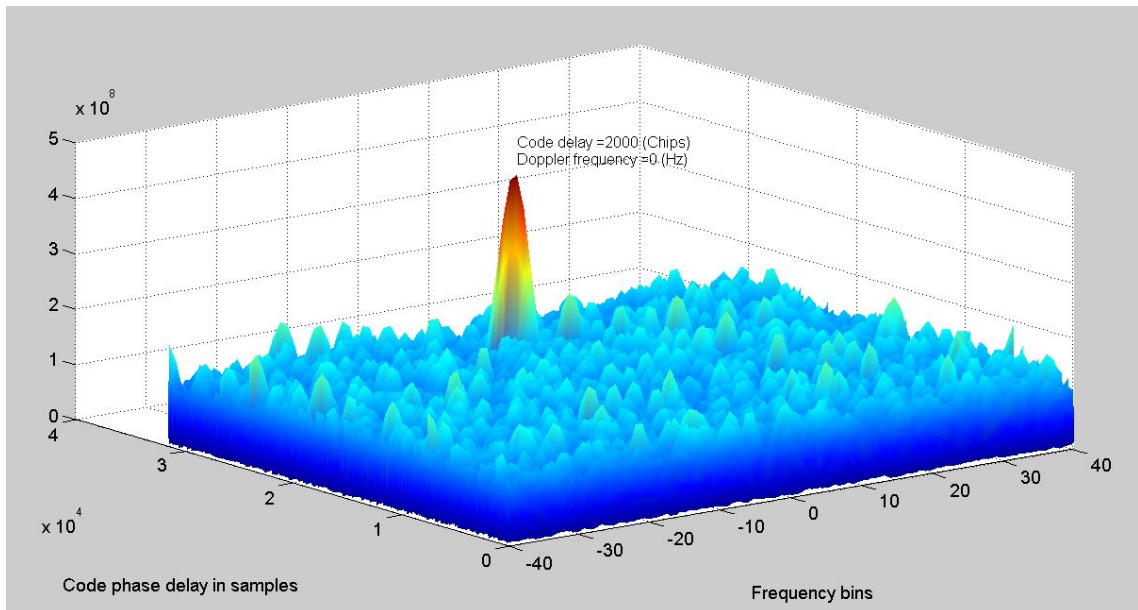


Figure 5.15 Zeroing method against one CWI.

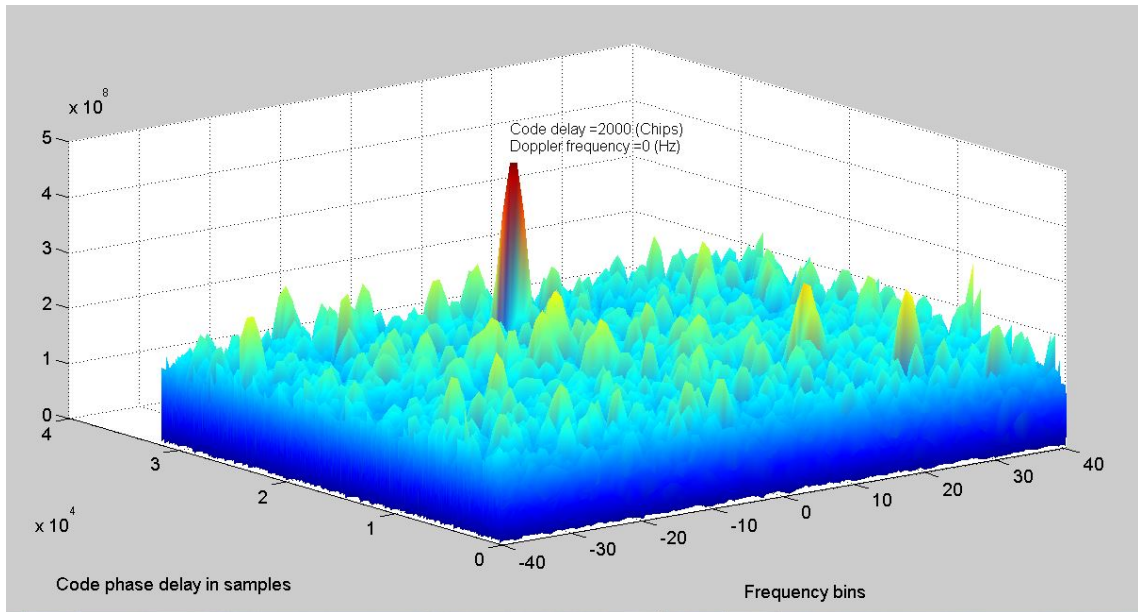


Figure 5.16 Notch-Filtering method against one CWI.

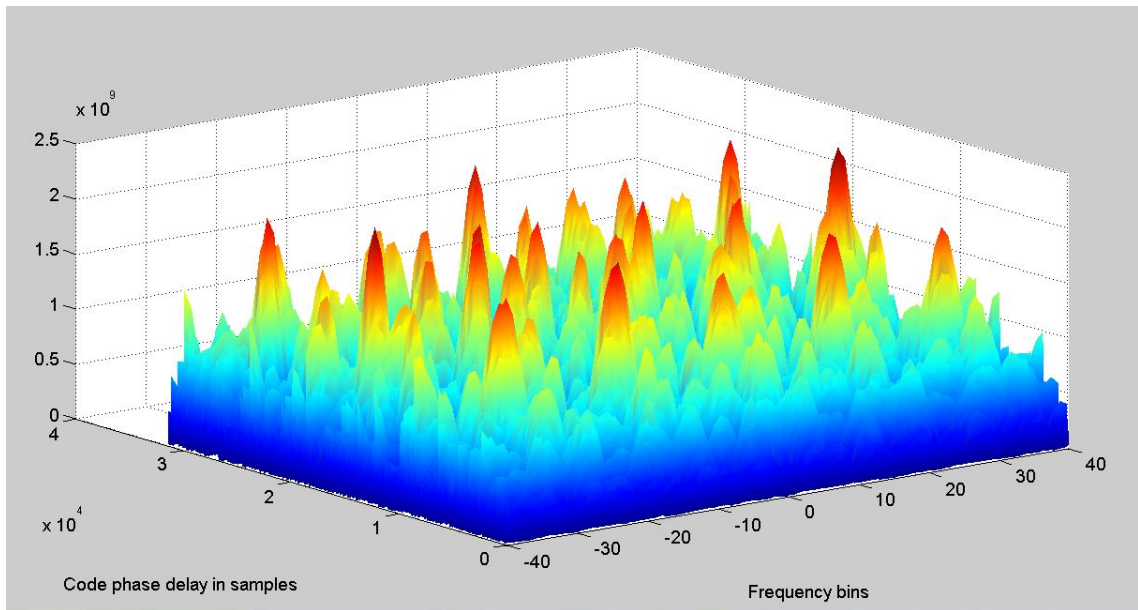


Figure 5.17 DME interference with 3000 pps density. No-mitigation technique is used.

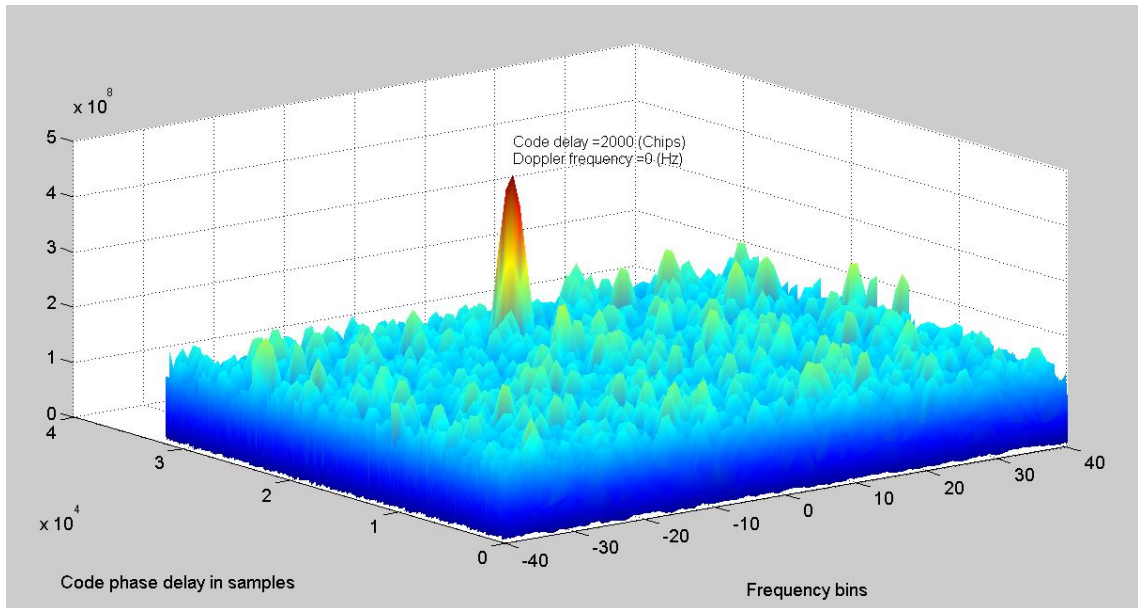


Figure 5.18 Notch-Filtering method against DME interference with 3000 pps density.

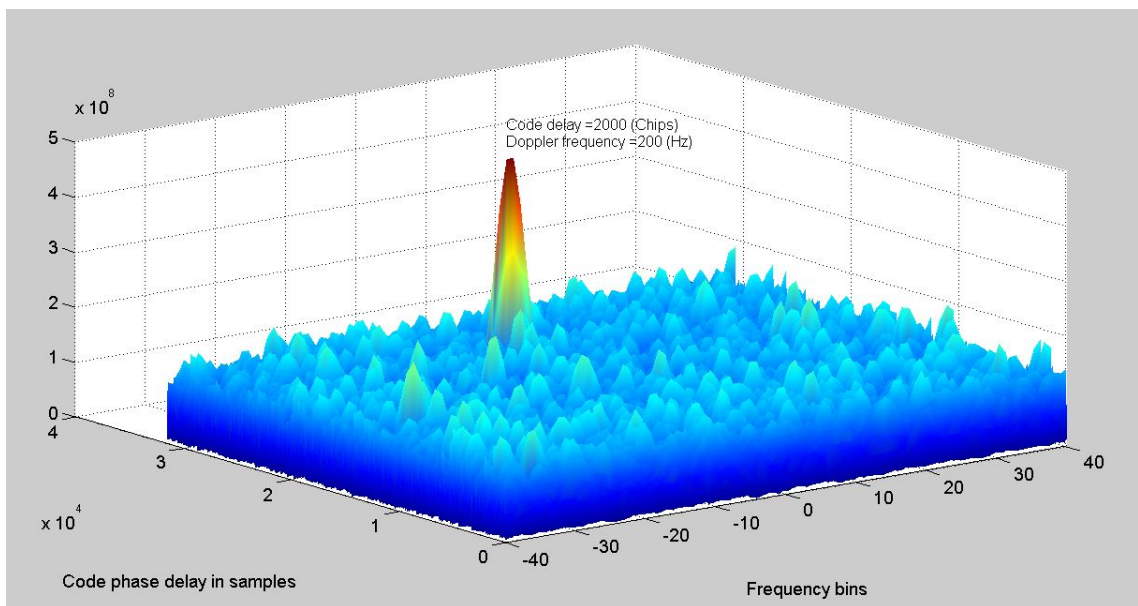


Figure 5.19 Blanking method against DME interference with 3000 pps density.

5.3.3 Tracking unit

Although this thesis is mainly focused on acquisition process in presence of signals outside the system, tracking block is also explained but in summary form.

Once the Galileo signal is acquired, a control flag is turn on (*TRACKING_ENABLE*)

to enable the tracking unit and then be able to refine the values given by the acquisition unit and then, demodulate the navigation data. This subsystem is formed by three main block: carrier wipe-off block, a discrete time Numerically controlled Oscillator (NCO) block and dual channel correlation and discriminator block as in figure 5.20

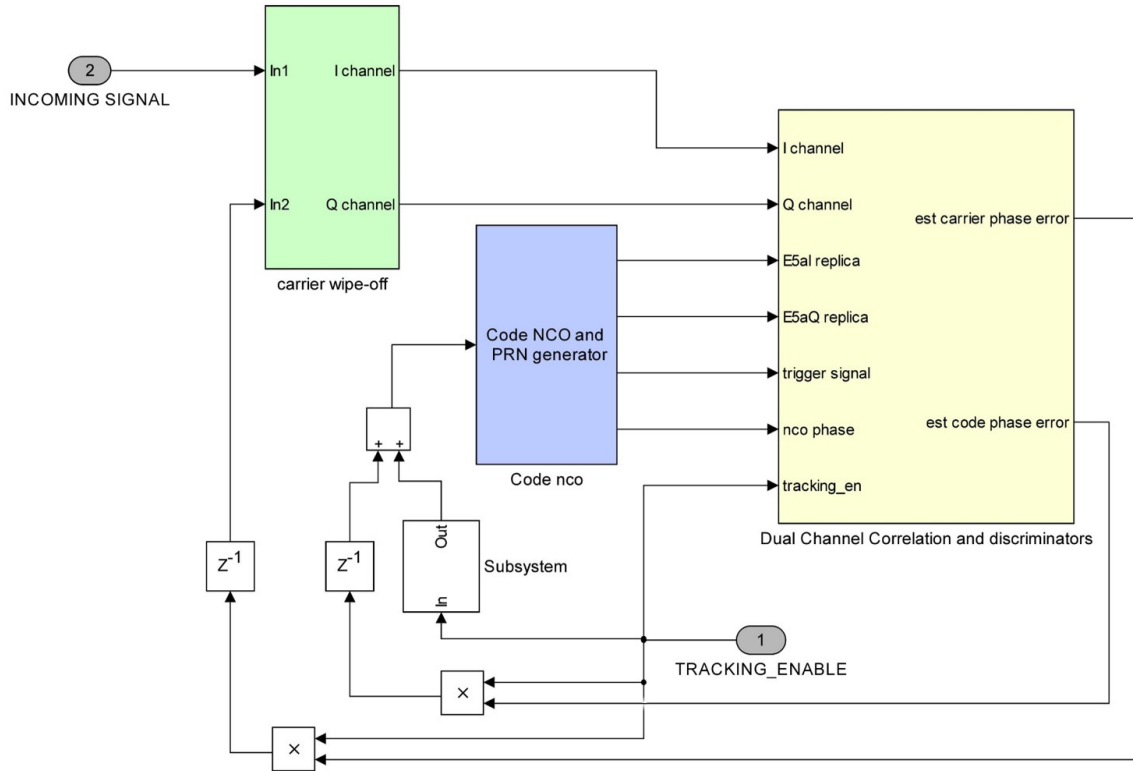


Figure 5.20 Tracking subsystem block diagram.

- The carrier wipe-off block (figure 5.21) down-converts the E5 signal to a baseband with the estimated frequency ($\hat{f}_{Doppler}$) and phase(θ) from Phase Locked Loop (PLL) and Frequency Locked Loop (FLL) in the correlation and discriminator block. After the carrier wipe-off, the real part and the imaginary part of the complex signal are separated as the in-phase (channel I) and the quad-phase (channel Q) channels.

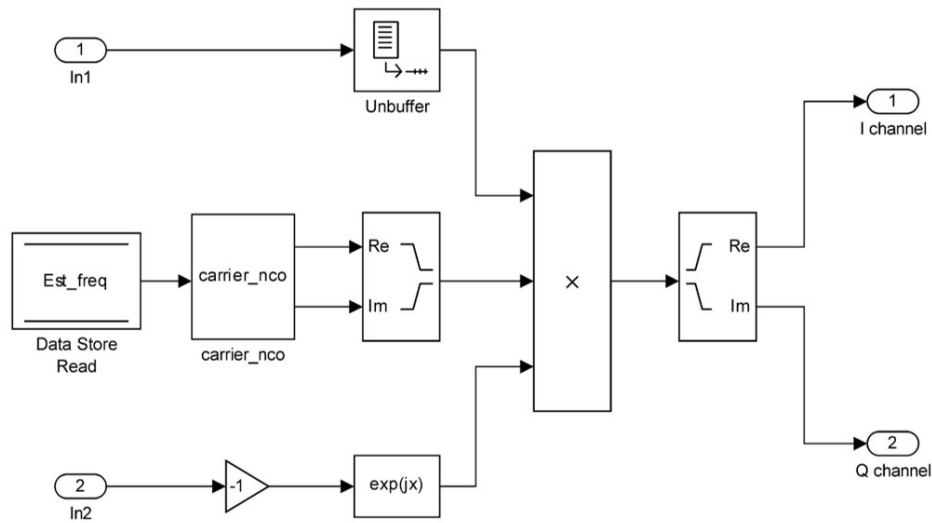


Figure 5.21 Carrier-wipe-off block diagram.

- An NCO is used to generate the local PRN reference code, which is shifted by the estimated code phase from the Delay Locked Loop (DLL) in the correlation and discriminator block. Only the E5a-I signal is generated in the NCO block. A feedback loop is in charge to join this block with the next.
- Inside dual channel correlation and discriminator block (5.22) just one channel is used for E5a signal. A PLL is implemented to track the central carrier and the Doppler frequency of the sideband E5a. Also a DLL is carried out to track the PRN code. This is possible using different correlator structures. Currently, in GE5-TUT, Early minus Late (EML) discriminator [3] and HRC [14] are used in DLL block as discriminator functions. An integrate and dump operation is applied to assess the correlations between the incoming signal and the replicas.

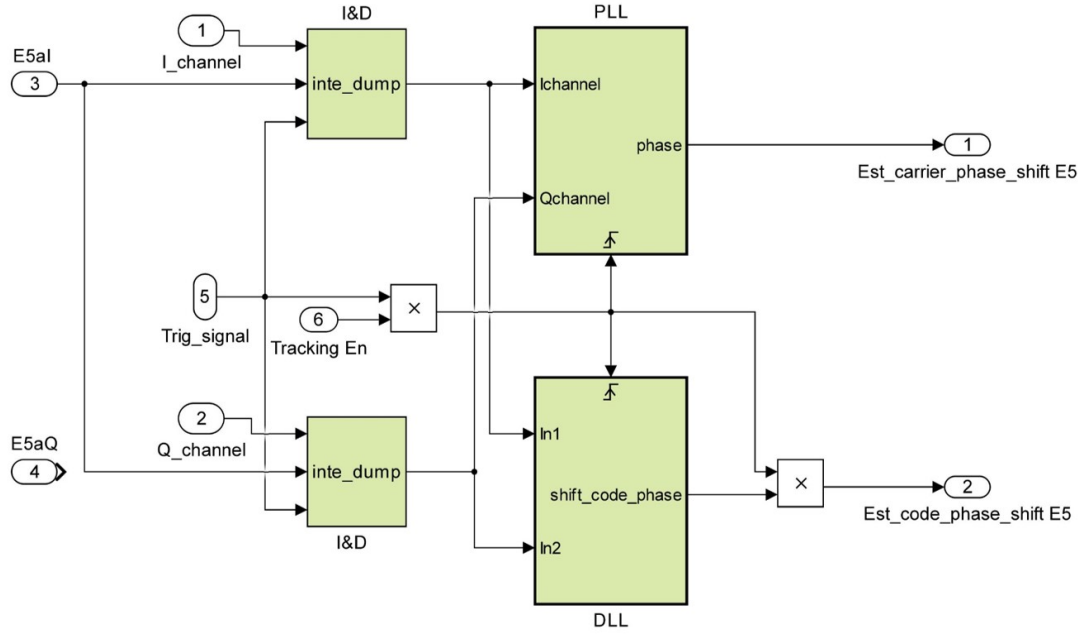


Figure 5.22 channel correlation and discriminator block diagram.

Figure 5.23 gives an idea of how big the tracking error can be along the simulation time. As can be observed, it magnitude is around few dozen of centimeters.

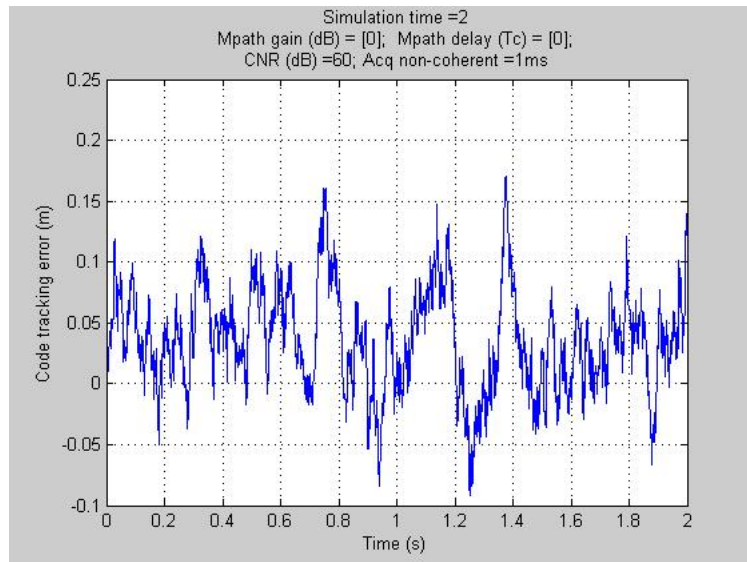
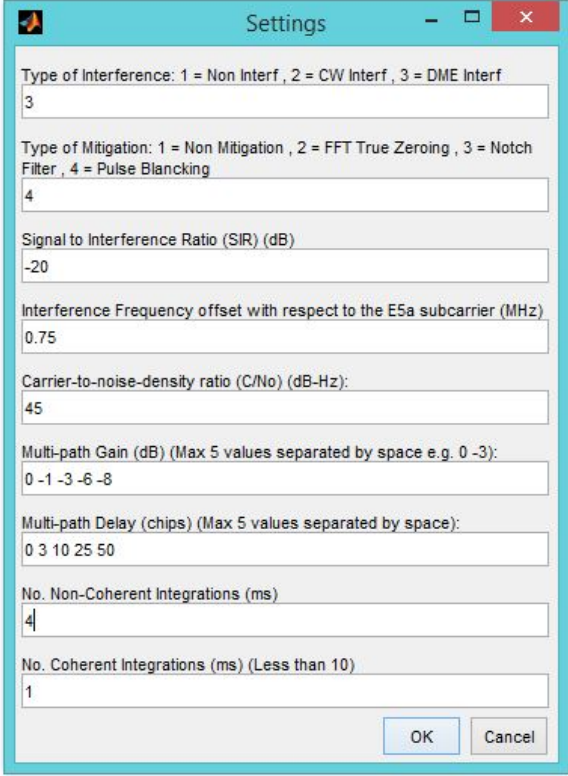


Figure 5.23 Tracking error along 0.5 second of simulation, 1 ms of non-coherent integration and $C/N_0 = 60$ dB/Hz.

5.4 Main variables and defined-user parameters

Along this chapter, it was mentioned that user is in charge of set some parameters through a pop-up menu when the simulation is launched. This menu is illustrated in figure 5.24 and table 5.1 reflect also the main variables and its current values.



The image shows a 'Settings' dialog box with the following parameters and values:

Parameter	Value
Type of Interference: 1 = Non Interf , 2 = CW Interf , 3 = DME Interf	3
Type of Mitigation: 1 = Non Mitigation , 2 = FFT True Zeroing , 3 = Notch Filter , 4 = Pulse Blanking	4
Signal to Interference Ratio (SIR) (dB)	-20
Interference Frequency offset with respect to the E5a subcarrier (MHz)	0.75
Carrier-to-noise-density ratio (C/No) (dB-Hz):	45
Multi-path Gain (dB) (Max 5 values separated by space e.g. 0 -3):	0 -1 -3 -6 -8
Multi-path Delay (chips) (Max 5 values separated by space):	0 3 10 25 50
No. Non-Coherent Integrations (ms)	4
No. Coherent Integrations (ms) (Less than 10)	1

Buttons: OK, Cancel

Figure 5.24 Initial pop-up menu.

Table 5.1 GE5-TUT main parameters.

Subsystem	Parameter	Description	Current value	Units
Transmitter block	sv	Satellite index for selecting the corresponding primary code	2	-
	fchip	Chip rate	10.23×10^6	chips/s
	fs	Sample rate	126×10^6	Hz
	K	Down sample factor	4	-
	fs_r	Sample rate after down sample block	31.5	Hz
	fIF	Intermediate frequency	20×10^6	Hz
	fsubcarr	E5 subcarrier frequency	15.345×10^6	Hz
	fBB	E5a central frequency	fIF - fsubcarr	Hz
Channel & Interference block	ID_Type_Interference	Type of interference (pop-up menu)	1	-
	P_sin	SIR (pop-up menu)	-10	dB
	Finterf	Interference Frequency offset with respect to the E5a subcarrier (pop-up menu)	0	MHz
	CNR	Carrier-to-noise-density ratio (C/No) (pop-up menu)	50	dB/Hz
	Mpath_gain	Multi-path Gain vector (pop-up menu)	[0, 0, 0, 0, 0]	dB
	Mpath_delay	Multi-path Delay vector (pop-up menu)	[0, 0, 0, 0, 0]	Chips
	fad_type	Type of multipath	“static”	-
	Dop_vec	Doppler-path spread vector for “fading” channel	[0, 0, 0, 0, 0]	Hz
Mitigation technique block	ID_Type_Mitigation	Type of mitigation technique (pop-up menu)	1	-
Acquisition block	frange	Doppler uncertainty domain	[fBB-2000 , fBB+2000]	Hz
	step_fre	Frequency step for acquisition search	200	Hz
	step_time_bin_chips	Time step for acquisition search	0.17	chips
	acq_non_coh_ind	Number of non-coherent integrations (pop-up menu)	1	ms
	acq_coh_ind	Number of coherent integrations (pop-up menu)	1	ms
Tracking block	delta	early-late spacing	0.05	Chips
	corr_range	Correlator range	[-1 : delta : 1]	Chips
	dll	DLL algorithm type	1 (EML)	-

6. SIMULATION RESULTS

In this chapter, we show the performance of the three proposed interference mitigation techniques for GE5-TUT simulator. The main goal of this thesis is the performance of the acquisition stage with and without interference mitigation. This will also illustrate the capacity to correctly detect the SIS in hostile environments or with high density of air traffic.

6.1 Performance criteria

As it was mentioned in section 5.3.2, GE5-TUT acquisition detection is implemented based on CFAR algorithm. The decision variable (X) is the ratio between the highest peak (Z_{m1}) of the correlation grid Z_i and the second highest peak (Z_{m2}) after zeroing the closest neighbors time-frequency bins of Z_{m1} [42]:

$$X = \frac{Z_{m1}}{Z_{m2}} \quad (6.1)$$

When $X > \gamma_{th}$, a detection is declared. This is a binary detection process in which there are two hypothesis. H_0 means the desired signal is absent (wrong detection) and H_1 is when desired signal is present (correct detection). Under these hypothesis, probability density functions (f_{X,H_0} and f_{X,H_1}) and cumulative distribution functions (F_{X,H_0} and F_{X,H_1}) of X can be obtained numerically. These lead to compute the false alarm (P_{fa}) and detection (P_d) probabilities:

$$P_{fa}(\gamma_{th}) = P(X \geq \gamma_{th}|H_0) = 1 - F_{X,H_0}(\gamma_{th}) = 1 - \int_{-\infty}^{\gamma_{th}} f_{X,H_0}(x) dx \quad (6.2a)$$

$$P_d(\gamma_{th}) = P(X \geq \gamma_{th}|H_1) = 1 - F_{X,H_1}(\gamma_{th}) = 1 - \int_{-\infty}^{\gamma_{th}} f_{X,H_1}(x) dx \quad (6.2b)$$

Figure 6.1 shows the general scenario for this binary detection process (CFAR detector). Currently, the threshold value is set to 1.3 to provide a good trade-off

between P_{fa} and P_d .

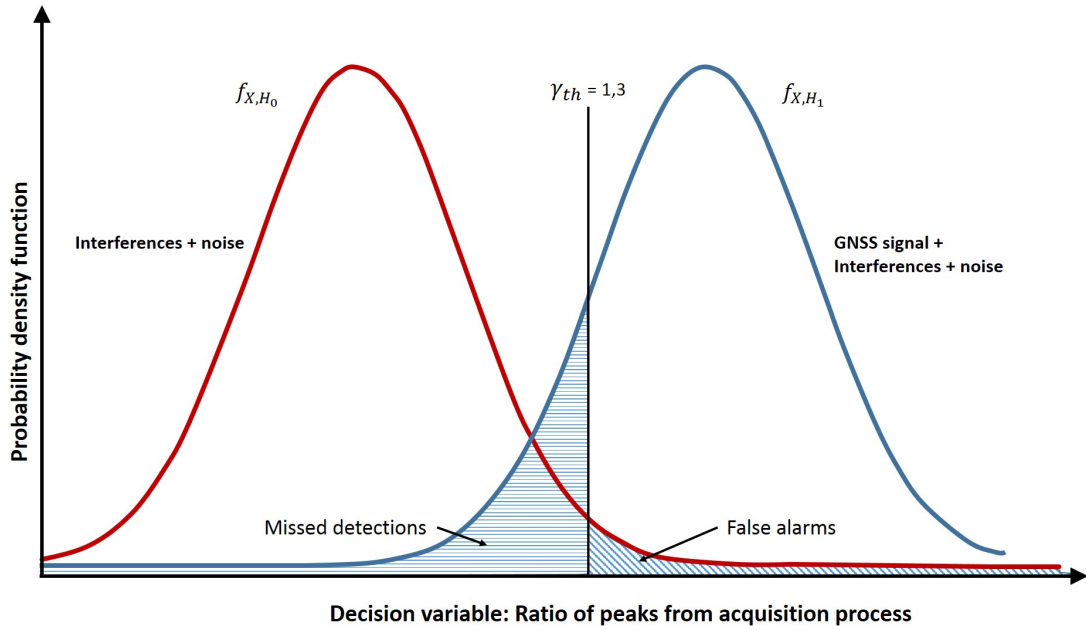


Figure 6.1 Statistical scenario.

To assess the P_d , the tracking block was unplugged and GE5-TUT was left to work just with the acquisition block to see how many right detections the system is able to detect for different values of SIR and C/N_0 . Figure 6.2 and 6.3 is the probability density functions representation for different situations, with and without mitigation technique, for CWI.

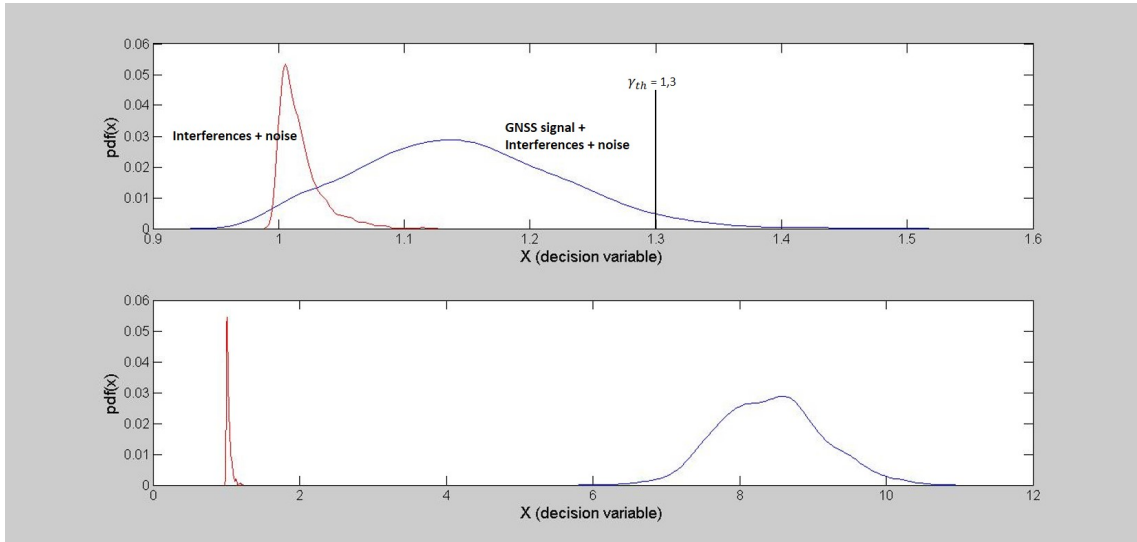


Figure 6.2 Statistical scenario for $SIR = -30$ dB and $C/N_0 = 50$ dB. Above no mitigation technique is applied while picture below shows the zeroing behavior.

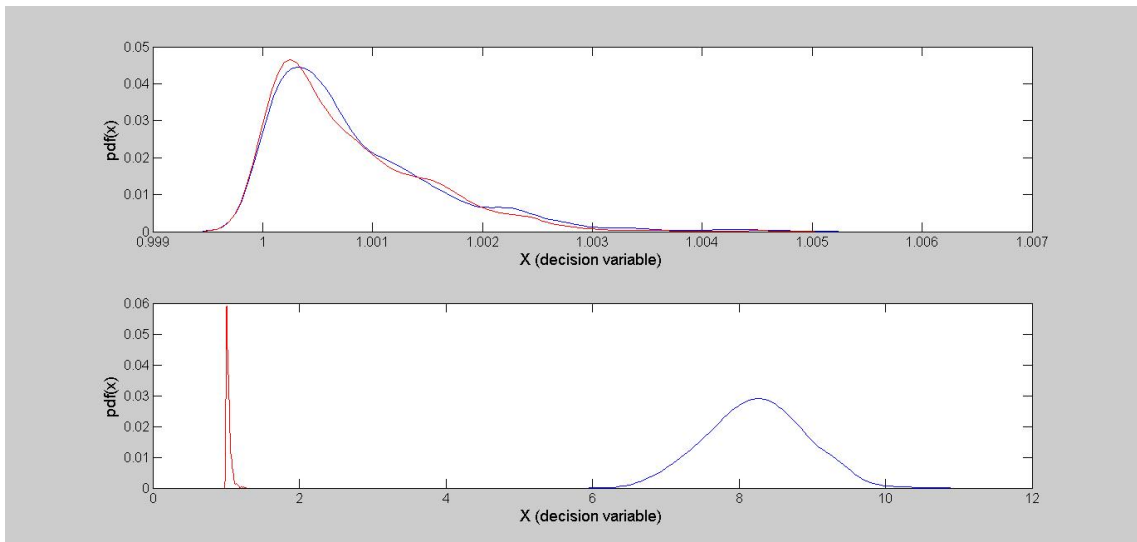


Figure 6.3 Statistical scenario for $SIR = -50$ dB and $C/N_0 = 50$ dB. Above no mitigation technique is applied while picture below shows the zeroing behavior.

Without any mitigation approach, the smaller the SIR value, the bigger the miss-detection probability is. The peaks ratio (X) is always smaller than the threshold (set to 1.3) and thus, detection is never declared. However, with zeroing technique, the decision variable is always above the threshold leading to correctly acquire the signal always.

6.2 Simulation results

Simulations were done for both cases, CWI and DME interferences. For the sake of simplicity, the multipath effect was not considered. The duration of each simulation was 10 seconds. Relevant user-defined parameters are: $N_{NC} = 20$, $N_C = 1$, $\Delta f_{interf} = 0$, $Mpath_delay = [0]$ and $Mpath_gain = [0]$. For each simulation, SIR and C/N_0 take different values. $SIR = 0, 15, 30, 45, 60$ dB and $C/N_0 = 35, 40, 41, 42, 43, 44, 45, 50$ dB/Hz. The rest of parameters are the same as shown in table 5.1. For the case in which DME interference is assessed, the density of pulses also varies. Firstly, it was set to 500 pps and later to 3000 pps. It is possible just adding delay blocks inside DME interference generator block.

The results are depicted in the next figures. First of all, figure 6.4 gives an idea to what extent interferences damage the acquisition process. It is possible to observe that the most harmful signal to receiver is the CWI. For example for $C/N_0 = 42$ dB/Hz, the P_d begins to rapidly decline from an interference power of 15 dB. On the other hand, the system performance starts to fall from 30 dB with 500 pps and 45 dB with 3000 pps.

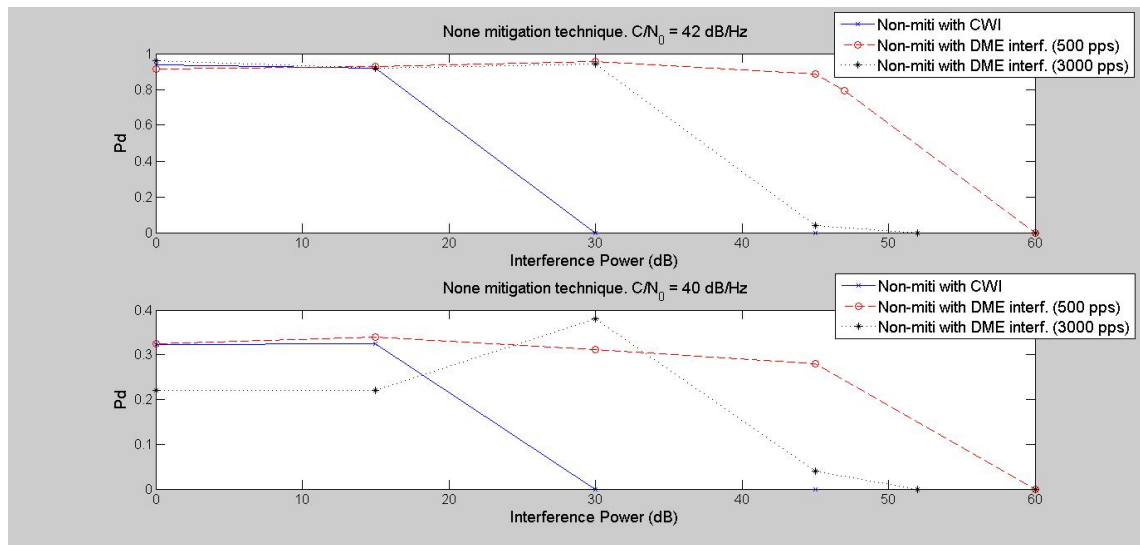


Figure 6.4 P_d performance without any mitigation technique and different values of interference power. CWI and DME signal are considered.

The CWI rejection methods performance is illustrated in figure 6.5.

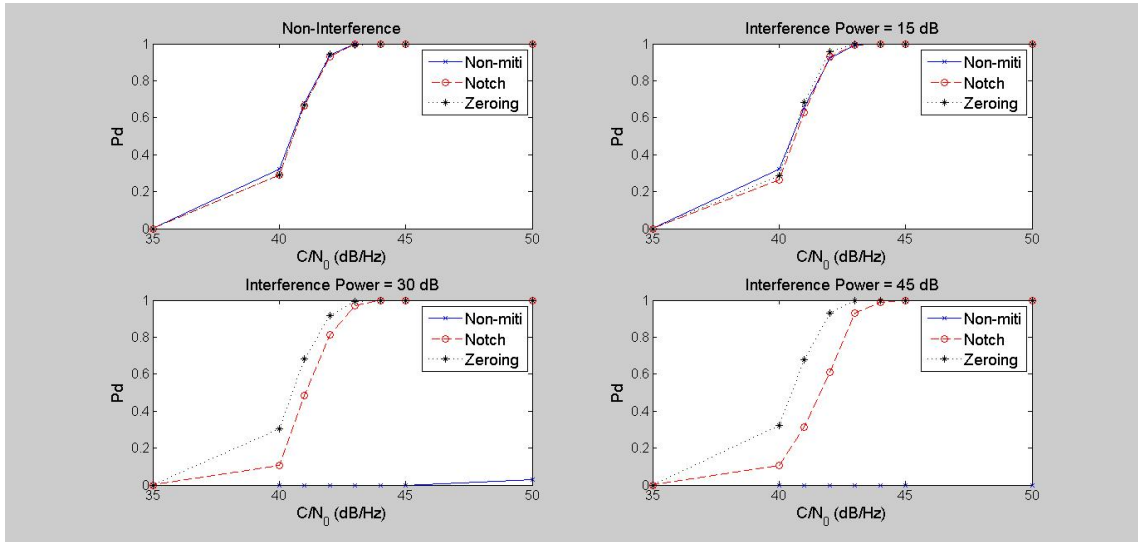


Figure 6.5 CWI rejection performance at interference powers between 0 and 45 dB.

Acquisition process withstands better DME interference due to its duty cycle is shorter than CWI. DME systems have been designed for air traffic which involves transmitting 2700 pps. In order to compare zones with high or low pulse density, figures 6.6 and figure 6.7 show the mitigation techniques performance in each of these environments.

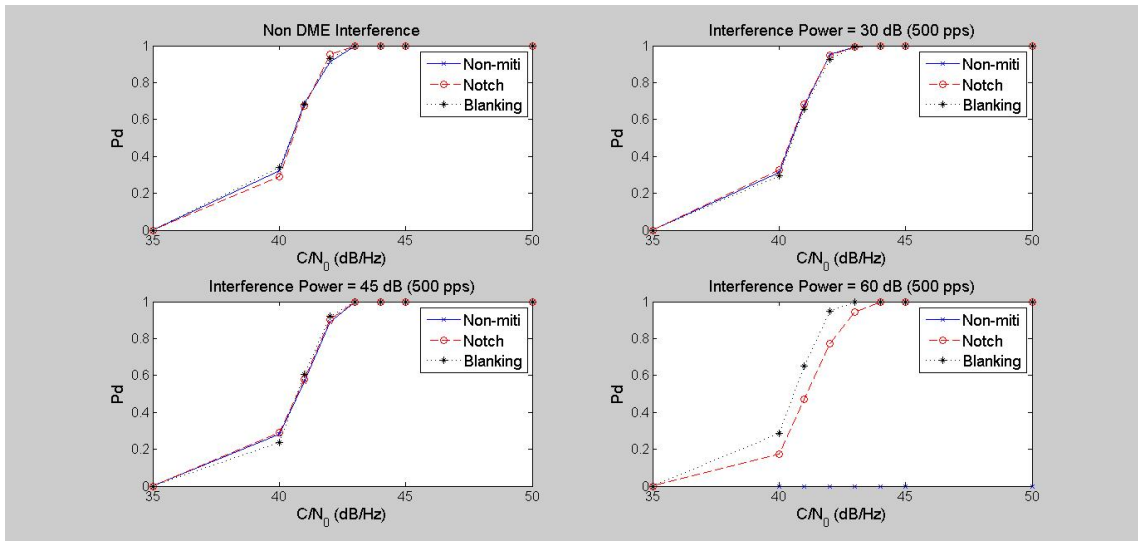


Figure 6.6 DME interference rejection performance at interference powers between 0 and 60 dB. Pulse density of 500 pps.

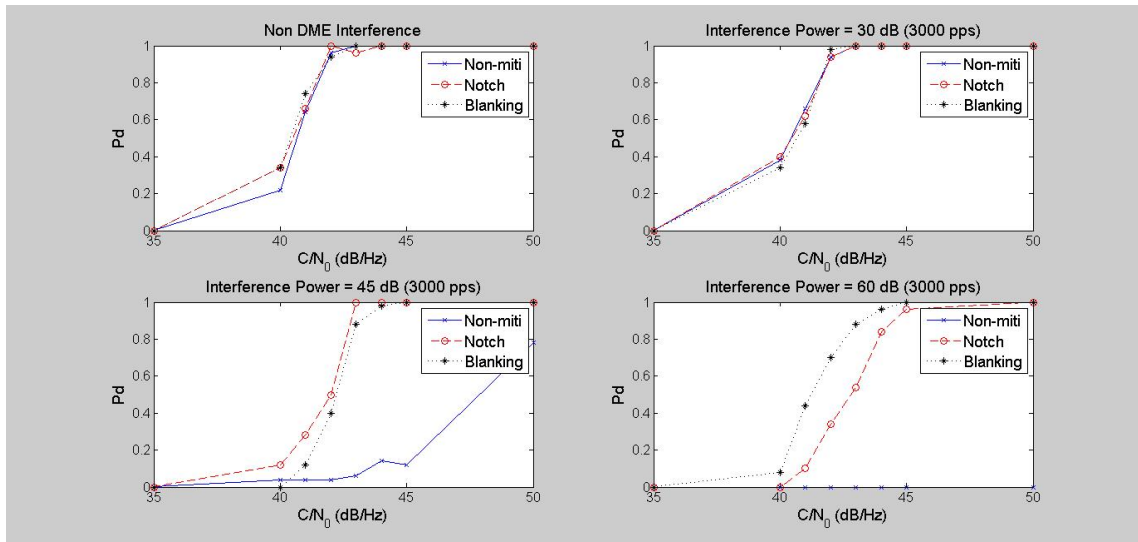


Figure 6.7 DME interference rejection performance at interference powers between 0 and 60 dB. Pulse density of 3000 pps.

For pulse density of 500 pps, acquisition process works reasonably well in presence of DME signals with a power of 45 dB, whilst for a density of 3000 pps, detections become worse before interferences reach 45 dB.

One way of evaluating the rejection methods was to fix C/N_0 and vary the value of the interference power (SIR) to see how Pd is changing. Figure 6.8 shows this situation for $C/N_0 = 42$ dB/Hz. One may conclude that notch filter method offers the worst performance of the three proposed approaches and it is the method which takes more time. For DME interferences the blanking pulse presents a high effectiveness. In the case of CWI, the zeroing method is the most effective.

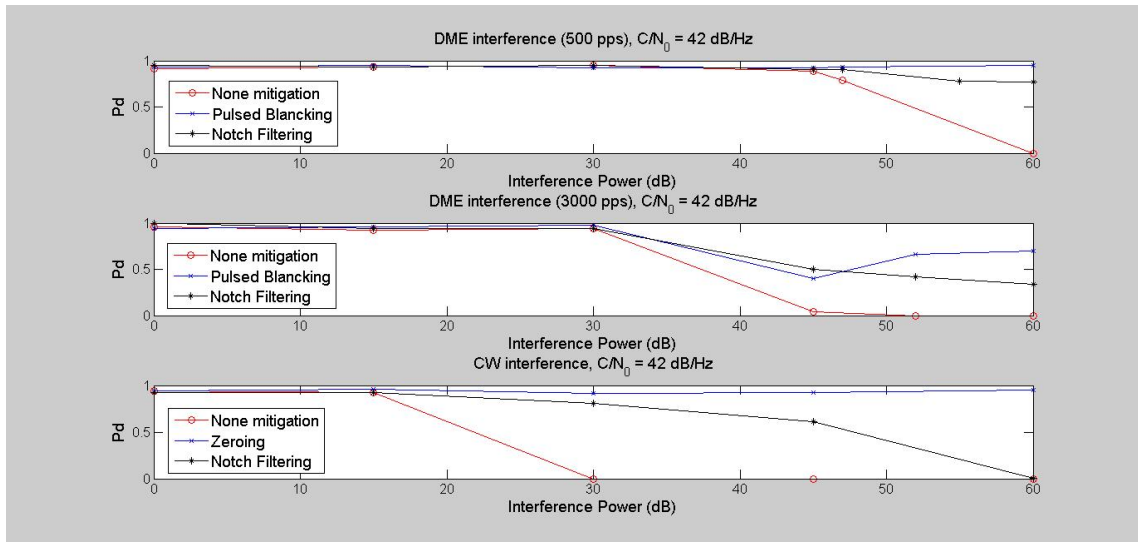


Figure 6.8 Mitigation techniques efficiency. C/N_0 was fixed to 42 dB/Hz.

In the light of the results obtained during the simulations, it may be said that blanking method for DME pulses and zeroing method for CWI are the most effective techniques to achieve a high number of detections. A trade-off between performance, versatility and computational load must be found, and notch filtering method is the least balanced in this regard.

Subjectively, if one mitigation technique between zeroing and blanking needs to be recommended to a GNSS devices designer, perhaps zeroing method would be the elected. The reason is that zeroing method works satisfactorily for CWIs and although it works badly for DME interferences, this kind of signals are less harming than CWIs. It is likely that DME/TACAN facilities will be phase-out as GNSS systems consolidate and become the air-navigation standard. However, DME is still widely used. On the other hand, Blanking only works for pulsed interferences.

7. CONCLUSIONS AND OPEN DIRECTIONS

The evolution of positioning services and deployment of incoming GNSS systems envisaged for the next years (BeiDou and Galileo) raise the need to reinforce the robustness of satellite communications. Thus, different research studies are currently under way in both the academic realm and business world.

This thesis is focused on Galileo E5 band, especially on the E5a component. The developed simulator (GE5-TUT) and the results obtained by the author provide a starting point for future research. The main objective has been to extend the provided TUT simulator to observe the effect of both CWI and DME signal, and to evaluate the different types of narrowband interference rejections such as blanking, zeroing and notch methods. The first one has proven to be the most appropriate for DME interferences and zeroing method for CWI. Dynamic notch filtering is the slowest approach even though it is useful for both types of harming signals. To analyze all of these, some math functions such as ACF or the time-frequency grid of the acquisition unit have been used.

Thanks to the features implemented until the present in GE5-TUT simulator, numerous studies could be made, in addition to those carried out in this thesis. Adding new error sources (ionosphere, troposphere, relativity effect...), more interference signals, new mitigation techniques, an impact assessment of the multipath effect together with some interferences or also investigate the frequency interferences dependence with respect to the Galileo E5 sub-carriers and its influence in the acquisition or tracking process. In short, a good baseline has been laid, but the GE5-TUT simulator could be enhanced as much as the user wants.

The running time required by the simulations has been one of the biggest bottlenecks. Luckily, thanks to the powerful resources from the Tampere University of Technology, this time was severely reduced. To get a handle on this, an 8-Core Desktop Processor (Intel(R) Core(TM) i7-4790 CPU @ 3.6GHz) needs around four hours to simulate 10 seconds (even more if notch filtering approach is running). Therefore, another possible task could be to optimize the running time of the blocks which form the simulator.

GE5-TUT has been developed with Matlab-Simulink 2014a - 64 bits. It was necessary to update the simulator because it was created with Matlab-Simulink 2007 - 32 bits. *Upgrade Advisor* is a Simulink update tool that comes by default (*Analysis-> Model Advisor-> Upgrade Advisor*). This simulator is planned to be an open source tool to be available at www.cs.tut.fi/tlt/pos under open-source license. It is highly recommended to update the model if new improvements are intended to be done in future studies to reduce any block running time.

BIBLIOGRAPHY

- [1] E. Anyaegbu, G. Brodin, J. Cooper, and E. Aguado, “An Integrated Pulsed Interference Mitigation for GNSS Receivers,” *The journal of navigation*, vol. 61, pp. 239–255, Apr. 2008.
- [2] M. Appel, A. Hornbostel, and C. Haettich, “Impact of Meaconing and Spoofing on Galileo Receiver Performance,” Institute of Communications and Navigation, German Aerospace Center (DLR), Oberpfaffenhofen, Germany, Oct. 2014.
- [3] A.V. Dierendonck and P. Fenton and T. Ford, “Theory and Performance of Narrow Correlator Spacing in a GPS Receiver,” *NAVIGATION. Journal of the Institute of navigation*, vol. 39, no. 3, pp. 265–283, 1992.
- [4] J. Ávila, “On Generalized Signal Waveforms for Satellite Navigation,” Ph.D. dissertation, University FAF Munich, Germany, June 2008.
- [5] A. Balaei, B. Motella, and A. Dempster, “GPS Interference detected in Sydney-Australia,” In Proceedings of IGNSS Conference, Sydney, Australia, Dec. 2007.
- [6] R. Barradas, “GNSS Applications,” 2011, Navipedia ESA-approved website.
- [7] R. Bucher and D. Misra, “A Synthesizable VHDL Model of the Exact Solution for Three-dimensional Hyperbolic Positioning System,” *VLSI Design*, vol. 15, no. 2, 2002.
- [8] M. Chavan, R. Chile, and S. Sawant, “Multipath Fading Channel Modeling and Performance Comparison of Wireless Channel Models,” in *International Journal of Electrical and Computer Engineering (IJECE)*, vol. 4, no. 2. International Research Publication House (IRPH), 2011, pp. 189–203.
- [9] J. Clynch, A. Parker, R. Adler, W. R. Vincent, P. McGill, and G. Badger, “The Hunt for RFI: Unjamming a Coast Harbor,” *GPS World*, Jan 2003.
- [10] “Galileo Ready Advanced Mass Market Receiver (GRAMMAR) project,” Available: http://www.dlr.de/kn/en/desktopdefault.aspx/tabid-4309/3222_read-20115/admin-1/, Coordinate by Institute of Communications and Navigation at German Aerospace Center (DLR), in collaboration with ACORDE TECHNOLOGIES S.A. (ACORDE) and Tampere University of Technology (TUT).

- [11] H. Diessongo, H. Bock, T. Schuler, S. Junker, and A. Kiroe, "Exploiting the Galileo E5 Wideband Signal," *Inside GNSS Magazine*, vol. 7, no. 5, pp. 64–73, Sep. 2012.
- [12] "Constellation Information," European GNSS Service Center, European GNSS Service Center website, Available: <http://www.gsc-europa.eu/system-status/Constellation-Information>.
- [13] *European GNSS (Galileo) Open Service Signal In Space Interface Control Document*, European Union, Sep. 2010.
- [14] F. Dovis and P. Mulassano and D. Margaria, "Multiresolution Acquisition Engine Tailored to the Galileo AltBOC Signals," in *Proceedings of the 20th International Technical Meeting of the Satellite Division of The Institute of Navigation (ION GNSS 2007)*. ION Publications, Sep. 2007, pp. 999 – 1007.
- [15] I. Fernandez, I. Rodríguez, G. Tobías, J. Calle, E. Carbonell, G. Seco-Granados, J. Simón, and R. Blasi, "Galileo's Commercial Service. Testing GNSS High Accuracy and Authentication," *Inside GNSS Magazine*, vol. 10, no. 1, pp. 38–48, Jan. 2015.
- [16] "Galileo service interruption for ground segment upgrade," Galileo GNSS blog, 2015, Available: <http://galileognss.eu/category/galileo-ground-segment/>.
- [17] G. X. Gao, "DME/TACAN Interference and its Mitigation in L5/E5 Bands," in *Proceedings of the 20th International Technical Meeting of the Satellite Division of The Institute of Navigation (ION GNSS 2007)*, Fort Worth, TX, Sep. 2007, pp. 1191–1200.
- [18] "China launches first of next-gen beidou satellites," GPS World staff, Mar. 2015, GPS World website.
- [19] R. Hranac and B. Currivan, "Digital Transmission: Carrier-to-Noise, Signal-to-Noise & Modulation Error Ratio," Cisco Systems, Inc. and Broadcom Corporation," White paper, 2006.
- [20] "SX3 multi-GNSS software receiver," IFEN Inc., 2015, Available: <http://www.ifen.com/products/sx3-gnss-solutions/sx3-gnss-software-receiver.html>.
- [21] "GLONASS constellation status," Information-Analytical Center of the Russian Federation, Available: <http://glonass-iac.ru/en/GLONASS/>.
- [22] Inside GNSS staff, "Exploiting the Galileo E5 Wideband Signal," Nov. 2014.

- [23] Ismael Colomina and Christian Miranda and M. Eulàlia Parés and Marcus Andreotti and Chris Hill and Pedro F. da Silva and João S. Silva and Tiago Peres and João F. Galera Monico and Paulo O. Camargo and Antonio Fernández and José Maria Palomo and João Moreira and Gustavo Streiff and Emerson Z. Granemann and Carmen Aguilera, “Galileo’s Surveying Potential: E5 Pseudorange Precision,” Mar. 2012.
- [24] J. Sanz and J.M. Juan and M. Hernández, “Antenna Phase Centre,” Navipedia ESA-approved website, 2011.
- [25] —, “Ionosphere-free Combination for Dual Frequency Receivers,” Navipedia ESA-approved website, 2011.
- [26] —, “Ionospheric Models for Single Frequency Receivers,” Navipedia ESA-approved website, 2011.
- [27] —, “Multipath,” Navipedia ESA-approved website, 2011.
- [28] J. Diez, A. Fernandez, and P. D’Angelo, “Granada: a low-cost commercial simulator for gnss receivers design and evaluation,” Proceedings of the Navitec 2006, Noordwijk, The Netherlands, pp. 11–13, Dec. 2006.
- [29] C. Jeffrey, *An Introduction to GNSS, GPS, GLONAS, Galileo and other Global Navigation Satellite Systems*, 1st ed. NovAtel Inc., 2010.
- [30] A. Joseph, “GNSS Solutions: Measuring GNSS Signal Strength,” *Inside GNSS*, vol. 5, no. 8, pp. 20–25, Nov. 2010.
- [31] Junhong Liu and Gu Defeng and Ju Bing and Yao Jing and Duan Xiaojun and Yi Dongyun, “Basic performance of BeiDou-2 navigation satellite system used in LEO satellites precise orbit determination,” *Chinese Journal of Aeronautics*, vol. 27, pp. 1251–1258, Oct 2014.
- [32] K. Borre, “The E1 Galileo Signal,” Aalborg University, Denmark, Tech. Rep., May 2009.
- [33] A. Lehner and A. Steingass, “A Novel Channel Model for Land Mobile Satellite Navigation,” in *Proceedings of the 18th International Technical Meeting of the Satellite Division of The Institute of Navigation (ION GNSS 2005)*, Long Beach Convention Center, Long Beach, CA, Sep. 2005, pp. 2132–2138.
- [34] A. Martellucci and R. P. Cerdeira, “Review of tropospheric, ionospheric and multipath data and models for Global Navigation Satellite Systems,” in *3rd European Conference on Antennas and Propagation (EuCAP) in 2009, Berlin (Germany)*. IEEE, Mar. 2009, pp. 3697–3702.

- [35] F. P. Martínez, *Sistemas de navegación por satélite*, 1st ed. Servicio de Publicaciones, E.T.S.I. Telecomunicación, 2000.
- [36] C. Matyszczyk, “Truck driver has GPS jammer, accidentally jams Newark airport,” CNET website, Aug. 2013.
- [37] O. Montenbruck, A. Hauschild, P. Steigenberger, U. Hugentobler, P. Teunissen, and S. Nakamura, “Initial assessment of the COMPASS/BeiDou-2 regional navigation satellite system,” *GPS Solutions*, vol. 7, no. 2, pp. 211–222, Apr. 2013.
- [38] A. Najmul, E. Lohan, and M. Renfors, “Moment based CNR estimators for BOC/BPSK modulated signal for Galileo/GPS,” in *Proceeding of the 5th workshop on positioning, navigation and communication 2008 (WPNC’08), Hannover, Germany*. IEEE, Mar. 2008, pp. 129–136.
- [39] Navipedia ESA-approved website, Available: http://www.navipedia.net/index.php/Road_Applications.
- [40] J. Nurmi, E. S. Lohan, S. Sand, and H. Hurskainen, *GALILEO Positioning Technology*, 1st ed. Springer, 2015.
- [41] “Space Segment,” Official U.S. Government information about the Global Positioning System (GPS) and related topics, GPS.gov website, Available: <http://www.gps.gov/systems/gps/>.
- [42] E. Pajala, E. S. Lohan, and M. Renfors, “CFAR detectors for hybrid-search acquisition of Galileo signals,” Jan. 2005.
- [43] S. Pullen and G. Gao, “GNSS Jamming in the Name of Privacy. Potential threat to GPS Aviation,” *Inside GNSS Magazine*, vol. 7, no. 2, pp. 34–43, Mar. 2012.
- [44] S. Pullen, G. Gao, C. Tedeschi, and J. Warburton, “The Impact of Uninformed RF Interference on GBAS and Potential Mitigations,” in *Proceedings of the 2012 International Technical Meeting of The Institute of Navigation*, Marriott Newport Beach Hotel & Spa, Newport Beach, CA, Jan. 2012, pp. 780–789.
- [45] “Ultra wide band (UWB) development and applications,” Radio-Electronics.Com, 2012, Available: http://www.radio-electronics.com/info/wireless/uwb/uwb_development.php.
- [46] Y. Rahayu, T. Rahman, R. Ngah, and P. Hall, “Ultra Wideband Technology and Its Applications,” in *5th IFIP International Conference on Wireless and*

- Optical Communications Networks, 2008. WOCN '08, Surabaya, Indonesia.* IEEE, May 2008, pp. 1–5.
- [47] L. Rusch and H. V. Poor, “Narrowband Interference Suppression in CDMA Spread Spectrum Communications,” in *IEEE Transactions on Communications*, vol. 42, no. 234. IEEE, Aug. 1994, pp. 1969–1979.
- [48] A. Rusu, E. Lohan, G. Seco, and I. Marghescu, “Investigation of Narrowband Interference Filtering Algorithms for Galileo CBOC Signals,” in *Proc. European Conference of Communications (ECCOM)*, Dec 2012.
- [49] Safa Dwoud, “GNSS principles and comparison,” Potsdam University, Jan. 2012.
- [50] J. Samson, “Interference in GNSS-bands,” European Space Agency, 2012.
- [51] J. Sanz, A. Rovira-Garcia, M. Hernández, J. Juan, J. Ventura-Traveset, C. López, and G. Hein, “The ESA/UPC GNSS-Lab Tool (gLAB): An advanced educational and professional package for GNSS data processing and analysis,” in *6th ESA Workshop on Satellite Navigation Technologies Multi-GNSS Navigation Technologies. Proceedings ISBN: 978-1-4673-2010-8, DOI: 10.1109/NAVITEC.2012.6423100.* Noordwijk, the Netherlands: gAGE-NAV,S.L, Dec. 2012.
- [52] N. C. Shivaramaiah and A. Dempster, “The Galileo E5 AltBOC: Understanding the Signal Structure,” in *International Global Navigation Satellite Systems Society IGNSS Symposium 2009*, Holiday Inn Surfers Paradise, Qld, Australia, Dec. 2009.
- [53] “Launch Schedule,” SPACEFLIGHT NOW, Available: <http://spaceflightnow.com/launch-schedule/>.
- [54] G. Stupak, “GLONASS Status and Development,” 5th Meeting of the International Committee on GNSS, Turin, Italy, 2010.
- [55] J. S. Subirana, J. J. Zornoza, and M. Hernández-Pajares, “Code Based Positioning (SPS),” Navipedia ESA-approved website, 2011.
- [56] K. Thomassen, “How GPS Works,” 2013, Avionics West GPS Training website.
- [57] J. B.-Y. Tsui, *Fundamentals of Global Positioning System Receivers: A Software Approach*, 2nd ed. Wiley-Interscience, Jan 2005, chapter 5: GPS C/A Code Signal Structure.

- [58] “GNSS Modernization,” UNAVCO, UNAVCO website, Available: <https://www.unavco.org/projects/project-support/gnss-support/gnss-modernization/gnss-modernization.html>.
- [59] Y.R. Chien and Y.C. Huang and D.N. Yang and H.W. Tsao, “A Novel Continuous Wave Interference Detectable Adaptive Notch Filter for GPS Receivers,” in *Global Telecommunications Conference (GLOBECOM 2010), 2010 IEEE*. Miami, Florida, USA: IEEE, Dec. 2010, pp. 1–6.
- [60] J. Zhang, “Advanced Signal Processing in Multi-mode Multi-frequency Receivers for Positioning Applications,” Ph.D. dissertation, Department of Communications Engineering, Tampere University of Technology, Tampere, Finland, Oct. 2013.
- [61] J. Zhang and E.-S. Lohan, “Effect and Mitigation of Narrowband Interference on Galileo E1 signal Acquisition and Tracking Accuracy,” in *International Conference on Localization and GNSS (ICL-GNSS), Tampere, Finland*. IEEE, June 2011, pp. 36–41.